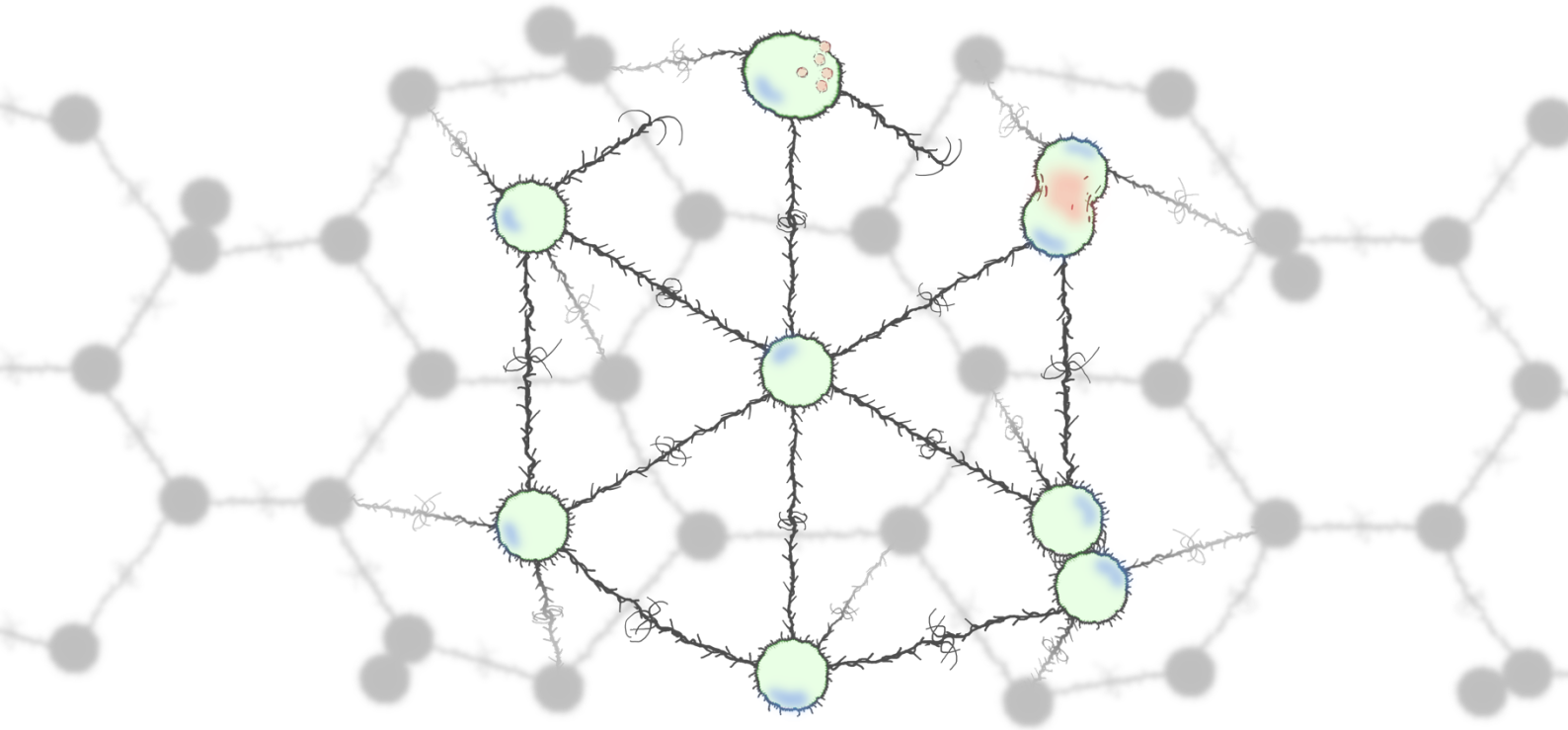

Imaging-based characterization of prokaryotic virocells at single-cell level

Dissertation

Zur Erlangung des Doktorgrades der Naturwissenschaften (Dr. rer. nat.)

Der Fakultät für Chemie der

Universität Duisburg-Essen

vorgelegt von

Indra Banas

2023

Image on title page: *Candidatus* Altiarchaeum hamiconexum cells forming hexagonal structures within biofilms by entangling their cell appendages, called *hami*. The cells are actively dividing, but also being targeted by a virus, resulting in virocells.

Das Promotionsgesuch wurde eingereicht am: 31.03.2023

Disputation am 29.08.2023

Diese Arbeit wurde angeleitet von: Prof. Dr. Alexander J. Probst

Prüfungsausschuss: Vorsitzender: Prof. Dr. Stephan Barcikowski

1. Gutachter: Prof. Dr. Alexander J. Probst

2. Gutachter: Prof. Dr. Andreas Klingl

3. Gutachterin: Prof. Dr. Ruth Schmitz-Streit

_____

Unterschrift: Indra Banas

Imaging-based characterization of prokaryotic virocells at single-cell level

Dissertation

For achieving the doctoral degree of natural sciences (Dr. rer. nat.)

At the faculty of Chemistry at the University of Duisburg-Essen

By

Indra Banas

2023

Key words:

virus, virocell, prokaryotes, archaea, terrestrial subsurface, microbial ecology, single-cell, microscopy, Raman spectroscopy, *in situ* characterization,

DOI: 10.17185/duepublico/79193
URN: urn:nbn:de:hbz:465-20231108-084823-6

This dissertation was performed under the auspices of

Prof. Dr. Alexander J. Probst (1st PhD supervisor)

Prof. Dr. Andreas Klingl (2nd PhD supervisor)

Prof. Dr. Ruth Schmitz-Streit (3rd referee)

At the Fakultät für Chemie under fullfillment of all guidelines according to the Promotionsordnung of the faculty

“l'essentiel est invisible pour les yeux” Antoine de Saint-Exupéry

Acknowledgements

Growing as person and as scientist in the way it happens during a PhD is not possible as an isolated person. Minds adhere to Newton's first law "an object will not change its motion unless a force acts on it". Therefore, I would like to acknowledge the forces that set my mind in motion.

I thank Prof. Alexander J. Probst as primary force during the past four years. From the first talk we had you focused on how you can contribute to my career and not just on how I can benefit your labs development. I was able to saturate and expand my scientific curiosity, while you made sure that I didn't lose track by overthinking. It is such a pleasure to work with you because you encourage us to tackle tasks, which mind sound insane to other people and made it work. You encouraged my application to the scholarship of the Studienstiftung des deutschen Volkes, to whom I am thankful for funding my PhD project.

Of course, this would not be possible without the amazing GEMs that you collected in your group. Even with major global boundaries, which paralyzed everyone in the past three years, our group mentality was always above average as we never let someone down. Abi, you glued us all together and always had a plan, no matter if it was a lab or personal emergency. André, you are the Post-doc (and now staff scientist) our lab needed for a long time and your presence enhances our coffee breaks, R scripts and drafts.

Hands up to the RGBG sampling Team, namely the NOVAC-girls (Vicky and Sarah) and Sophie. Our trips were always intensive experiences, we withstood every meteorological and technical difficulty and always succeeded as team. Our science would not be as much fun without sampling trips. Vicky, without your fearless and consequent attitude, my experiments would have never left the preliminary stage. Thank you, Sarah, for always having my back, as co-driver with the best playlist and most patient and sharp-sighted office ally. Together with Sophie and her unbreakable ambition to engage me into more self-organization, your honest and elucidating feedback make me a more intelligible person.

I would also like to thank the people behind the scenes. Prof. Andreas Klingl for being my second supervisor and demonstrating what kind of amazing structure conversation I can achieve if I try enough. The team at EMU for never ending discussions on sample preparation improvements during long days, a coffee or quick lunch breaks and your intensive training, which enables me to generate the micrographs I can present in this thesis. And to

Prof. Reinhard Rachel, for providing space in lab during sampling trips, fruitful discussions and for introducing me to the life science community in the German society of electron microscopy (DGE), which opened a broader perspective than any literature review.

Since I honestly did not learn about acknowledgements before my PhD, I also want to thank Prof. Dr. Hans-Curt Flemming for being my mentor during my undergraduate time. Thank you for creating Water Science, for engaging me with your passion for science and for encouraging me to face my archenemy, the English language. You opened my mind in all directions of the world and I hope I make good use of it.

Beside my colleagues I would also like to thank the JCF community, especially my senior spokespersons, who got me engaged in this network and the national board members and Team leaders. During the time, where social interaction was reduced to online Meetings, this community demonstrated that we could use it to stay connected and explore new possibilities.

Last but not least I want to thank my family and friends. I am grateful for my parents and grandparents to raise me and let me grow apart. Your constant engagement inspired me to become the person I am today. And for my brother, who followed me, even I if always used him to perform and cover up my mischief. I am now blessed with an amazing husband, he is usually not the fastest, but always there, when he is needed. Thank you Jarno for enduring me, when I am head at the clouds and for catching me, when I am coming back to the ground to fast. Especially during the roller coaster of the past weeks. Of course, we are both lucky, that we found a friend like Kira, who decided to tag along after her mandatory time. Thank you for the Wednesday evenings, no matter where we had our glass of wine, for listening, no matter how much I talk and still having advice.

There are still more people, my club members and dance partners, who made my time after work also fun and constructive.

But I would like to conclude with: Thank you, vacuum-packed instant Ramen, for saturating and satisfying me many home offices lunches and evenings. Life would have been sad without you.

Thanks

List of Publications

Indra Banas (née Monsees) has authored six publications in total, whereas she is first author for three publications The individual publications are listed below, categorized into published and in revision.

1. **Monsees, I**., Klingl, A., & Probst, A. J. (2019). Kleine Zellen, große Wirkung—Bakterien der Candidate Phyla Radiation**. BIOspektrum**, 25(7), 719-721.
2. **Monsees, I.,** Turzynski, V., Esser, S. P., Soares, A., Timmermann, L. I., Weidenbach, K., ... & Probst, A. J. (2022). Label-Free Raman Microspectroscopy for Identifying Prokaryotic Virocells. **Msystems**, 7(1), e01505-21.
3. **Banas I.**, Esser, S. P., Turzynski, V., Soares, A., Novikova, P., May, P., Moraru, C., Hasenberg, M., Wilmes, P., Klingl, A., Probst, A. J. (2023) Spatio-functional organization in virocells of small uncultivated archaea from the deep biosphere. **Revisied for The ISME Journal**
4. Rahlff, J., Turzynski, V., Esser, S. P., **Monsees, I**., Bornemann, T. L., Figueroa-Gonzalez, P. A., ... & Probst, A. J. (2021). Lytic archaeal viruses infect abundant primary producers in Earth's crust. **Nature communications**, 12(1), 1-12.
5. Turzynski, V., **Monsees, I**., Moraru, C., & Probst, A. J. (2021). Imaging Techniques for Detecting Prokaryotic Viruses in Environmental Samples. ***Viruses***, *13*(11), 2126.
6. Esser, S.P., Rahlff, J., Zhao, W., Predl, M., Plewka, J., Sures, K., Wimmer, F., Lee, J., Adam, P.S., McGonigle, J., Turzynski, V., **Banas, I.,** ... & Probst, A.J., 2023. CRISPR-mediated symbiosis of uncultivated archaea. **In revision for Nature Microbiologie**

Conference Proceedings

The work included in this thesis was presented and discussed at four in person conferences as three Posters (Microscopy conference 2019, Vereinigung für Allgemeine und Angewandte Mikrobiologie (Vaam) 2020, International Society for Microbial Ecology 2022) and one oral presentation (Microscopy conference 2023). In addition, one poster (Scix20) and three presentations (Micrsocopy conference 2021, Scix21 and VAAM 2022) were included in online conferences.

Table of content

1. Abstract

Viruses are assumed to be the most abundant entity on earth, when quantified as viral particles (virions). However, without metabolism these virions are of low ecological impact. Only encountering a potential host triggers their ecological role. For one decade, the virocell concept addresses the need to change the perspective of how to access the impact of viruses on ecosystems. The imbalance between properties of isolated viruses and the actual environmental diversity provided by microscopic and metagenomic studies on morphological and genomic traits of uncultivated viruses point out the need combine culture independent tools for virocell studies in microbial ecology.

This thesis aims to identify and characterize prokaryotic virocells at the single-cell level, using imaging-based techniques. We provide an insight into biochemical changes of prokaryotic virocells under laboratory conditions using Raman microspectroscopy. The analyses of single-cell spectra allowed reduction of multivariate data into a ratio for univariate virocell identification. The biomolecular assignment of observed spectral changes are consistent with characteristics of the virion composition and their maturation stages. In addition, we established a correlative light and electron microscopy approach, which allows the study of morphological traits of indigenous archaeal virocells identified based on metagenomic data. Examining individual environmental virocells in detail revealed their increase in cell size, putative viral particles on the cells surface and indices of the intracellular organization of virus replication. In a future perspective, further application and combination of the different approaches are discussed to point out how virocells and their impact on ecosystems can be accessed *in situ* using multimodal imaging approaches.

In summary, this thesis provides a substantial overview of imaging techniques and data processing to identify and characterize individual virocells and provides guidance for future experimental design to address different levels of the ecological impact of virocells throughout their lifecycle.

2. Introduction

2.1. The unexplored majority

Microbial ecology: from meta- to single-cell-omics

While the existence of microorganisms has been known for more than two centuries (Leeuwenhoek, 1800), methods to attain the identity and metabolic capacities of microorganisms that escape isolation and cultivation under laboratory conditions only emerged in the second half of the last century (Head et al., 1998). The awareness of the majority of microorganism being uncultivated became a central dogma of microbial ecology (Head et al., 1998) and drives scientific efforts until today. Microbes occur in high abundances in spheres of Earth, influencing ecosystems and global biogeochemical cycles significantly (Ladau and Eloe-Fadrosh, 2019). Understanding the effects of microbial interactions paves the way for modifying them, for engineering natural and anthropogenic systems to tackle global challenges, namely planetary sustainability, and human health (Verstraete et al., 2022).

The recent advances in digitalization have allowed new computational capabilities for research evolved from conventional Life Sciences (Krüger et al., 2020). Previously interdisciplinary approaches become new key disciplines. Biological methods are no longer cultivation based as faster computational methods allow generation of high-throughput data (Caicedo et al., 2017; Hériché et al., 2019; Luscombe et al., 2001)). This increasing complexity can now be used to formulate new scientific hypotheses. Multivariate data analyses allow more complex statistical calculations within shorter time (Ali et al., 2018). This interdisciplinary field of research that combines biology, statistics and computer sciences is nowadays named Bioinformatics (Luscombe et al., 2001).

Bioinformatics covers a wide variety of disciplines according to the nature of the data (e.g. DNA sequences, micrographs or spectra) (Chen et al., 2020; Luscombe et al., 2001; Vicar et al., 2019). With the description of 16S rRNA gene as a universal marker gene with highly conserved and nine variable regions (Abellan-Schneyder et al., 2021) and the availability of sequencing, microorganisms were phylogenetically classified based on their genetic information and not on morphology and metabolic characteristics only (Woese, 1998), which sheds light on the uncultivated majority of life on earth (Head et al., 1998). The high-throughput analysis of molecular information obtained from cellular components as DNA, RNA, proteins, lipids, or metabolites are denominated as respective -omics approaches

(Micheel et al., 2012). The combination of these techniques has allowed new insights into microbial communities by being combined into multi-omics studies (Krüger et al., 2020).

To study the ecological role of prokaryotes, not only 16S rRNA genes are recovered. Near-complete genomes of microorganisms can be reconstructed, allowing predictions of their metabolism (Anantharaman et al., 2016). Metagenomics represent a method to recover high amounts of microbial genomes from complex ecosystems (Anantharaman et al., 2016), but they tend to fall short on microorganisms with low abundance or high genomic heterogeneity (Dam et al., 2020). To tackle these short comes, single-cell genomics amplifies genomes of individual cells after an isolation process like Fluorescence-activated cell sorting (FACS), optical tweezers or microfluidic chips, allowing complete genome recovery (Woyke et al., 2010). Cells can even be sorted based on specific fluorescent labels, indicating degradation of specific substrates or facilitating enrichment of low abundant cells of interest (Kaster and Sobol, 2020). This function driven single-cell genomics only provides information about the metabolic potential of an uncultivated microbial cell, yet to explore the activity, the actual expressed genes need to be identified using transcriptomics (Kaster and Sobol, 2020). Transcriptomics processes RNA instead of DNA (Wang et al., 2009), which is challenging in prokaryotic cells as they have significantly lower amount of RNA than eukaryotic cells (Imdahl et al., 2020) and only a small fraction represents the messenger RNA (mRNA), the RNA of interest (Kaster and Sobol, 2020). In eukaryotic studies, single-cell transcriptomics help to reveal gene expression dependent sub-population patterns (Chen et al., 2017; de Bekker et al., 2011), which can provide *e.g.*, a detailed understanding how cells response to viral infections (Ku et al., 2020; Rosenwasser et al., 2019). Although, transferring single-cell transcriptomics methods form eukaryotic to prokaryotic cells is challenging, protocols adapting to prokaryotic limitations are being published for laboratory conditions (Chen et al., 2017; Imdahl et al., 2020)

With regard to transferring single-cell techniques to environmental samples to tackle the characterization of the uncultivated majority there is still major one challenge: samples are not fixed for transcriptomic analyses. Samples are frozen subsequently to sampling until processing in the laboratory, which works well for metatranscriptomic analyses relying on the isolation of total RNA from frozen samples (Auer et al., 2014). However, the microfluidic separation of cells for single-cell methods, is a lengthy process (Lee et al., 2021b). During this time the transcriptome might be altered irreversible (Imdahl et al., 2020). At the same time,

the sorting process of environmental samples has two additional challenges in comparison to cultures: Firstly, cells are mixed or attached to other materials, which interfere with the separation process. Secondly, the majority of cells is suspected to live in biofilms instead as free planktonic cells, with strong intercellular connections via extracellular polymeric substances (EPS) (Flemming and Wuertz, 2019).

Despite the advances in technology and cost reduction (Metzker, 2010) and the possibility to resolve analyses down to the single-cell level (Kaster and Sobol, 2020), the extraction of biomolecules leads to a loss of spatial information at the microbial relevant scale. To circumvent this loss, and overcome current processing limitations, microscopy and spectroscopy techniques can provide spatial context of the sample, including genomically derived information, while generating data for bioinformatical processing (Lee et al., 2021b, 2021a; Moter and Göbel, 2000).

Shedding light on microbial interactions

At the same time as sequencing technologies evolved, scientists began to link phylogenetic information to microscopic methods and put them into a spatial context (Giovannoni et al., 1988). The technique to use fluorophores attached to oligonucleotide probes targeting the 16S rRNA was established as fluorescence *in situ* hybridization (FISH) (Figure 2.1 A) (Amann et al., 1990) and is nowadays adapted to a broad variety of challenges. FISH can verify hypothesizes, *e.g.,* about syntrophic relationships of different microorganisms predicted from metagenomes by *in situ* co-occurrence (Schreiber et al., 2010). For environmental microbial samples, especially to tackle a low cellular number of ribosomes, a signal amplification via tyramide signal amplification (TSA) and horseradish peroxidase (HRP) was introduced (catalyzed reporter deposition FISH [CARD-FISH]) (Figure 2.1 B) (Pernthaler et al., 2002). This protocol opened new possibilities to detect microorganisms of interest in complex matrices and slow growing or little active cells (Matturro et al., 2021).

CARD-FISH was further modified and resulted in the first protocol to indicate the presence of a gene within cells of an environmental sample (geneFISH) (Moraru et al., 2010). The authors designed HRP-labelled dsDNA polynucleotide probes targeting the ammonia monooxygenase alpha subunit (*amo*A) encoding gene of *Crenarchaetota* (Figure 2.1 C). Since dsDNA polynucleotides are used, both strands of the genome can be labeled simultaneously, further amplifying the signal (Barrero-Canosa et al., 2017). The protocol was established on *E. coli* cells with *amo*A-containing plasmids and then used to detect bacterial cells containing

the gene in seawater samples (Moraru et al., 2010). However, this approach is quite time consuming - two amplification steps are performed one after another - and does not allow quantification (Barrero-Canosa et al., 2017). Barrero-Canosa and colleagues overcame these drawbacks by introducing direct-geneFISH (DGF) in 2016 (Barrero-Canosa et al., 2017). They replaced the two amplification steps by one hybridization step using a 16S rRNA targeting oligonucleotide probe for cell identification (Figure 2.1 A) and several multi labeled dsDNA polynucleotides, all targeting the same gene of interest, within (Figure 2.1 D) (Barrero-Canosa et al., 2017). Additionally, the directly labeled polynucleotides allowed quantification, which was not possible using amplification (Barrero-Canosa et al., 2017).

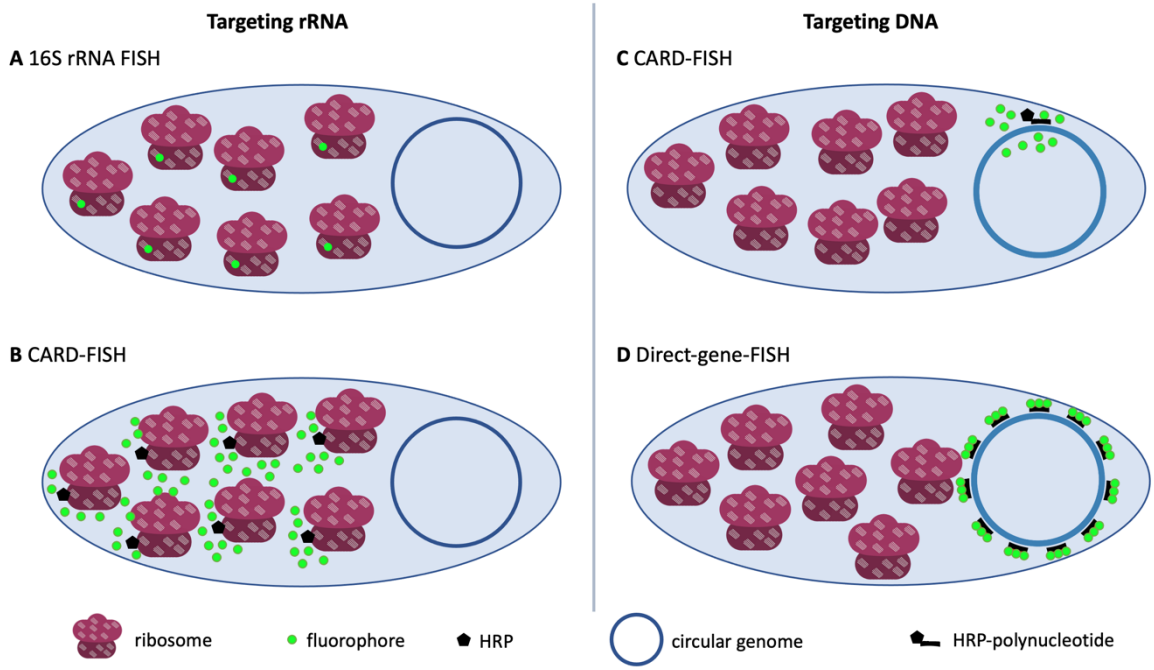

Figure 2.1 | **Examples of FISH approaches in prokaryotic cells. (A)** Conventional 16S rRNA FISH using mono-labeled oligonucleotides; **(B)** CARD-FISH targeting rRNA using HRP-labeled oligonucleotides; **(C)** CARD-FISH targeting a gene using a HRP-labeled polynucleotide; **(D)** Direct-geneFISH using several multi labeled polynucleotides, targeting a circular genome. For targeting accessible rRNA of the ribosomes (white spots) usually oligonucleotide (about 15-20 nucleotides) is used (A and B), for genes polynucleotides (about 300 nucleotides) are used (C and D). The genome and the polynucleotides are ds-DNA.

In a recent study, McIlroy and colleges observed morphological differences using FISH for the most frequent species in a bioreactor (McIlroy et al., 2023). Based on these microscopic observations, they performed metatranscriptomics to point out metabolic differences of these morphologies, while the genomes were found to be identical (McIlroy et al., 2023). They demonstrated, how FISH allows visualization of (meta-) genomically derived data and simultaneously paves the way for more in-depth *in silico* studies (McIlroy et al., 2023). While

McIlroy and colleagues used FISH and -omics side by side, other techniques allow direct linkage of phylogenomic identity of individual cells and metabolic capacities. The combination of different optical modalities to the same sample are summarized as multimodal approaches (Schie et al., 2021).

One technique to implement into such a multimodal approach is Raman spectroscopy. It measures the change of wavelength of photons from a monochromatic light source due to inelastic scattering, which is specific for different chemical bonds (Lee et al., 2021a). By coupling light microscopy and Raman spectroscopy, Raman microspectroscopy, a non-destructive, label-free technique that allows fast and cheap insights into microbial cells became available (Puppels et al., 1990). Databases of pure compounds and theoretical spectra now allow identification of biomolecular classes within complex biological spectra (De Gelder et al., 2007). In combination with FISH (Raman-FISH), individual cells can be identified and their metabolic potential can be accessed (Huang et al., 2007). The potential for degradation of specific compounds and fast identification within actively growing cultures can be elucidated by labeling the compound of interest *e.g.* with stable isotopes of carbon (^{13}C), nitrogen (^{15}N) or hydrogen (D) (Huang et al., 2007; Muhamadali et al., 2015; Wang et al., 2016). The integration of heavy isotopes causes a reduction of the resulting peaks wavenumbers, a so-called red shift, which is visible by eye (Huang et al., 2004). The application of multivariate data analysis on the spectral data allows label-free, in-depth insights into biochemical changes between cells (Neugebauer et al., 2007), but requires a sufficient sample size for statistical significance of the results (Ali et al., 2018). Since multivariate data analyses represents a high-throughput method, scientist introduced the terms ramanomics and ramanome to point out its potential power to bring "omics"-methods down to a non-destructive cellular level (Kuzmin et al., 2017; Teng et al., 2016). Simultaneously, a protocol allowing Raman-activated cell sorting (RACS) of prokaryotic cells was improved to enable sorting of up to 500 cells/h based on stable isotope labeling or molecules exhibiting strong Raman peaks, mainly associated to cytochromes (Lee et al., 2021b). This protocol presents the feasibility to be adapted to other molecular signals, if they cause strong Raman peaks or can be reduced to ratios of respective peak areas. For sorting cells based on the incorporation of ^{13}C, RACS compares the intensity of the peak assigned to ^{13}C incorporation into phenylalanine with the intensity of unlabeled (^{12}C) phenylalanine (Lee et al., 2021b) as it was proposed by *Huang et al*. (Huang et al., 2007).

Raman-FISH, ramanomics and RACS underline the high potential Raman spectroscopy harbors for microbial applications (Kuzmin et al., 2017; Lee et al., 2021b, 2021a; Teng et al., 2016). For spectral acquisition of microbial samples requiring high analytical sensitivity currently dried cells are used (Lee et al., 2021a). However, future technical improvements of detector sensitivity and inclusion of machine learning will support the emergence of live cell measurements in more fields of microbial ecology (Lee et al., 2021a).

Characterization beyond the diffraction limit

While light microscopy related studies allow conclusions about single microbial cells, more detailed information about cellular ultrastructure cannot be achieved due to limited resolution (de Boer et al., 2015). Super resolution imaging was able to overcome this limitation and demonstrate resolution down to 10-30 nm to localize single proteins in bacterial cells (Altinoglu et al., 2019). Various super resolution microscopy methods were introduced in the past decade (*e.g.,* photoactivation localization microscopy (PALM), stochastic optical reconstruction microscopy (STORM) and structured illumination microscopy (SIM)). However, all of these depend on cultivation of the organism to genetically modify proteins of interest or immunolabeling (Singh and Kenney, 2021).

To resolve the ultrastructure of microbial cells in the nanometer or angstrom (Å) range electron microscopy (EM) techniques are used (de Boer et al., 2015). Nevertheless, the respective imaging technique needs to be chosen in dependence of the desired information. Scanning electron microscopy (SEM) creates a surface overview of the sample at nanometer resolution (Kremer et al., 2015). This resolution allows the elucidation of morphological features of microbial cells, their surroundings, and respective changes due to external influences (Fleeman et al., 2023; Nyongesa et al., 2022; Serra et al., 2013).

Higher magnifications than SEM can be achieved by transmission electron microscopy (TEM). For TEM imaging, microbial samples are examined deposited on a grid, either as whole cells or embedded in resin as thin section (Perras et al., 2014). These thin sections allow a resolution in the angstrom range (Kremer et al., 2015) and enable insight into cells to visualize the ultrastructure of the cytoplasmic membrane, intracellular components, and processes like sporulation (Bechtel and Bulla, 1976; Perras et al., 2014). High resolution comes with a reduced field of view and therefore requires a high concentration of biological microbial material (Golding et al., 2016). For cultivated samples or almost monospecies environmental biofilms, proteins of interest can be extracted and then be localized within the cellular

ultrastructure and as cellular appendages using immunogold labeling of embedded cells or after deposition of cells on a TEM grid (Moissl et al., 2005; Sakoula et al., 2022). However, protein labeling requires extensive preparation, as the protein needs to be purified in a sufficient amount to produce respective antibodies, by injection into mammals, *e.g.* rabbits. The antibodies need to be purified form the blood as well, so they can be applied to the sample (Flechsler et al., 2020).

The time-consuming preparation of antibodies for immunogold labeling in EM explains, why labelling of probes used for FISH with gold particles is an emerging contemplation. Linking phylogeny with ultrastructural details of cells morphology or microbial interactions within environmental samples will pave the way for faster, more in-depth studies (Schmidt et al., 2012). To avoid possible low signal to noise ratio between nanogold probes and natural inorganic background, Schmidt and colleagues introduced a CARD-FISH-based approach with autometallographic enhancement of nanogold after deposition within microbial cells, called Gold-FISH (Schmidt et al., 2012). They demonstrated enrichment of gold in microbial cells of environmental samples with sufficient concentration for detection during SEM using the backscattered electron detector (BSE), but also pointed out the challenge of non-specific signals from minerals (Schmidt et al., 2012). In 2015, two studies trying to address the challenges of this method were published: Polygold-FISH kept the initial Gold-FISH protocol and only replaced the gold enhancement step by applying multiple probes for the same organisms, but did not apply this protocol to environmental samples (Almstrand et al., 2015). At the same time, Ye and colleagues addressed the need for permeabilization to allow insertion of large molecules in previous protocols which affects cellular ultrastructure (Ye et al., 2015). They adapted the original FISH protocol by replacing fluorophores with nanogold particles attached to oligonucleotides with a 5' thiol-modification (Gold *in situ* hybridization, short GISH) (Ye et al., 2015). Nevertheless, they also found gold-enhancement leading to non-specific binding to iron oxide using energy dispersive spectroscopy (EDS) within their charcoal sample representing environmental conditions (Ye et al., 2015).

Emergence by correlation

So far, all studies illustrate the potential and challenges of *in situ* hybridization using probes detectable using electron microscopy (Almstrand et al., 2015; Schmidt et al., 2012; Ye et al., 2015). However, a more recent study adapted the CARD-FISH protocol and exchanged the amplification step by intracellular silver deposition in dependence to the horseradish

peroxidase labeled probes (Berg et al., 2020). With this silver deposition *in situ* hybridization (silver-DISH) protocol, not only was it possible to differentiate microbial cells within an environmental sample, but to also demonstrate for the first time a surface-enhanced Raman spectra (SERS) effect specifically within labeled cells (Berg et al., 2020). The applicability of metal probes for multiple techniques constitutes new possibilities for multimodal studies of environmental microbial samples and therefore for more complex *in situ* studies for microbial ecology.

If light and electron microscopy are coupled in a multimodal setting, the workflow is described as correlative light and electron microscopy (CLEM) (Walter et al., 2020). Correlating EM methods with FISH allows the detection of more than one probe within the sample and directly links (meta-) genomically derived information to spatial organization or morphology (Knierim et al., 2012; McGlynn et al., 2018). This allows to explore microbial interactions even in environmental samples (Schaible et al., 2022). For example, Li *et al.* illustrated the morphologies of different uncultivated magnetotactic bacteria within an environmental sample (Li et al., 2017). Linking FM with SEM or TEM, they correlated the phylogenetic identity with the presence of magnetosomes, which display a high contrast to other molecules due to their high electron density (Li et al., 2017). McGlynn and colleagues first correlated FM and TEM of thin sections to define distinct ultrastructural characteristics of different anaerobic methanotrophic archaea within multicell environmental consortia (McGlynn et al., 2018). Based on these morphological traits they performed an additional EM study to measure and compare the biovolume of the different prokaryotes within the consortia and found a correlation between cell size and intracellular polyphosphate-like granules (McGlynn et al., 2018). CLEM and its expansion to multimodal approaches requires thoughtful design of experiment and sample preparation (Walter et al., 2020). Considerations for multimodal experiments start with the sample fixation, as glutaraldehyde is important for ultrastructure conservation, but causes autofluorescence (McGlynn et al., 2018). Moreover, the FISH protocol and the order in which the different techniques are applied need to be contemplated (Schaible et al., 2022). The correct design of experiment allows coupling CLEM to Raman microspectroscopy, nano-scale secondary ion mass spectrometry (Nano-SIMS) and EDS to identify intracellular granules using multimodal approaches (McGlynn et al., 2018; Schaible et al., 2022).

Consequently, *in situ* hybridization-based approaches hold the key to resolve genomically derived data on a microbial relevant scale within in environmental samples, down to the single-cell level. Implemented in multimodal settings, they can confirm biochemical characteristics of single-cells and in EM settings, they can elucidate morphological traits of microorganisms.

2.2. Viruses and virocells

Classifying the smallest microbial entity

In addition to the challenge of isolating and characterizing microbial cells, studying viruses that infect them presents unique challenges (Kieft and Anantharaman, 2022a). Understanding and detecting viruses plays a crucial role in understanding structure and health of ecosystems and individuals (Suttle, 2005; Vincent and Vardi, 2023). Around 1970, two methods of functionally characterizing viruses were proposed: the Baltimore classification proposed to sort viruses based on the transmission of their genetic information (Baltimore, 1971). These can be double- or single-stranded (ds/ss) RNA or DNA which are transcribed into messenger mRNA within the host cell (Baltimore, 1971). Another system is based on the morphologies of isolated viral particles (virions) known from TEM micrographs (Bradley, 1967). In general, the nucleic acid core of a virion is surrounded by a capsid consisting of proteins, which can in addition be enveloped by lipids (Dion et al., 2020). The manifold ratios and shapes of these macromolecules are illustrated in the diversity of viral shapes known today (Dion et al., 2020).

For viruses, it was noted that most representatives show no universal marker gene like the 16S rRNA gene for prokaryotes, indicating no monophyletic origin of viruses (Rohwer and Edwards, 2002). However, genetic studies show several genes that, on one hand, are shared between groups of viruses and, on the other hand, only have distant homologs in organisms (Koonin et al., 2006). These genes are collected under the term “viral hallmark genes” and encode, for example, capsid proteins, proteins for genome replication or for DNA packaging (Koonin et al., 2006). These genes can be used to prove the viral character of putative viral sequences in metagenomic datasets (Dutilh et al., 2021). Simultaneously, virions contain genetic fragments of their former hosts, called auxiliary metabolic genes (AMG), which can be expressed during consecutive infections (Sun et al., 2022). Therefore, viruses influence their ecosystems as mobile genetic elements between host cells, enhancing horizontal gene transfer (Rohwer et al., 2009).

To lyse or not to lyse — viral lifestyles

Besides the ongoing discussion on taxonomical classification, it is extensively discussed what should be considered a virus (Forterre, 2011). The methods used for traditional virus classification only consider the characteristics of virions which are released into the environment (Baltimore, 1971; Bradley, 1967). Another characteristic of viruses is their lifestyle within their respective host, which significantly influences its ecological impact (Zhang et al., 2022). Initially, they were differentiated into lytic and lysogenic lifestyles (Lwoff, 1953). On one hand, lytic infection results in lyses of the host cells and the release of organic matter and virions (Correa et al., 2021). Lysis can result in an huge impact on geochemical cycles, especially carbon cycling, as for example described by the viral shunt in aquatic ecosystems (Suttle, 2005; Wilhelm and Suttle, 1999) and shape the microbial community (Thingstad et al., 2014; Zhang et al., 2022). On the other hand, lysogenic infection cycles describe virus replication within the cell without causing lysis, by integrating the viral genome into the host genome (Mäntynen et al., 2021). Once the virus is integrated into the host genome, the expression of AMG can enhance the fitness of the host, for example by encoding metabolic or antibiotic resistance genes (Correa et al., 2021; Kieft and Anantharaman, 2022b; Sun et al., 2022). Nowadays, the majority of prokaryotic viruses is suggested to be temperate viruses, which are able to switch between lysogeny and lytic infection cycles (Zhang et al., 2022). The factors influencing the transition of a temperate virus are *e.g*. nutrient availability, temperature or host density (Zhang et al., 2022). To graduate an infection continuum between lytic and lysogenic states, more lifestyles have been described: Pseudolysogeny, where the viral genome is within the host cell without being replicated and chronic viral infections, in which virions are produced without lysis of the host cell either by continuous excretion of the particles through the membrane or accumulation of the particles within the host cell (Mäntynen et al., 2021).

To emphasize that viruses as microbial entities are not just their virions, but also include their maturation within host cells, Forterre proposed calling infected cells producing virions "virocells" (Forterre, 2011). In contrast, cells undergoing metabolism to divide into new cells are termed "ribocells" (Forterre, 2011). With this terminology, lytic viruses would be virocells and lysogenic and pseudolysogenic lifestyles result in ribocells. To describe chronic infections, the term ribovirocells is proposed (Forterre, 2013). In alignment with the diversity of viral lifestyles and the virocell concept, Correa and colleagues emphasize to change the

perspective of microbial ecology on viruses (Correa et al., 2021). By quantification of virions, viruses seem to outnumber possible hosts, but this does not necessarily correlate to actual successful infections (Forterre, 2013). Virions might be immobilized by attachment to a matrix (Kimura et al., 2008), or the host might have developed effective defense mechanisms (Daly et al., 2019). Under consideration of the virocell concept, viruses cannot be more abundant than other microorganisms (Forterre, 2011). To quantify the proliferation of all viral lifestyles, similarly to epidemiology, a reproduction number could be implemented to indicate how many new infected cells are produced from one infected cell (Correa et al., 2021).

Under laboratory conditions, time-resolved metabolomic studies have shown great potential to link the changes within the transcriptome, lipidome and proteome of different virocells to viral proliferation, in comparison to respective uninfected ribocells, or ribocells infected with a lysogenic virus (Ankrah et al., 2014; De Smet et al., 2016; Howard-Varona et al., 2020; Rosenwasser et al., 2014). However, all these studies were performed at population level and therefore display an average of the actual infection dynamics (Figure 2.2 left panel) (Ku et al., 2020).

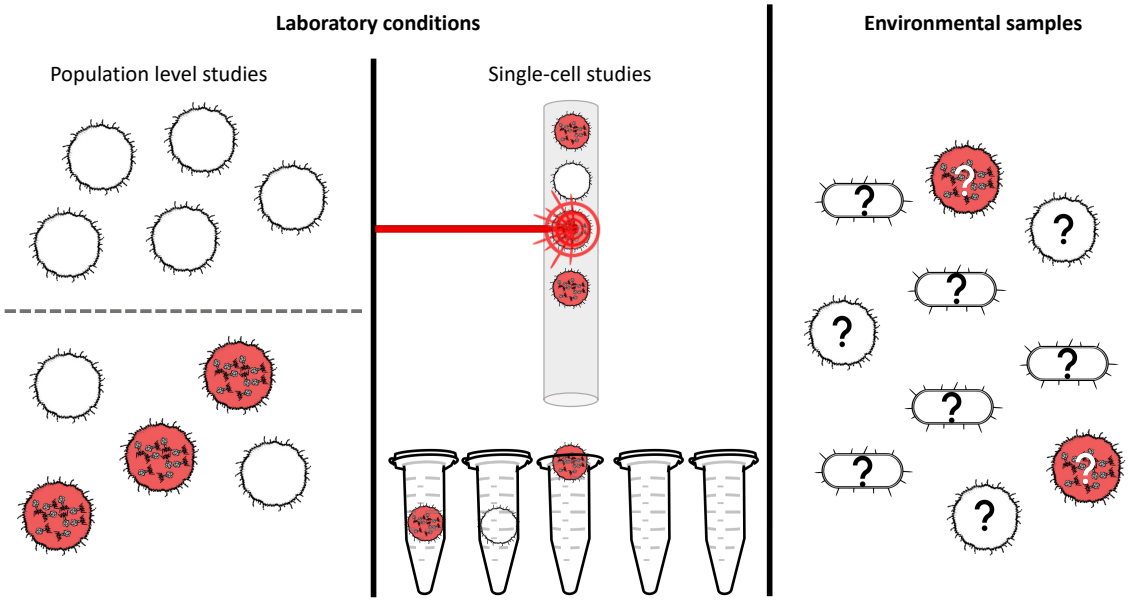

Figure 2.2| Challenges studying virocells. White cells are ribocells, red virus filled cells are virocells. During growth dependent studies in the laboratory, infection conditions can be defined and controlled. **Left panel**: Analyses on the population level lacks resolution, since the sampling time point will never display the same progress of infection in each cell. **Middle panel**: FACS allows sorting of infected cultures for single-cell studies. **Right panel:** Under environmental conditions the infection state of a sample cannot be defined, therefore no control group is available. Currently, no methods are available to identify a virocell prior to analysis.

As introduced in section 2.1, single-cell methods aim to show the phenotypic diversity overseen by population level experiments (Figure 2.2 middle panel). Single-cell genomics has

been proven to be able to capture novel viruses and virus-host systems (Dam et al., 2020; Džunková, 2022; Kaster and Sobol, 2020). During consecutive studies Rosenwasser and colleagues demonstrated, how single-cell methods can uncover maturation of eukaryotic virocells, based on their model system *Emiliania huxleyi* and the large *E. huxleyi* virus (EhV) (Ku et al., 2020; Rosenwasser et al., 2019, 2014). First, they conducted a population level transcriptomic and metabolomic study to demonstrate how the virus remodels the host metabolism towards the transcription of its own lipid metabolism (Rosenwasser et al., 2014). Consecutively, they sorted individual cells using microfluids prior to compare host and viral gene expression over time (Rosenwasser et al., 2019). They were able to show that during different sampling time points, the heterogeny of viral gene expression is better resolved than in population level experiments and allows the creation of a pseudotemporal scale of virocell maturation (Rosenwasser et al., 2019). Simultaneously, they were able to identify the expression profile of a virus resistant sub population, which was concealed during population level experiments (Rosenwasser et al., 2019). Finally, they used FACS and single-cell RNA-sequencing to define seven maturation stages along the pseudotemporal scale and tracked the host mitochondrial, chloroplast and nuclear derived mRNA shutdown during virocell maturation (Ku et al., 2020). Similar to eukaryotic systems (Ku et al., 2020; Rosenwasser et al., 2019), the availability of single-cell transcriptomics of prokaryotic cells (Imdahl et al., 2020) will most likely be able to describe transcriptomic development within virocells with a previously unseen detailedness, allowing an understanding of mechanisms involving viral infection, maturation and host defense. A first insight into the potential of single-cell transcriptomics to study prokaryotic virocells is already provided by Raman microspectroscopy combined with trapping individual cells using an optical tweezer (Chen et al., 2009; Wu et al., 2021). However, measuring single-cells until viral induced lysis is rather time consuming, resulting in few replicates (Chen et al., 2009; Wu et al., 2021, p. 21) limiting insights into phenotypic heterogeneity (Dam et al., 2020)

To match the metagenomically predicted diversity of viruses, it is necessary to move away from a virion-centric view towards the better understanding of temperate phages on a transcriptomic level (Howard-Varona et al., 2020, 2017). For this purpose, isolated virus-host systems can be used to establish single-cell methods with increased temporal and spatial resolution of virus-host interactions (Howard-Varona et al., 2017; Vincent and Vardi, 2023; Wu et al., 2021, p. 21). Additionally, monitoring individual cells prior to genomic or

transcriptomic analyses using a quick and non-destructive method would allow more in-depth analyses of intra cellular changes (Lee et al., 2021b). Demonstrating the ability to track massive metabolic changes on the short temporal scale of virocell maturation at single-cell level (Wu et al., 2021, p. 21) paves the way to understand metabolic more subtle but persistent effect of lysogenic ribocells and the initiation of transition into a lytic state. Ultimately, the methods will allow identification and transcriptomic exploration of environmental viruses (Figure 2.2 right panel) (Howard-Varona et al., 2017, p. 20).

Luminary in shape and escape - Archaeal viruses

Among prokaryotic viruses, archaeal viruses have been discovered to display a variety of morphologies unseen in other viruses (Krupovic et al., 2018). Comparing proteomes of archaeal virus with other viral or microbial proteins revealed that even with the increasing amount of available data, only about 25% have identifiable homologs outside of the archaeal virome (Dutilh et al., 2021). There are even isolated archaeal viruses without any genes shared with other known viruses (Wagner et al., 2017; Weidenbach et al., 2017). However, with regard to the evolutionary relationship of archaeal viruses, structural studies using cryo-electron microscopy helped to find similarities to other viruses within capsid protein structures, which were not predictable using genomic studies (Prangishvili et al., 2017).

Nevertheless, studies with a resolution to predict protein structures down to the angstrom level are generally performed on cultivated representatives, as a high amount of purified virions is required (DiMaio et al., 2015; Kasson et al., 2017; Wang et al., 2019). Besides the unique structure of archaeal virions, infected archaeal cells also harbor previously unknown characteristic. They display outstanding egress mechanisms during lytic and chronic infections such as virus-associated pyramids, budding or enzymes specialized on the degradation of archaeal cell walls (Baquero et al., 2021) and drastic morphological alteration of the host, like a 20-fold increase in cell size (Liu et al., 2021).

The various studies performed on isolated or enriched (putative) virus-host systems highlight the expected diversity of the currently unexplored mechanisms expected in uncultivated environmental systems (Gehlert et al., 2022; Kieft and Anantharaman, 2022a; Krupovic et al., 2018; Prangishvili et al., 2017; Sharma et al., 2018; Wang et al., 2022). Recent studies started to link the genomic identity of archaeal viruses to fluorescence microscopy (Hochstein et al., 2016; Rahlff et al., 2021). To overcome weak fluorescence signals, Hochstein and colleagues adapted a CARD-FISH protocol (Figure 2.1 C) achieving dual viral and cellular

FISH (viral FISH) (Hochstein et al., 2016). They designed four polynucleotide probes targeting the predicted viral genome. In addition to reveal the co-occurrence of fluorescence signals of virus and archaea, they were able to infect an isolated closely related strain and purify virions for TEM imaging (Hochstein et al., 2016). In comparison, Rahlff *et al*. used eleven polynucleotides instead of a signal amplification step in a protocol derived from direct-geneFISH (Figure 2.1 D) and therefore called virus-targeted direct-geneFISH (virusFISH) (Rahlff et al., 2021). With this method they were able to illustrate different infection stages of a putative lytic virus within environmental archaeal biofilms with no isolated relative of the *Candidatus* phylum Altiarchaeota (Dombrowski et al., 2019). To underline the viral character of the putative virus, they were able to show intracellular putative virions in TEM micrographs of ultra-thin sections of these biofilms (Rahlff et al., 2021). These studies linked virus and host signals, but do not transfer these results directly to ultrastructural images.

While CLEM is slowly emerging into microbial ecology (Schaible et al., 2022), it has rarely been used to study microbial virocells. The first link of a bacteriophage fluorescence signal to electron microscopic images was presented by Jahn *et al.* (Jahn et al., 2021). They localized a putative bacteriophage signal within bacterial cells in sponge tissue and putative phage particles inside the sponge phagosome. Hybridization was performed on the viral genome only, without linking it visually to its potential bacterial host. Instead, only the 4',6-Diamidino-2-phenylindol (DAPI) signal, which binds unspecific to DNA, was used to overlay fluorescence and electron micrographs on embedded sponge tissue (Jahn et al., 2021). This study points out that visual colocalization of viral and host genomes in virocells using CLEM is technically feasible; yet no publication has so far bridged this gap of application for characterization of uncultivated virocells *in situ.*

Virocells directing carbon cycling in the deep terrestrial subsurface

The deep subsurface is estimated to hold about 15% of the global and the majority of bacterial and archaeal biomass (Bar-On et al., 2018) and consequently represents a reservoir for novel microbial phyla (Magnabosco et al., 2018). About one third of all prokaryotic cells is estimated to live in the deep continental subsurface and the majority is expected to life in biofilms, where microbial interactions and processes are facilitated in comparison to planktonic lifestyles (Flemming and Wuertz, 2019). Metagenomic studies reveal the close linkage of microbial processes like energy metabolism to biogeochemical cycling of carbon, nitrogen, sulfur and other elements (Anantharaman et al., 2016; Hernsdorf et al., 2017). Noteworthy, the majority

of these subsurface organisms does not contain genes for complete pathways, but the respective genes are rather distributed among several organisms (Anantharaman et al., 2016). As biofilms create gradients and retain nutrients, they represent a hotspot for metabolic handoffs driving geomicrobiological processes in the deep continental subsurface (Anantharaman et al., 2016; Flemming and Wuertz, 2019), which need to be understood to tackle ongoing challenges derived from anthropologically-driven climate change (Hernsdorf et al., 2017).

In alignment with the importance of understanding the biogeochemical impact of microorganisms of the deep subsurface is the understanding of their viruses and how they may affect abundance and metabolisms of their host (Cai et al., 2023). Unlike surface environments, where ribocells will eventually be grazed and the organic carbon be transferred to higher trophic levels (Suttle, 2005), the deep subsurface is dominated by prokaryotes (Bar-On et al., 2018). Therefore, deep subsurface lytic viruses have a higher impact on microbial mortality, community composition and nutrient availability than in surface ecosystems (Cai et al., 2023). Consequently, to understand carbon cycling in the deep subsurface, we need to be able to quantify virus infected cells and to distinguish virocells from ribocells. By doing so, studies targeting specifically virocells might be able to shed light on the actual impact of viruses on the carbon cycle within the continental subsurface (Cai et al., 2023).

First evidences for *Ca.* A. hamiconexum being targeted by viruses in the continental subsurface were the identification of a clustered, regularly-interspaced short palindromic repeat (CRISPR) system using metagenomics (Probst et al., 2014) and infrequent micrographs showing virus-like particles (Probst and Moissl-Eichinger, 2015). The motivation to further elucidate this virus-host system is not only arising from the interest to shed light on novel viruses, but also the unique characteristics of the host and the role of the virus-host system in the continental subsurfaces carbon cycle (Rahlff et al., 2021).

The first described representatives of *Ca.* Altiarchaeum were discovered over 20 years ago, when the ubiquity of archaea across Earth's biomes was recognized (Moissl et al., 2003). *Ca* Altiarchaeum was initially found in a striking biofilm morphology in the outlet of cold sulfidic springs and was postulated to have a symbiotic lifestyle with sulfide oxidizing bacteria (Moissl et al., 2002; Rudolph et al., 2004, 2001). Later, *Ca.* Altiarchaeum was found to originate from the spring water itself and therefore from the deep continental subsurface, where it was found to form almost pure archaeal monospecies biofilms (Henneberger et al., 2006).

In the past two decades, *Ca.* A. hamiconexum was studied intensively *in situ* and *in silico* to access its contribution on its ecosystem and was located based on sequencing data in subsurface ecosystems across the globe. Within these ecosystems, it is frequently one of the most abundant species (Hernsdorf et al., 2017; Probst et al., 2018, 2014). However, there is no cultivated representative of Altiarchaeota and their phylogenetic placement between Euryarchaeota and the DPANN (Diapherotrites, Parvarchaeota, Aenigmarchaeota, Nanoarchaeota, Nanohaloarchaeota)-superphylum is not yet concluded (Dombrowski et al., 2019). In the Mühlbacher Schwefelquelle (MSI) in Bavaria, Germany, microscopic studies revealed a highly conserved structure between individual archaeal cells of the biofilm. Cells are organized in a reoccurring hexagonal pattern, maintaining a distance of about 4 µm to each other due to their unique cell appendages- the *hami* (Henneberger et al., 2006). The protein structure of *hami* (singular *hamus*) was examined using electron microscopical techniques (Moissl et al., 2005). About 100 *hami* occur per cell, each about 2 µm in length and consisting of a prickle and a hook region which are anchored within the double membrane (Moissl et al., 2005; Perras et al., 2014). Additionally, the combination of metagenomics and stable isotope analysis of the lipids indicates that *Ca.* A. hamiconexum should be capable of fixing carbon dioxide via a novel type of archaeal reductive acetyl-CoA pathway (Probst et al., 2014). The ability to fix carbon dioxide strongly suggests an autotrophic lifestyle in an anoxic, nutrient-limited environment (Probst et al., 2014). Despite this, the electron donor and acceptor have not been identified yet (Probst and Moissl-Eichinger, 2015).

In contrast to subsurface groundwater systems, hypotheses about large scale impact of microbial interactions based on laboratory experiments can be upscaled into mesocosms within aquatic surface ecosystems(Vincent and Vardi, 2023). These mesocosms allows to build an intermediate between laboratory conditions and the actual environment, to better estimate microbial impact on larger spatiotemporal scales (Vincent and Vardi, 2023). For the deep subsurface, upscaling of laboratory experiments is far more difficult, as gaining access to the ecosystem is in most cases linked to major interference with the initial ecosystem composition (Daly et al., 2019) and the majority of phyla lack any cultivated representatives (Probst et al., 2018). Therefore, there is a high scientific interest in distortion-free sampling of a subsurface ecosystem, while accumulating high cell numbers of an organism of interest. At MSI, *Ca.* A. hamiconexum biofilm flocks are continually flushed from the subsurface to the surface along with the groundwater flow (Henneberger et al., 2006), enabling such a distortion

free sampling for metagenomic and *in situ* studies of a subsurface primary producer and its putative lytic virus (Probst et al., 2014; Rahlff et al., 2021).

Imaging-based characterization of prokaryotic virocells at single-cell level

Metagenomic and spectroscopical studies allow to predict the metabolic potential of the uncultivated majority of environmental microbial communities and cells (Anantharaman et al., 2016; Probst et al., 2014). Single-cell transcriptomics links this potential with actual activity, helps to fully resolves the population heterogeneity and is about to overcome the final challenges to be broadly applicable for prokaryotic systems (Kaster and Sobol, 2020). In the meantime, imaging-based techniques are already able to link identity and function down to a single-cell level (Barrero-Canosa et al., 2017; Moraru et al., 2010), and multimodal approaches coupling microscopy, spectroscopy and -omics increase the spatial or temporal resolution of ecologically driven research questions (Huang et al., 2007; Lee et al., 2021b; Li et al., 2017; Schaible et al., 2022). However, the transfer of these multimodal single-cell approaches to prokaryotic virocells is lacking. This transfer will promote our understanding of host defense mechanisms, the transition between viral lifestyles, viral maturation stages and the impact of virocells on biochemical cycles.

Raman microspectroscopy can track biochemical changes during lytic infection of single-cells trapped by an optical tweezer (Chen et al., 2009; Wu et al., 2021). Combined with multivariate analyses univariate marker for different maturation stages along a pseudotemporal scale can be defined, as demonstrated in other systems (Ku et al., 2020; Rosenwasser et al., 2019; Teng et al., 2016; Wang et al., 2016). Once these markers are established, they can be applied to enhance sorting processes (Lee et al., 2021b), by linking multimodal and -omic studies along the pseudotemporal scale.

Genome-informed microscopy based on metagenomics allows us to localize a putative viral genome in an environmental biofilm of an abundant, carbon fixing archaeon, from a prokaryotic environment (Rahlff et al., 2021). Fluorescence signals of virusFISH indicate a lytic character, but without identification of viral hallmark genes, the targeted virus remains a putative virus and its genome remains uncorrelated to observed virus like particles (Rahlff et al., 2021). CLEM has the potential to bridge the gap between the presence of a putative viral genome and morphological changes of virocells in comparison to ribocells. These morphological traits might correlate with the presence of VLP on or within the virocell and

point out possibilities for label-free multimodal or microscopic *in situ* elucidation virion structure.

Ultimately, non-destructive or *in situ* identification of morphological and biochemical traits can help to characterize and quantify environmental prokaryotic virocells, whose contribution to the global carbon cycle is potentially significant, as the contribution of viruses to the total biomass is underestimated based on the mass of virions instead of accounting virus infected cells, especially virocells, and their effect on the ecosystem.

2.3. Scope of the thesis

This thesis explores microscopic and spectroscopic methods to identify and characterize prokaryotic virocells with single-cell resolution. The potential of imaging-based methods to promote single-cell transcriptomics of prokaryotic systems was assessed in section 2.1. Consecutively, section 2.2 elaborates the rising interest in studying not only virions but also virocells to access the metabolic impact of viral infections on ecosystems and biogeochemical cycles and the potential for imaging-based techniques to do so. To close the gap of knowledge, a laboratory study was conducted first, to evaluate the feasibility of Raman microspectroscopy for label-free identification of individual virocells within a population. Secondly, virusFISH was used for virocell identification within a biofilm and correlated with SEM for further ultrastructural characterization of environmental archaeal virocells.

Identification of biochemical changes in prokaryotic virocells

A non-destructive identification method needs to be available, to work towards an improved and reliable virocell characterization *in situ* and possibly *in vivo*. This facilitates more extensive downstream analyses, like single-cell-omics, and time resolved experiments of virocell maturation from infection to cell lysis.

The manuscript **'Label-Free Raman Microspectroscopy for Identifying Prokaryotic Virocells'** (section 3.1) provides evidence that multivariate data analysis of microbial Raman spectra can extract wavenumbers significantly altered within virocells compared to ribocells of different virus-host systems. A ratio was composed based on these wavenumbers, enabling identification of individual virocells within a population.

Description of morphological changes of environmental virocells

With the availability of an imaging based *in situ* method to identify virocells, established by Rahlff *et al*. (Rahlff et al., 2021), environmental virus-host systems can be

studied via correlative approaches to elucidate morphological changes during proceeding virocell maturation.

The submitted manuscript **'Spatio-functional organization in virocells of small uncultivated archaea from the deep biosphere'** (section 3.2) successfully uses CLEM to quantify the increase of virocell size in comparison to ribocells and to link potential virus like particles to the genomic identity of the respective virus. This allows linking predicted viral genomes to viral structures and virocell morphology, without cultivation of the respective host.

3. Publications

Two articles are incorporated in this quasi-cumulative dissertation. One has been published in mSystems, the other has been revised for The ISME journal, both being peer-reviewed journals, with the PhD student Indra Banas as a first author. The related supplemental information and raw data is supplied on the supporting CD. The structure of the data is listed in section 7.

Declaration of scientific contribution

Indra Banas contributions to the manuscripts are as followed:

1. Monsees, I., Turzynski, V., Esser, S. P., Soares, A., Timmermann, L. I., Weidenbach, K., ... & Probst, A. J. (2022). Label-Free Raman Microspectroscopy for Identifying Prokaryotic Virocells. Msystems, 7(1), e01505-21. Indra Banas designed the experiment, performed most of the measurements and data analyses and prepared the manuscript including most Figures and the supplemental Material. She incorporated the requested revisions.

2. Banas, I. Esser, S. P., Turzynski, V., Soares, A., Novikova, P., May, P., Moraru, C., Hasenberg, M., Wilmes, P., Klingl, A., Probst, A. J. (revised for The ISME journal) 'Spatio-functional organization in virocells of small uncultivated archaea from the deep biosphere'. Indra Banas performed sampling, sample preparation, image acquisition and analyses of the correlative workflow. She wrote the manuscript and prepared the main Figures as well as the majority of supplementary Figures. In addition, she organized the submission of all data to Figshare.

3.1. Label-Free Raman Microspectroscopy for Identifying Prokaryotic Virocells

Indra Monsees,[a] Victoria Turzynski,[a] Sarah P. Esser,[a] André Soares,[a] Lara I. Timmermann,[a] Katrin Weidenbach,[b] Jarno Banas,[e] Michael Kloster,[c] Bánk Beszteri,[c] Ruth A. Schmitz,[b] Alexander J. Probst[a,d]

[a]Group for Aquatic Microbial Ecology, Environmental Microbiology and Biotechnology, University Duisburg-Essen, Essen, Germany
[b]Institute for General Microbiology, Christian Albrechts University, Kiel, Germany
[c]Phycology Group, Faculty of Biology, University Duisburg-Essen, Essen, Germany
[d]Centre of Water and Environmental Research (ZWU), University of Duisburg-Essen, Essen, Germany
[e]Essen, Germany

Editor Joanne B. Emerson, University of California, Davis

Address correspondence to Indra Monsees, Indra.monsees@uni-due.de, or Alexander J. Probst, alexander.probst@uni-due.de.
The authors declare no conflict of interest.
Received 11 January 2022
Accepted 11 January 2022
Published 15 February 2022
[This article was published on 15 February 2022 with an error in Acknowledgments. A name was removed in the current version, posted on 24 February 2022.]

Abstract

Raman microspectroscopy has been used to thoroughly assess growth dynamics and heterogeneity of prokaryotic cells, yet little is known about how the chemistry of individual cells changes during infection with virulent viruses, resulting in so-called virocells. Here, we investigate biochemical changes of bacterial and archaeal cells of three different species in laboratory cultures before and after addition of their respective viruses using single-cell Raman microspectroscopy. By applying multivariate statistics, we identified significant differences in the spectra of single cells with/without addition of virulent dsRNA phage (*phi6*) for *Pseudomonas syringae*. A general ratio of wavenumbers that contributed the greatest differences in the recorded spectra was defined as an indicator for virocells. Based on reference spectra, this difference is likely attributable to an increase in nucleic acid versus protein ratio of virocells. This method also proved successful for identification of *Bacillus subtilis* cells infected with the double-stranded DNA (dsDNA) phage *phi29*, displaying a decrease in respective ratio, but failed for archaeal virocells (*Methanosarcina mazei* with the dsDNA *methanosarcina* spherical virus) due to autofluorescence. Multivariate and univariate analyses suggest that Raman spectral data of infected cells can also be used to explore the complex biology behind viral infections of bacteria. Using this method, we confirmed the previously described two-stage infection of *P. syringae's phi6* and that infection of *B. subtilis* with *phi29* results in a stress response within single cells. We conclude that Raman microspectroscopy is a promising tool for chemical identification of Gram-positive and Gram-negative virocells undergoing infection with virulent DNA or RNA viruses.

Importance

Viruses are highly diverse biological entities shaping many ecosystems across Earth. However, understanding the infection of individual microbial cells and the related biochemical changes remains limited. Using Raman microspectroscopy in conjunction with univariate and multivariate statistics, we established a marker for identification of infected Gram-positive and Gram-negative bacteria. This nondestructive, label-free analytical method at single-cell resolution paves the way for future studies geared towards analyzing virus-host systems of prokaryotes to further understand the complex chemistry and function of virocells.

Keywords bacteriophage, phage, phi29, phi6, virus

Introduction

Viruses substantially influence global ecosystems and biogeochemical cycles by infecting host populations. Predation can cause release of organic carbon and also enhance horizontal gene transfer (Rohwer et al., 2009), as viruses can act as mobile genetic elements (MGEs). Those viruses that infect bacteria have the specific denotation bacteriophages, or just phages (Ackermann, 2003, p. 19). Viruses are generally differentiated based on the type of genetic information stored in their viral particle, either single- or double-stranded DNA (dsDNA) or RNA (Baltimore, 1971). Prokaryotic viruses are also categorized based on their reproduction cycle as lysogenic or lytic (although other strategies, like chronic infection or pseudolysogeny, have been reported infrequently (Hobbs and Abedon, 2016)). Viruses can insert their genome into the plasmid or genome of an infected host and proliferate along with host reproduction (lysogeny). A lytic strategy involves the reorganization of host metabolism envisaging reproduction of virions and, ultimately, cell lysis. A host cell infected with a virulent virus is referred to as a virocell and needs to be differentiated from ribocells, cells that generally proliferate irrespective of an infection (Forterre, 2013). In a recent study, transcriptomics and proteomics were used to investigate whether metabolic differences between uninfected cells and virocells can impact an entire ecosystem (Howard-Varona et al., 2020). However, the study of virocells generally necessitates nondestructive techniques that can capture virocell characteristics at the single-cell level prior to cell lysis.

The development of confocal Raman microspectroscopy has enabled the measurement of single microbial cells (Puppels et al., 1990), which consequently opened the possibility to gain insights into the heterogeneity of microbial communities (Schuster et al., 2000). The combination of Raman microspectroscopy instruments with multivariate data analysis of digitally recorded spectra allowed for further increases in sensitivity in the last 2 decades, resulting in the detection of biochemical differences between bacterial species across growth phases (Huang et al., 2004). In this context, multivariate statistical analysis of Raman spectra has been used to differentiate single cells based on discrete wavenumbers corresponding to biochemical compounds. Huang and colleagues described a correlation between the fraction of ^{13}C in the carbon source and a ratio shift based on Raman peaks of unlabeled [^{12}C] phenylalanine and ^{13}C-labeled phenylalanine (Huang et al., 2007). The ratio between isotopically labeled and unlabeled molecules can be applied to identify key degraders in mixed cultures and allows specific cell sorting for single-cell methods (Lee et al., 2019).

However, this sensitivity is also the bottleneck of this technique, as demonstrated by García-Timermans *et al.*, who highlighted the influence of the sample preparation on the recorded spectra (García-Timermans et al., 2018). Such differences complicate the construction of a public database and comparability of spectra across studies. Nevertheless, the comparison of selected wavenumbers between individual spectra of a single study is crucial for expeditious categorization of single cells based on their chemical composition.

In this study, the high sensitivity of Raman microspectroscopy to identify and characterize microstructural intracellular changes as well as viruses and their effects on host metabolism was used to test the suitability of this technology for differentiating uninfected cells from virocells (Figure 3.1). To this end, three different model host-virus systems, including virulent DNA and RNA viruses, were used to analyze and monitor chemical changes during infection at the single-cell level using Raman microspectroscopy.

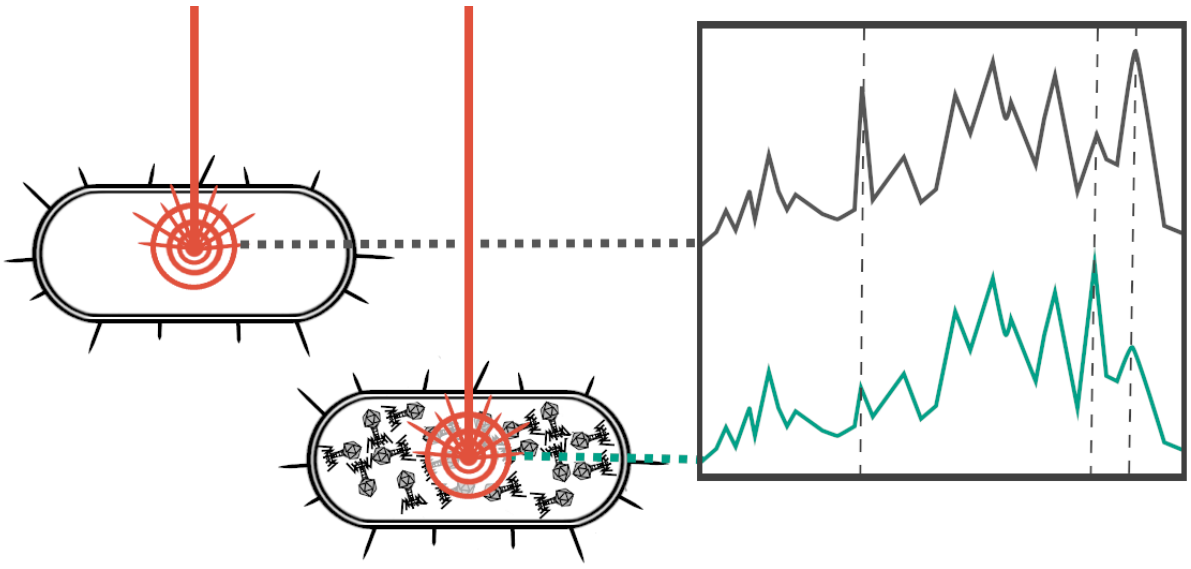

Figure 3.1 | Conceptual figure for the study. Laser of the Raman microspectroscope is focused on a single microbial cell. The presence of virions replicated inside the cell alters the Raman spectrum, especially in the determined areas. Virocells can be determined by calculation of a ratio based on these intensities.

Results

Significant differences in the chemical composition of infected and uninfected cultures of *P. syringae*. For establishing the differences between virocells and noninfected cells, we used the well-known virus host system of *P. syringae* (Gram-negative) and its phage, *phi6* (Xin et al., 2018). *phi6* has already been studied via Raman microspectroscopy in past decades but never in association with its host (Benevides et al., 1997). *phi6* is a double-stranded RNA (dsRNA) phage of the order *Mindivirales* (Laurinavičius et al., 2004; Mönttinen et al., 2021), and its maturation is described to take place in two steps (Bamford et al., 1976). Addition of *phi6* to *P. syringae* cultures resulted in the expected decline in optical density, enabling us to harvest cell populations representing a mixture of virocells and uninfected cells (Figure 3.2 A). We used this cell population and a culture without phage addition for comparison in single-cell Raman microspectroscopy. In doing so, we successfully measured 448 high-quality spectra of individual *P. syringae* cells, of which 198 cells were measured after addition of *phi6*. The other 250 spectra were reference spectra from uninfected cells of *P. syringae*. Inspection of the spectra and comparison to previously published Raman spectra of bacteria confirmed the typically expected peaks for biomolecules, confirming the measurement of actual microbial cells (Huang et al., 2004).

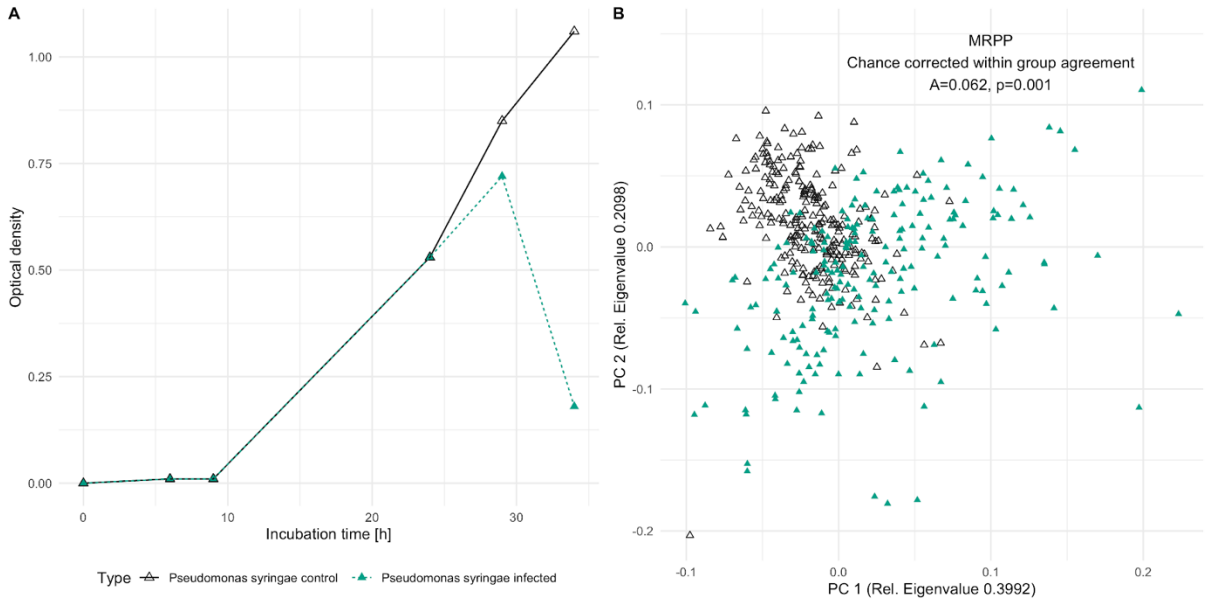

Figure 3.2 | *Pseudomonas syringae* cultures with (green, filled triangles) and without (black, empty triangles) addition of phage *phi6* after 24 h. (A) Growth curve determined by optical density. The drop in optical density corresponds to phage-mediated cell lysis after 34 h. **(B)** Principal component analyses of *P. syringae* single-cell Raman spectra after lysis (after 34 h) (ordination analyses based on Euclidean distance and spectral contrast angle revealed nearly identical results; see Fig. S1) and the result of the MRPP for control sample versus infected sample.

Using the individual spectra of each measured cell, we computed an ordination analysis comparing individual cells of cultures with and without phage addition, which showed substantial differences (Figure 3.2 B). Importantly, the two data sets (with and without phage addition) were not entirely separated along principal component 1 (PC 1) or PC 2 but showed differences along both PCs, which agrees with the above-mentioned mixture of virocells and uninfected cells in populations after phage addition. To test the observed differences for significance, a multiresponse permutation procedure (MRPP) was applied, because in addition to the *P* value for significance, it provides chance-corrected within-group agreement (A), which displays the difference between the groups (Kattenborn et al., 2019; Mielke, 1991). MRPP analysis displayed a highly significant *P* value (<0.001), with a chance-corrected within group agreement of 0.062. Consequently, phage addition and infection showed a significant and substantial change in the (bio)chemical composition of individual cells resulting in virocells.

To challenge the results of the observed differences between cultures with and without phage addition, we applied the abovementioned multivariate analysis to two different time points of the same uninfected culture of *P. syringae*. This experiment was set out with the aim of testing the null hypothesis that the differences between infected and noninfected cultures originates from variation during growth phases of cultures, which is known to exist in bacteria (Huang et al., 2004). The respective PCA (see Fig. S2 in the supplemental material), which also includes data from the infected cell culture, displays a difference of two time points along PC 2. However, the intragroup dissimilarity of the two individual time points was substantially lower than that for the population infected with phage, particularly along the major component of the PCA. Although the MRPP testing for differences between the uninfected cultures at the two time points resulted in a significant *P* value (0.002), the chance-corrected within-group agreement was less than a sixth (0.009) of those identified for differences between cultures with and without phage addition. Moreover, comparing the combination of both time points of the uninfected culture to one with phage addition, we identified a highly significant difference (MRPP, $P < 0.001$, $A = 0.06$). Based on these observations the null hypothesis was rejected, supporting the working hypothesis that uninfected cultures can be distinguished from cultures with virocells using Raman spectroscopy.

Differentiating wavenumbers of uninfected cells and virocells are attributable to nucleic acid and protein Raman shifts in *P. syringae*. To investigate the exact differences between cultures with and without phage addition as displayed in the PCA (Figure 3.2 B), we used the system of *P. syringae-phi6* for an in-depth statistical analysis. Comparing the contrast plot of phage-infected and noninfected cultures with the major two components of the PCA highlighted the contribution of the individual wavenumbers that discriminate the two groups (cultures with and without phage addition) (Figure 3.3 A). Six wavenumbers were identified as local maxima/minima displaying the differences between the average spectra of the two groups with a high contribution to the PCA or a high density at the contrast plots, and these are assigned to their respective biomolecules in Table 3.1.

Table 3.1 | Wavenumbers assigned to biomolecules of microbial cells and their density in the contrast plots of infected and uninfected cells.

	Density[a] of:		
Wavenumber (1/cm)	***P. syringae***	***B. subtilis***	**Peak assignment (Benevides et al., 2003, 1997, 1996; De Gelder et al., 2007)**
623	-0.0103	0.0000	623 adenine
645	-0.0047	0.0003	645 cytosine, adenine
669	0.0139	0.0066	668 guanine
726	0.0031	0.0180	723/724 adenine
748	-0.0094	-0.0154	740 thymine
784	0.0634	0.03444	785 cytosine/ uracil
855	-0.0399	0.0049	848 ribose /O-P-O stretch
902	-0.0471	-0.0042	Various metabolites
961	-0.0598	0.0006	960 valine/leucine
1005	**-0.1428**	**0.0020**	**1004 Phenylalanine**
1034	-0.0626	0.0014	1035 proteins/ 1034 Phosphoenolpyruvate
1096	-0.0084	0.0078	1101 PO_2^-
1175	-0.0207	-0.0035	1174 L-histidine
1241	-0.0018	0.0189	1230- 1310 amide III interval, 1240 uracil
1336	0.0442	0.0072	1337 adenine
1452	-0.0466	-0.0090	1440 lipids
1482	0.0922	0.0346	1482 guanine/adenine
1577	**0.1333**	**-0.0207**	**1573 adenine, guanine**
1671	**-0.1031**	**0.0397**	**1640-1680 amide, 11671 thymine**

[a]A high positive density refers to prominence in infected cells, and a negative value refers to wavenumbers more prominent in the control sample. Boldface indicates wavenumbers chosen for calculating the ratio for differentiating virocells from uninfected cells.

Three of the wavenumbers with the highest density in the contrast plot were assigned to nucleic acids (785, 1,483, and 1,576 1/cm), of which one was significantly higher in cultures infected with phage based on a Wilcoxon test ($P_{785} = 0.15$, $P_{1483} = 0.71$, $P_{1576} = 2.2 \cdot 10^{-16}$, respectively). In contrast, peaks assigned to proteins (1,003 and 1,671 1/cm) and lipids (1,448 1/cm) are more prominent in the control sample, and the corresponding *P* values of

the proteins were significant (Wilcoxon test, $P_{1003} = 1.7 \cdot 10^{-15}$, $P_{1671} = 2.2 \cdot 10^{-16}$, $P_{1448} = 0.71$, respectively). It is noteworthy that the wavenumbers associated with (highly) significant changes (1,003, 1,576, and 1,671 1/cm) contributed to PC 1, while the other three with insignificant changes between phage infected and noninfected contributed more to PC 2 (785, 1,440, and 1,483 1/cm) (Figure 3.3 A). The intensities (I) of three wavenumbers with significant *P* values were used to determine a differentiator for univariate differentiation of *P. syringae* virocells from uninfected cells (Equation 3.1):

$$\mathrm{Ratio}_{\mathrm{virocell}} = \frac{\text{Nucleic acids}}{\text{Proteins}} = \frac{\mathrm{I}_{1576} \times 2}{\mathrm{I}_{1003} \times \mathrm{I}_{1671}} \tag{3.1}$$

with wavenumbers assigned to proteins (1,003 and 1,671 1/cm) in the denominator and the nucleic acid peak (1,576 1/cm) in the numerator. The Shapiro test demonstrated that the ratios based on spectra of the control sample based on Equation 3.1 were normally distributed ($P = 0.07$) and those of the infected sample were not ($P = 5.99 \cdot 10^{-9}$), which was expected since the latter represent a mixture of virocells and uninfected cells. The calculated confidence intervals indicate that *P. syringae* cells of the control group do not exceed a ratio above 1.06 (99% probability), while this threshold was indeed exceeded (with a probability of 45%, 66 of 198 cells) in the sample after phage addition. Consequently, Equation 3.1 can be used to identify potential virocells in cultures of *P. syringae* (Figure 3.3 C).

Validation of selected wavenumbers for virocell identification of *P. syringae* via VIP of the OPLS analysis model indicates high influence by peak shoulders. The average Raman spectra of the control sample and the infected sample show clear differences in the intensity of prominent biomolecule peaks chosen for the ratio determination (Figure 3.3 B). However, plotting the peak maxima of the variable importance on projection (VIP) of the orthogonal partial least square model (OPLS) together with the average Raman spectra revealed that the differences in virocells are sometimes not only represented by the maximum of the peak but also by its shoulders. This is a fine detail that is overseen by just visually inspecting the average spectra. The peaks can be assigned to their biomolecular origin (chemical bond) since their position does not change with a change in the molecular environment. However, the width of the peak is dependent on the composition of the molecule surrounding the polarized bond (Thomas, 1999). Although the intensity change cannot be determined between two groups, this approach confirms the selected wavenumbers for the determined ratio for virocell identification in *P. syringae.*

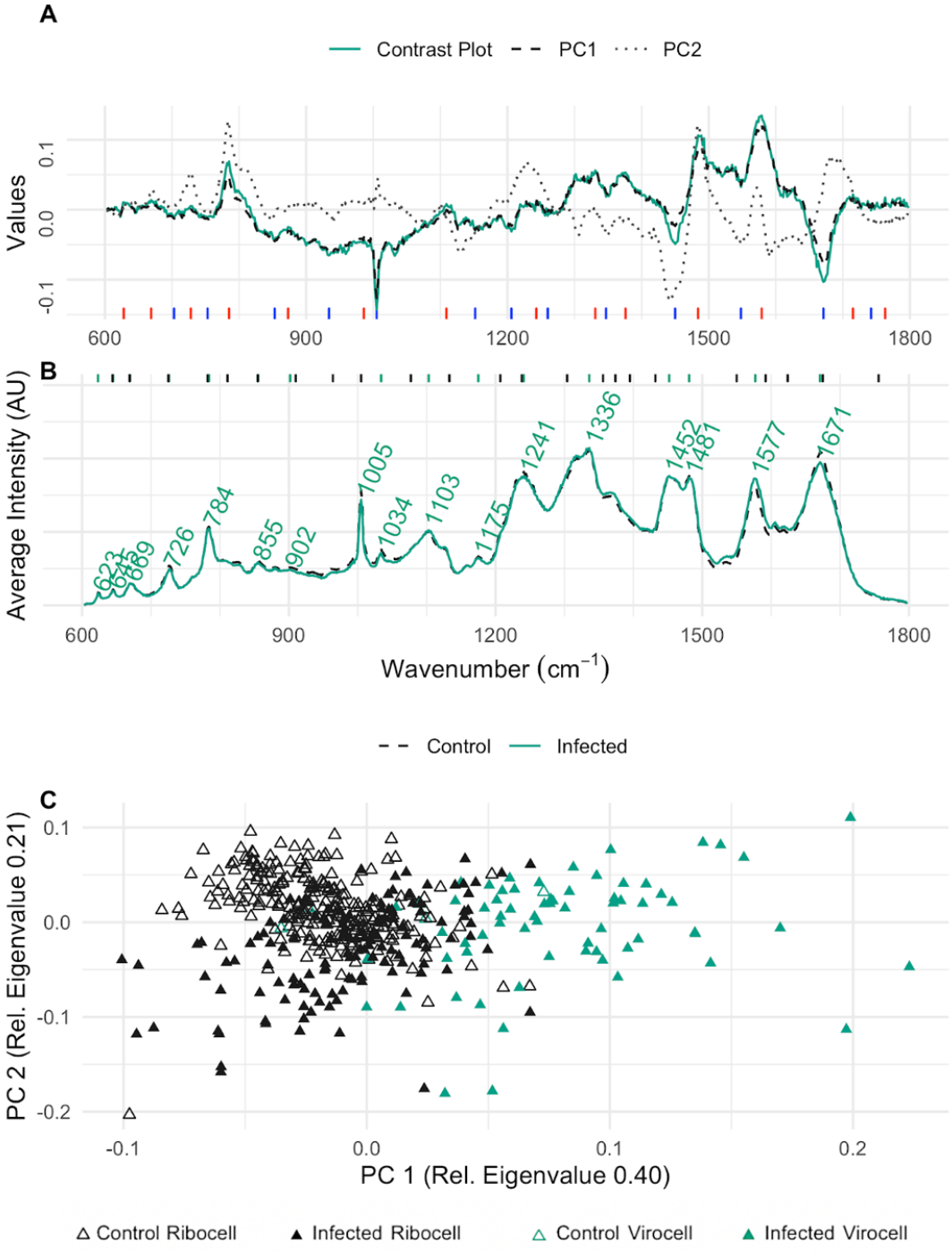

Figure 3.3 | Evaluation of wavenumbers for virocell identification in *P. syringae*. (A) Contrast plot (green) of potential infected cells compared to the wavenumber influence on PC 1 (black, dashed) and PC 2 (gray, line dotted). Blue lines at the bottom indicate wavenumbers that decreased in virocells, and red lines indicate wavenumbers increasing in virocells. **(B)** Average Raman spectra of the samples with (green, solid) and without (black, dashed) phage addition. Green lines at the top indicate the positions of the labeled peaks in the Raman spectra, and black lines indicate peak maxima of the variable importance on projection of the orthogonal partial least-square model. **(C)** PCA of single-cell Raman spectra from infected cultures (filled triangle) and cultures without phage addition (empty triangle); virocells identified based on the determined ratio are shown as filled triangles in green.

Applicability of virocell identification across three different species. Based on the differentiating ratio determined for virocells and uninfected cells of *P. syringae* (Equation 3.1), we tested its applicability to other microbial species by repeating the analysis performed with *P. syringae-phi6* for *B. subtilis-phi29* and *M. mazei-methanosarcina* spherical virus (MetSV). We calculated the ratios (Equation 3.1) for cultures with and without virus addition, which showed a significant difference for *P. syringae* and *B. subtilis* ($P < 0.0001$) (Figure 3.4). By contrast, only a trend was revealed for the *M. mazei*-MetSV system ($P < 0.0649$) (Figure 3.4) without visible differences in PCA and contrast plot analysis (Fig. S3).

As a model system for Gram-positive bacteria, *Bacillus subtilis* was chosen as a representative, as it is a well-studied model organism with its dsDNA phage *phi29* of the order *Caudovirales*, which is among the smallest known dsDNA phages (Meijer et al., 2001). For the *B. subtilis-phi29* system, a group of potential virocells could be differentiated from the control sample along PC 2 (Figure 3.5 C), yet the contrast plot (Figure 3.5 A) shows a lower density range than the one for *P. syringae* (Figure 3.3 A). The highest values contributing to spectra of infected cells were associated with nucleic acids and proteins (Wilcoxon test, $P_{785} = 3.4 \cdot 10^{-11}$, $P_{1483} = 3.0 \cdot 10^{-12}$, $P_{1003} = 0.15$, and $P_{1671} = 9.5 \cdot 10^{-12}$), while peaks with the wavenumbers for hydrocarbons and nucleic acids were enriched in uninfected cells ($P_{1131} = 1.7 \cdot 10^{-8}$, $P_{1550} < 2.2 \cdot 10^{-16}$, and $P_{1589} < 2.2 \cdot 10^{-16}$). Importantly, these identified wavenumbers included the same wavenumbers that were determined for the ratio (Equation 3.1) for *P. syringae*. Although the associated signals of biomolecules were inverted compared to those for *P. syringae*, *i.e.*, proteins were substantially higher in designated virocells and nucleic acids declined, the respective ratio (Equation 3.1) can still be used to identify potential virocells of *B. subtilis* in Raman spectroscopy (Figure 3.5).

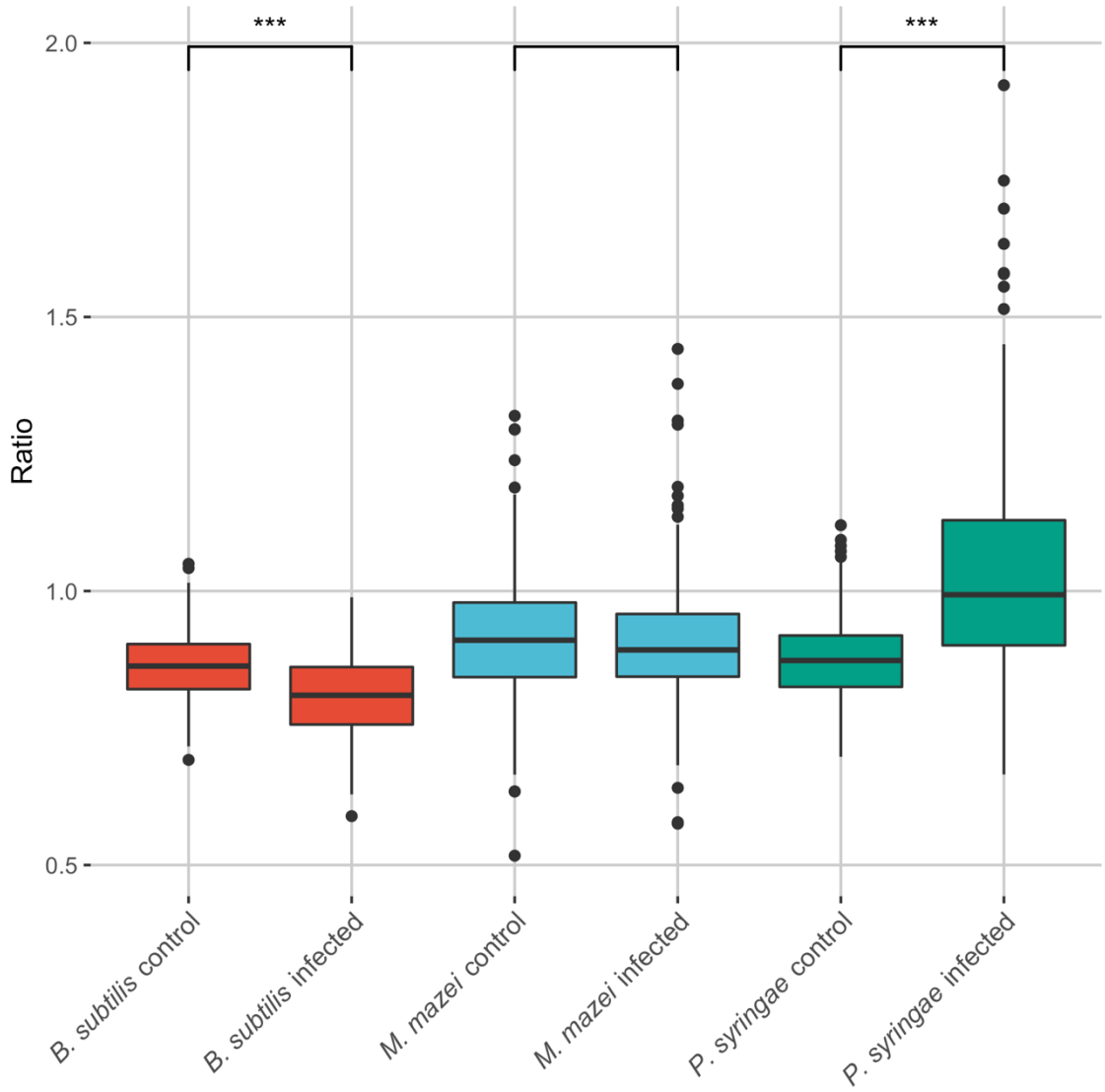

Figure 3.4 | Boxplot of the determined ratio for control (no virus addition) and infected (with virus addition) samples of *B. subtilis* (red), *M. mazei* (blue), and *P. syringae* (green). Asterisks indicate significance according to Wilcoxon test (***, highly significant, $P < 0.0001$; no asterisk, not significant, $P < 0.06$). For the exact number of spectra per sample see Table S1, and for a detailed multiple comparison across species (based on Dunn's test) see Table S2.

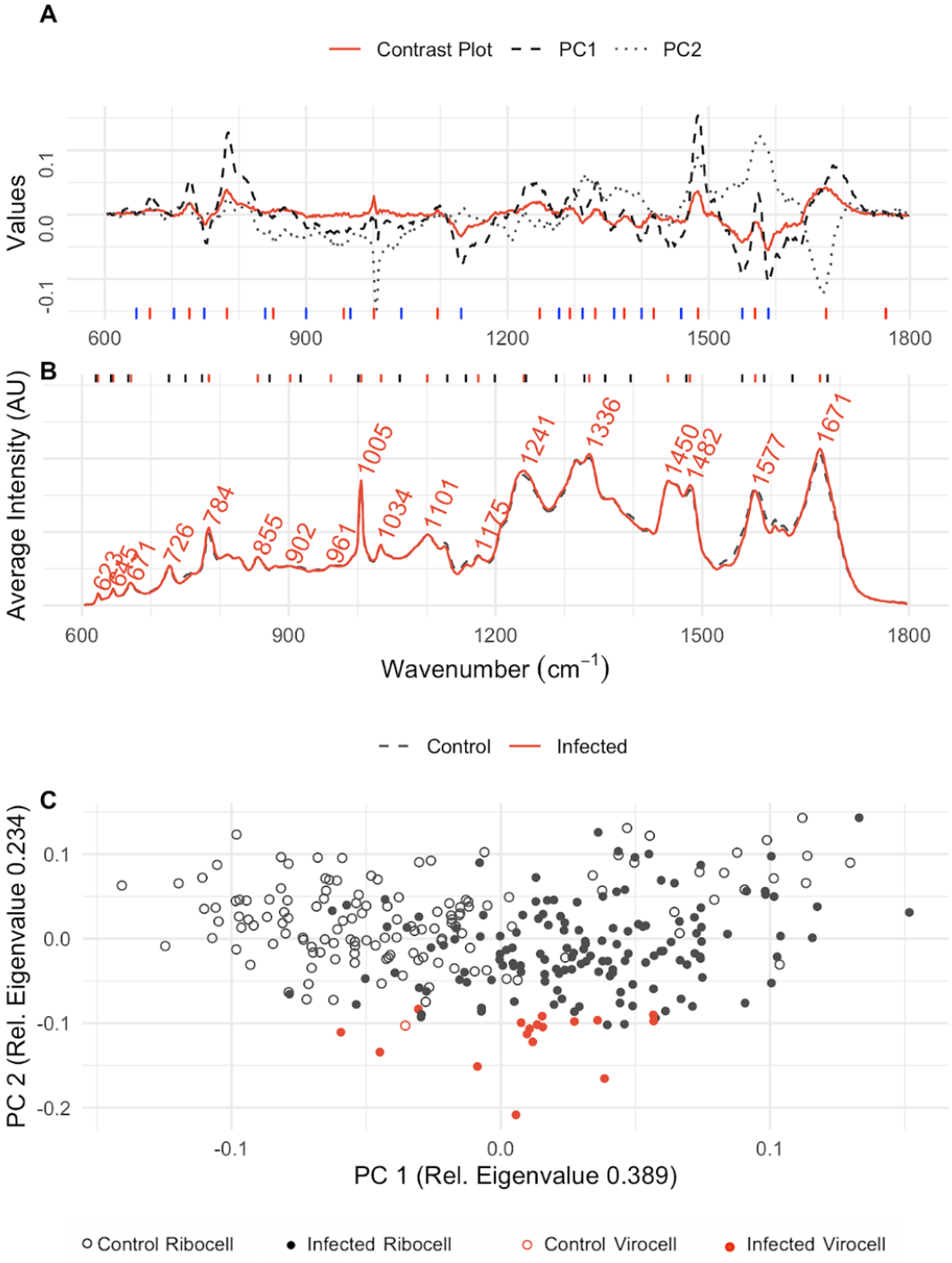

Figure 3.5 | Evaluation of wavenumbers for virocell identification in *B. subtilis*. (A) Contrast plot (red) of potential infected cells compared to the wavenumber influence on PC 1 (black, dashed) and PC 2 (gray, dotted). Long, blue lines at the bottom indicate wavenumbers that decrease in virocells, and red lines indicate wavenumbers increasing in virocells. **(B)** Average Raman spectra of the samples with (red, solid) and without phage (black, dashed) addition. Red lines at the top indicate the positions of the labeled peaks in the Raman spectra, and black lines indicate peaks of the OPLS importance. **(C)** PCA of single-cell Raman spectra from infected cultures (filled dots) and cultures without phage addition (empty dots); virocells identified based on the determined ratio are shown as filled dots in red.

As an archaeal system, we chose the anaerobic methane producer *Methanosarcina mazei* and its first identified and isolated virus, MetSV, which is classified as a dsDNA virus (Weidenbach et al., 2017). The PCA of *M. mazei* is presented in Fig. S3. In contrast to the bacterial systems, no difference between the control and infected cultures was observed. For instance, the chance-corrected within-group agreement of these cultures was lower than the chance-corrected within-group agreement across uninfected Pseudomonas cultures (after 24 h), displaying little variance in the spectra of ribocells and virocells of *M. mazei* (A = 0.006872 for *M. mazei*, A = 0.009298 for *P. syringae*). During spectral acquisition of *M. mazei* cells, the raw spectra displayed a high background signal. This background signal was associated with autofluorescence of the methanogen, since it could be reduced by applying laser bleaching (30 s). This led to a higher dispersion of individual spectra of the same sample in ordination analysis. Figure S4 displays the dispersion of the archaeal sample set compared to the bacterial data sets. The bleaching time reduced the dispersion but was insufficient for enabling a differentiation between infected and noninfected samples.

Discussion

In this work, we measured several hundred individual bacterial and archaeal cells (see Fig. S4 in the supplemental material) to identify common changes in Raman spectra due to viral infections. One major challenge associated with measuring cultures of infected cells was their heterogeneity, meaning the culture consisting of uninfected cells and virocells at the same time. However, we were able to identify a specific ratio of Raman spectra that allowed us to differentiate virocells and ribocells in the cultures of *P. syringae* and *B. subtilis*. This ratio was based on the wavenumbers 1,003, 1,576, and 1,671 1/cm, which can be assigned to proteins and nucleic acid changes based on existing literature of recoded Raman spectra (Benevides et al., 1997; De Gelder et al., 2007).

Overcoming challenges in identifying a Raman spectrum-based marker for virocells. For identification of a Raman spectrum-based marker of virocells, it was mandatory to use univariate and multivariate statistics in concert. Neither univariate nor multivariate statistics alone were successful in identifying the respective wavenumbers necessary for the differentiation of virocells from uninfected cells.

To initially identify a set of wavenumbers that showed differences between these two cell types, we applied a multivariate analysis, resulting in six wavenumbers, which were further filtered based on a Wilcoxon test to create the respective equation for differentiation of the two cell types. This was partly because multiple PCs can contribute to differences in

statistical populations at various intensities, while we focused only on the two PCs with the greatest eigenvalues. Two peaks contributing substantially to PC 2 of both bacteria studied here are assigned to guanine (1,483 1/cm) (De Gelder et al., 2007) and the ring breathing of cytosine and uracil (785 1/cm) (Benevides et al., 1997). Although this suggests a strong involvement of nucleic acid changes in uninfected versus virocells, the Wilcoxon test did not indicate a significant difference demonstrating an insufficient picture provided by multivariate data analysis (MRPP). On the other hand, using univariate statistics alone, the highest differences for the populations of *B. subtilis* did not occur at the maximum of the peak (1,579 1/cm), which we determined from using both methods. Instead, the contrast plot had the highest values at the shoulders of the maximum peak, at 1,550 1/cm and 1,589 1/cm, suggesting that the peak position must be considered in Raman spectra via multivariate statistics. The reason for this phenomenon of the breadth of the peak can be traced back to the chemical environment of the molecule, as the Raman shift is characteristic for the polarized chemical bond (Benevides et al., 1996; Prescott et al., 1985; Thomas, 1999). Several studies about differences of Raman spectra of packed and unpacked viral DNA/ RNA and protein/oligonucleotide interactions have been performed in the past and describe altered base environments as the reason for the observation of such perturbations (Benevides et al., 1996; Prescott et al., 1985; Thomas, 1999).

***phi29* likely causes a stress response in *B. subtilis*.** The determined equation for differentiating virocells from ribocells in the *P. syringae-phi6* system could also be applied to the *B. subtilis-phi29* system. However, the ratio used for the differentiation was significantly lower in the *B. subtilis* system, which is in stark contrast to the significantly higher ratio for *P. syringae*. The respective wavenumbers attributable to proteins (1,003 and 1,671 1/cm) showed an increase in intensity in *B. subtilis*, and nucleic acids (1,576 1/cm) appeared to decrease substantially during infection with *phi29*. A drop in nucleic acid content and increase in protein content (as observed here for virocells of *B. subtilis*) is complementary to multiple biological processes that can be observed for bacteria. Chemicals like ethanol can cause a similar change in the protein and nucleic acid content, which represents a stress response by the bacterium. This stress response was detected based on the same changes in the wavenumbers as those observed here (Teng et al., 2016). However, the induction of temperate phage in *B. subtilis* was shown to result in a decrease of the Raman shifts at 782 and 1,095 1/cm and only a slight decrease at 1,452 and 1,659 1/cm (Wu et al., 2020). The

authors of the aforementioned study concluded that these measurements likely stem from the fact that the measured cell had ruptured and an empty cellular hull had been measured (consisting of proteins and lipids, while nucleic acids are lost during lysis). They used Raman shifts around 1,095 1/cm and 785 1/cm to measure the respective differences in the nucleic acid, neither of which showed a significant difference in our data sets. Comparing these previous findings to our results for *B. subtilis*, some likely cannot differentiate between *B. subtilis* cells showing a stress response and a respective virocell. We conclude that *phi29* causes a stress response in *B. subtilis* during infection, which we measured during Raman spectra acquisition.

High sensitivity of Raman spectra mirrors different types of phage infection. The changes in nucleic acid and protein content are contradictory in the *P. syringae* and the *B. subtilis* system and could not be attributed solely to complex stress responses but rather to different types of phages. While *phi6* infecting *P. syringae* is a nontailed RNA phage with a lipid membrane (Laurinavičius et al., 2004; Vidaver et al., 1973), *phi29* is a DNA phage with a complex polypeptide structure consisting of a phage head and a phage tail (Hemphill and Whiteley, 1975). Consequently, an increase in the protein content during *phi29* replication can be associated with an increase in protein content in the cell. The wavenumber 1,671 1/cm was previously associated not only with the amides but also with thymine, a central component of DNA but not RNA (Table 3.1). Comparing the RNA phage *phi6* and the DNA phage *phi29*, we did observe a difference at the thymine concentration at this wavelength. A similar trend (increase in thymine/protein concentration) was also observed for the *M. mazei* system, which is also based on a DNA virus. We conclude that the putative increase of proteins measured at 1,671 1/cm stems from an increase in protein and thymine concentration at the same time, reflecting the difference in DNA and RNA phage used in the experiments.

Beyond the different types of phages, the relatively slow maturation of the *phi6* virions usually encompasses two different stages within the *P. syringae* host. After 45 min, 50 nm particles can be observed within the host, and after 80 min these particles are covered by the viral membrane (Bamford et al., 1976). The plot of the PCA in Figure 3.2 shows that infected cultures of *P. syringae* differed along both components. Component one was used for the ratio determination, but the ratio did not include spectra of individual virocells that showed a difference along component two. The shift of these virocells along PC2 was associated with a single wavenumber at 1,448 1/cm. This wavenumber indicates an increase of lipids, which

agrees with the production of lipid membranes for viral particle maturation (Bamford et al., 1976). Consequently, we succeeded not only in identification of virocells of *P. syringae* but also in distinguishing the two infection stages during *phi6* maturation based on our Raman spectra.

Conclusions. Our data, encompassing 1,287 Raman spectra acquired for individual cells of three different microbial species with and without virus addition, suggest that at least bacterial virocells can be differentiated from uninfected cells. We present a ratio of three wavenumbers that can be utilized to quickly perform this differentiation, although the type of phage (RNA versus DNA) and different infection stages can influence the detection. Beyond detection, Raman spectra of individual cells are sensitive enough to capture essential information on the biology of individual phage-host systems. Namely, DNA and RNA phages and stress responses to the differentiation of maturation stages of phages within the microbial host cell can be robustly identified. We predict that the identification of such cells in batch culture experiments and ultimately in environmental samples will aid studying the biology of individual virocells and, thus, expand our understanding of the complex interplay of phages and hosts along with their associated biochemistry.

Materials and methods

Cultivation of model systems and sampling strategy. Two cultures of *Pseudomonas syringae* (DSM21482) were incubated at 25°C with 150 rpm in tryptone soya broth (DSM medium 545). After 24 h, the cultures reached the exponential growth phase; 1 vol% glycerol stock of the phage *phi6* (DSM21518) was added to one culture, and the second culture was kept uninfected as a negative control. Samples for Raman microspectroscopy were taken prior to phage addition and 10 h after infection, indicated by a drop of the optical density (OD).

Bacillus subtilis (DSM5547) was incubated at 37°C with 150 rpm in DSM medium 545. After 4 h, the cultures reached the exponential growth phase, and 10 vol% of a phage *phi29* solution (DSM5546) was added to one culture; the second culture was kept uninfected as a control. The shaking was reduced to 80 rpm. Samples for Raman microspectroscopy were taken when the optical density dropped 2 h after infection (see Fig. S5 in the supplemental material).

Methanosarcina mazei (DSM3647) was grown in minimal medium under anaerobic conditions with an N_2-CO2 (80:20) atmosphere in closed serum bottles without shaking at 37°C. As energy and carbon sources, 150 mM methanol and 40 mM acetate were added.

Furthermore, medium was supplemented with 2 mM cysteine and 1 mM sodium sulfide as described previously (Deppenmeier et al., 1990; Ehlers et al., 2002). When the sample reached turbidity at an OD at 600 nm (OD_{600}) of approximately 0.2, cultures were infected with 1% filtrated MetSV lysate (Weidenbach et al., 2017). Samples for Raman spectroscopy were taken anaerobically before and 180 min and 210 min after infection.

Sample preparation for Raman microspectroscopy. Samples for Raman microspectroscopy were taken at respective time points from the model systems (described above); 1 ml of the culture was washed with 1 ml 1X phosphate-buffered saline (PBS; pH 7.4; Sigma-Aldrich), followed by resuspension in 0.45 ml 1X PBS and 0.15 ml 4% formaldehyde (Thermo Scientific) solution (fixation at 4°C for 3 h). Afterwards the sample was again washed in 0.5 ml 1X PBS and dehydrated at room temperature in 50 vol% and 80 vol% ethanol (Fisher Scientific) for 10 min each. Finally, the preparation was stored in 0.15 ml 96% ethanol at -20°C until spectral acquisition. Throughout all steps mentioned above, washing was done by pelleting of samples via centrifugation at 2,000 X g for 10 min, followed by discarding the supernatant.

Raman spectral acquisition. Raman spectral acquisition was performed using a Renishaw in via a Raman microspectroscope with a 532-nm Nd:YAG laser and 1,800-l/mm grating equipped with a Leica DM2700M microscope. A 100X dry objective with a numerical aperture of 0.85 was used. Daily calibration was performed using a silicon wafer (Renishaw). For each dehydrated sample (preparation as described above), a drop was placed on a highly polished steel slide (Renishaw) and air dried. Figure S6 displays the even distribution of cells on the slide. For *Pseudomonas syringae*, a spectral acquisition of 25 to 30 s at 10% laser power was used, and for *Bacillus subtilis*, three accumulations of 25 s and 5% laser power were used. For cells of *Methanosarcina mazei,* a 15 s bleaching step prior to 30 s measurement at 5% laser power was necessary to reduce the florescent background. At least 50 cells per drop were measured, and at minimum three drops per sample were used.

Multivariate statistical analyses. The spectra were imported to R (Team, 2018) as SPC files and processed using the R package *MicroRaman* (García-Timermans et al., 2018). The spectral data were trimmed to a range of 600 to 1,800 1/cm. After background subtraction using the statistics-sensitive nonlinear iterative peak-clipping (SNIP) algorithm (Ryan et al., 1988), data were normalized using total ion current (TIC) (Gibb and Strimmer, 2012). These preprocessed data were used to calculate principal component analyses (PCA) (Oksanen et al., 2013) and dendrograms based on Euclidian distance (Ward D2 clustering) (Team, 2018). PCA results were

compared to principal coordinate analyses (Paradis and Schliep, 2019) based on spectral contrast angle dissimilarities (García-Timermans et al., 2018). Spectra of cells burnt during spectral acquisition, spectra of low intensity, and those containing cosmic rays were identified and removed from the data set. Wavenumbers causing differences between infected and uninfected spectra were identified using a contrast plot (García-Timermans et al., 2018) and the influence on the principal components. Differences between the samples were assessed via a multiresponse permutation procedure (MRPP) using 999 Monte Carlo permutations (Kattenborn et al., 2019; Mielke, 1991).

An orthogonal partial least square analysis (OPLS) (Thévenot et al., 2015) was performed on the baseline-corrected data. The spectra were divided into "Species_control" or "Species_infected" according to the sample their originated from. The variable importance on projection (VIP) for each wavenumber in the range of 600 to 1,800 1/cm was determined and compared with the density of the contrast plot and the principal components.

The mean spectrum of each class was calculated by determining the mean intensity at each wavenumber.

Determination of differentiating ratio of virocells and uninfected cells. Different combinations of the intensities of the three wavenumbers with the most influence in the contrast plots (contrasting virocells and uninfected cells) of the *P. syringae-phi6* system were further analyzed. The average intensities and the standard deviations were calculated for the normalized data of the uninfected cells and potential virocells. A Shapiro test for normal distribution then was performed, and a Wilcoxon test for nonnormally distributed data was used to test if the data from infected and uninfected cells show a significant difference. For each ratio, a cutoff value was defined to declare a cell was infected. The 99% confidence interval was calculated for the infected group and the control group, and afterwards the number of false-positive spectra inside the control group was determined. The results derived from the *P. syringae-phi6* system for identification of differentiating wavenumbers was then applied to the other virus-host systems and a Dunn's test was performed to differentiate between host type coupled to infected/ uninfected cultures (https://github.com/cran/dunn.test) (Dinno and Dinno, 2017).

To identify the respective Raman spectra and relate them to biomolecules, we followed various publications by G. J. Thomas and coworkers, which resulted in a collection of Raman spectra of nucleic acids and proteins (Benevides et al., 1997), and De Gelder *et al*. (De

Gelder et al., 2007), who conducted a study on pure solutions of biomolecules. The assignments are summarized in Table 3.1.

Supplemental material

The supplemental material is available online under:
https://journals.asm.org/doi/full/10.1128/msystems.01505-21 as well as Supporting data I on the CD.

FIG S1, TIF file, 15.6 MB. FIG S2, TIF file, 7.8 MB. FIG S3, TIF file, 15.6 MB. FIG S4, TIF file, 7.8 MB. FIG S5, TIF file, 6.7 MB. FIG S6, JPG file, 0.1 MB.

TABLE S1, PDF file, 0.03 MB. TABLE S2, PDF file, 0.1 MB. TABLE S3, PDF file, 0.02 MB.

Acknowledgments

This work was funded by German Research Foundation (DFG grant PR1603/2-1). I.M. was supported by the German Academic Scholarship Foundation, and A.J.P. acknowledges funding by the Ministry of Culture and Science of North Rhine-Westphalia (Nachwuchsgruppe “Dr. Alexander Probst”). We acknowledge support by the Open Access Publication Fund of the University of Duisburg-Essen. We thank Sabrina Eisfeld and Agathe Materla for lab management and technical assistance. Priyanka Mishra and Rainer Meckenstock are acknowledged for support with the Raman microspectroscope. We declare no conflict of interest.

3.2. Spatio-functional organization in virocells of small uncultivated archaea from the deep biosphere

Indra Banas[1], Sarah P. Esser[1], Victoria Turzynski[1], André Soares[1], Polina Novikova[2], Patrick May[2], Cristina Moraru[3], Mike Hasenberg[4], Paul Wilmes[2,5], Andreas Klingl[6]*, and Alexander J. Probst[1,7]*

[1] Environmental Metagenomics, Research Center One Health Ruhr of the University Alliance Ruhr, Faculty of Chemistry, University of Duisburg-Essen

[2] Luxembourg Centre for Systems Biomedicine, University of Luxembourg, Esch-sur-Alzette, Luxembourg

[3]Institute for Chemistry and Biology of the Marine Environment (ICBM), Carl-von-Ossietzky-University Oldenburg, Oldenburg, Germany

[4] Imaging Center Essen, EMU, Essen, Germany

[5] Department of Life Sciences and Medicine, Faculty of Science, Technology and Medicine, University of Luxembourg, Belvaux, Luxembourg

[6]Plant Development & Electron Microscopy, Biocenter LMU Munich, Planegg-Martinsried, Germany

[7] Centre of Water and Environmental Research (ZWU), University of Duisburg-Essen, Essen, Germany

*to whom the correspondence should be addressed:
andreas.klingl@biologie.uni-muenchen.de and alexander.probst@uni-due.de

Publication information:
Article was revised for The ISME journal
Revised 31.03.2023
running title: Spatio-functional organization in virocells of small uncultivated archaea from the deep biosphere

The authors declare no competing interest. All data is publicly available.

Abstract

Despite important ecological roles posited for virocells (*i.e.*, cells infected with viruses), studying individual cells *in situ* is technically challenging. We introduce here a novel correlative microscopic approach to study the ecophysiology of virocells. By conducting concerted virusFISH, 16S rRNA FISH, and scanning electron microscopy interrogations of uncultivated archaea, we linked morphologies of various altiarchaeal cells to corresponding phylogenetic signals and indigenous virus infections. While uninfected cells exhibited moderate separation between fluorescence signals of ribosomes and DNA, virocells displayed complete cellular segregation of chromosomal DNA from viral DNA, the latter co-localizing with host ribosome signals. A similar spatial separation was observed in dividing cells, with viral signals congregating near ribosomes at the septum. These observations suggest that replication of these uncultivated viruses occurs alongside host ribosomes, which are used to generate the required proteins for virion assembly. Heavily infected cells sometimes displayed virus-like particles attached to their surface, which agree with virus structures in cells observed via transmission electron microscopy. Consequently, this approach is the first to link genomes of uncultivated viruses to their respective structures and host cells. Our findings shed new light on the complex ecophysiology of archaeal virocells in deep subsurface biofilms and provide a solid framework for future *in situ* studies of virocells.

Results and discussion

Most *in situ* studies on environmental prokaryotic lytic viruses focus on free virions or their genomes (Turzynski et al., 2021). Recently, the scientific community has begun to investigate ecological roles of the virocells, which are cells that have fallen victim to viral infection and are subject to metabolic conversion (Howard-Varona et al., 2020). Host molecular machinery is typically reprogrammed rapidly to facilitate virus replication (Forterre, 2013), and can even result in distinct cellular compartmentalization for reproduction in the case of highly evolved bacterial jumbo phages (Chaikeeratisak et al., 2017). Viruses that infect archaea often possess distinct virion structures, biochemical properties, egress mechanisms, and coordinated virocell takeover motifs (as reviewed in (Liu et al., 2021; Prangishvili et al., 2017)). As all of these reports have arisen from isolated archaeal cultures, the scientific community lacks an understanding of the structure and organization of virocells of the uncultivated majority (Turzynski et al., 2021).

Recently, advances in fluorescence *in situ* hybridization (FISH) enabled researchers to detect an uncultivated viruses via tagging the viral genome (Jahn et al., 2021; Rahlff et al., 2021) and Schaible *et al*. to correlated FISH imaging with scanning electron microscopy (SEM) (Schaible et al., 2022) for identification of specific prokaryotes using 16S rRNA tagging. However, the combination of virusFISH (*i.e.*, virus-targeted direct-geneFISH) with SEM has not been established, as virusFISH protocols necessitate 300 base pairs double-stranded probes to enter target cells and thus a harsh temperature treatment of cells, which results in disintegration of the cellular ultrastructure (Sup. II Fig. S1). Here we report a novel correlative microscopic approach to study the ecophysiology of indigenous, uncultivated archaeal virocells by conducting concerted virusFISH, 16S rRNA-based FISH, and SEM analyses. Applied to uncultivated archaea from the deep biosphere, we linked morphologies of various *Candidatus* Altiarchaeum hamiconexum cells to corresponding nucleic acid signals.

Carbon fixing members of the uncultivated archaeal genus *Candidatus* Altiarchaeum dominate deep subsurface ecosystems worldwide (Probst et al., 2014) with uncultivated lytic ds-DNA viruses infecting these archaea and causing profound consequences on carbon cycling in the deep biosphere (Rahlff et al., 2021). The genome of the ds-DNA virus primarily targeting *Ca*. A. hamiconexum and tagged via virusFISH, however, has not been predicted to encode any viral hallmark genes in a previous study (Rahlff et al., 2021), which is not surprising since most archaeal viruses encode for novel or previously unknown proteins (Prangishvili et al., 2017). By modeling protein tertiary structure from predicted viral genes with AlphaFold (Jumper et al., 2021) and correlating results to annotations of function, we identified a novel auxiliary metabolic gene (*i.e.*, Ni-Fe hydrogenase), a gene encoding a capsid protein, and other virus-associated proteins encoded in the circular viral genome (Sup. II Fig. S2, Sup. II Table S1). Given this *in silico* evidence confirming the viral nature of the tagged genome, we examined the ultrastructure of *Ca*. A. hamiconexum virocells using a novel correlative microscopic approach.

Conserving cellular ultrastructure is particularly challenging when preparing samples for (virus)FISH and subsequent SEM. A distinct characteristic of *Ca*. A. hamiconexum are their extracellular hami structures, which are extracellular cell surface appendages with a basal barbwire structure and nano-grappling terminal hooks to interconnect cells (Moissl et al., 2005). By carefully balancing fixation reagent concentrations with critical point drying (for details please see Suppl. Methods, Sup. II Fig S1 illustrates insufficient sample preservation for

comparison), we successfully preserved the hami, and thus ultrastructure of *Ca*. A. hamiconexum cells throughout virusFISH preparation (Figure 3.6). Using gridded coverslips to ensure proper correlation of fluorescence and SEM signals (Figure 3.6 a, Sup. II Fig S3), spatial separation between ribosomes and chromosomal DNA was apparent in most uninfected cells. Although this phenomenon has previously been observed for archaea larger than altiarchaeal cells (i.e., Asgardarchaeota) (Avci et al., 2021), we observe a comparable segregation in ribocells (cells showing no infection) of small Altiarchaea of the DPANN superphylum (700-800 nm diameter). A similar segregation was observed in cells undergoing division, with DNA localizing about the outer poles of each of the daughter cells. At the same time, our approach enabled the infrequent detection of small DNA-filled vesicles (diameter: 250-300 nm, n=3) attached to Ca. A. hamiconexum ribocells (Figure 3.6 b). We hypothesize that these vesicles play an important role in inter-kingdom lateral gene transfer, which has recently been reported in *Ca*. Altiarchaea (Bornemann et al., 2022).

Altiarchaeal cells infected with uncultivated viruses (infection rate 5% (Turzynski et al., 2023)) were 10 —20% larger and slightly more spherical than their ribocell counterparts (Figure 3.7 b; 30 infected and 145 non-infected cells; Wilcox test, p value < 0.001; Sup. II Table S2, Sup. II Figs. S9, S10). Virocell enlargement has been reported previously in pure culture, with infected *Sulfolobus islandicus* cells increasing their size by several orders of magnitude (Liu et al., 2021). In dividing *Ca*. A. hamiconexum cells, virus signals accumulated along the cell division septum, indicating that viral reproduction occurs in the cytosol between the two daughter cells (Figure 3.6 d,e). This spatial separation of chromosomal DNA, ribosomes, and virion synthesis was also observed in individual cocci (Figure 3.6 f, g). Upon comparing these observations with ultrathin sections of *Ca*. A. hamiconexum cells, we confirmed a distinct segregation of viral reproduction activities from other cytosolic spaces (Figure 3.7 c, Sup. II Fig. S12). An accumulation of virus signals arranged in sphere-like intracellular structures observed via fluorescence microscopy suggested an organized packing of virions (Figure 3.6 g, Figure 3.7 a). However, virocells did not exhibit these sphere-like structures in most instances, but rather a dense agglomeration of virus signals (*e.g.*, virus signals in Figure 3.7 a). These observations most likely reflect different stages of the viral reproduction cycle, yet all of these are spatially separated from host chromosomes.

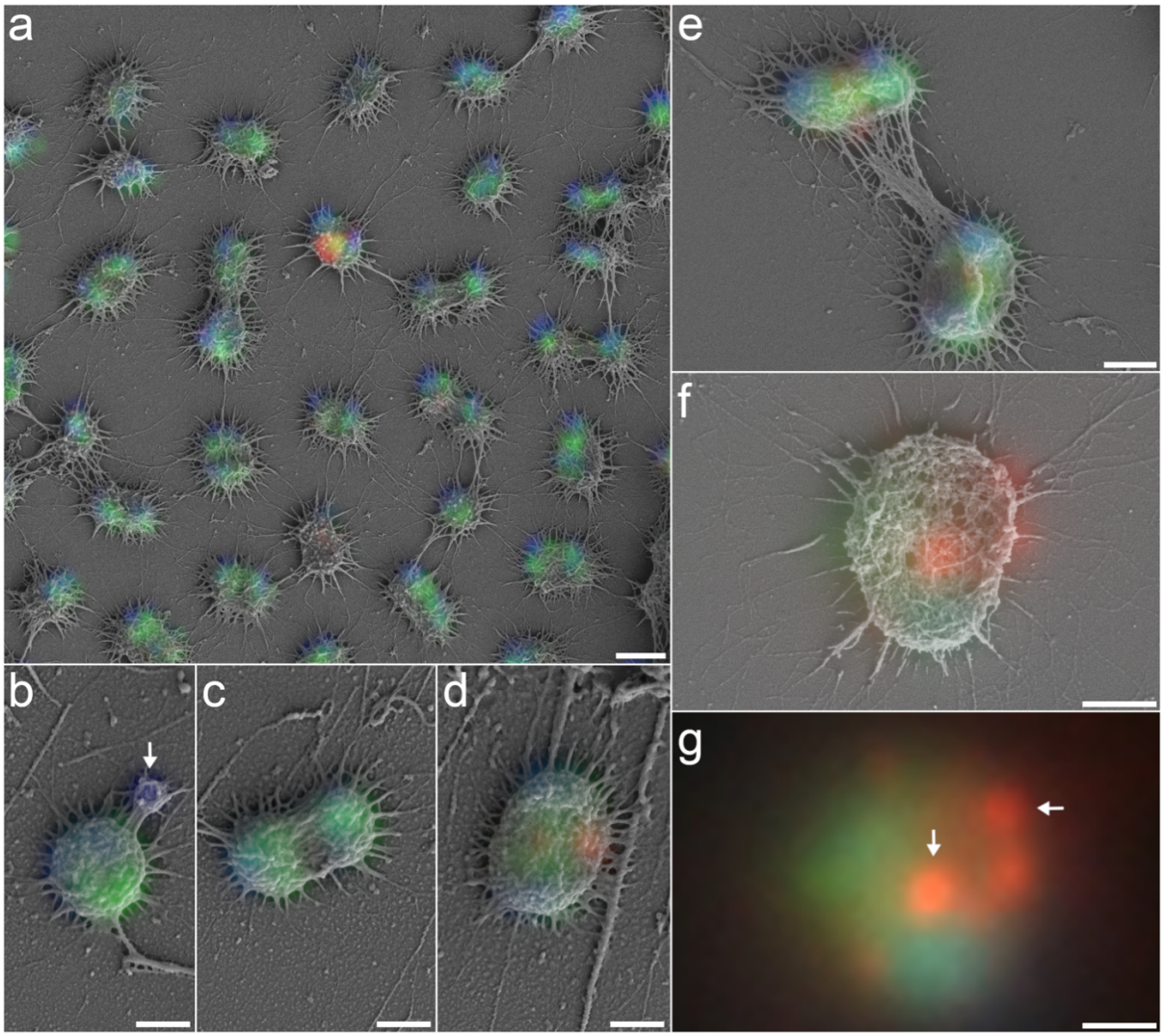

Figure 3.6 | Overlays of fluorescence and scanning electron micrographs of naturally occurring *Ca*. A. hamiconexum biofilms. Blue fluorescence signal corresponds to DAPI, green to the SMARCH714 probe (Moissl et al., 2003) labeling the 16S rRNA of *Ca.* A. hamiconexum (Atto 488) and red the virusFISH probes (Rahlff et al., 2021) labeling the viral genome (Alexa594); **a:** overview of single infected cell between multiple non infected cells demonstrating the successful correlation of the two imaging techniques due to sample preservation. **b:** uninfected single cell. Arrow points at a putative vesicle. **c:** uninfected dividing cells. **d:** infected swollen cell. **e:** dividing infected cells. **f:** single infected cell. **g:** overlay of the fluorescence images of f. Arrows point at spherical viral signals. Scale bars: 1 µm (a), 500 nm (b-g.) We provide a color-blind friendly image of this figure as Fig. S4; single channel images are provided as Fig. S5-S8

Strong virus signals not segregating into individual spheres often co-occurred with changes to the host cell's surface structure. These alterations manifested as small virus-like particles (VLPs) attached to the surfaces of *Ca*. A. hamiconexum cells (Figure 3.7 a). While the virion architecture of these uncultivated viruses remains unknown, these structures agree with transmission electron microscopy (TEM) images herein and elsewhere (Probst and Moissl-Eichinger, 2015; Rahlff et al., 2021). We compared the size of intracellular putative VLPs of TEM thin sections and the extracellular VLPs identified via correlative microscopy finding a significant difference in size [average diameter of VLPs in TEM 53 nm (n=56) vs. SEM 65 nm

(n=71) t-test *p* value= $2.7 \cdot 10^{-11}$; Sup. II Table S3, Figure 3.7, Sup. II S11, Sup. II S12]. Although the difference in size might be due to the application of different imaging techniques or the different states of virus maturation (*e.g.*, intracellular and extracellular, presence of the capsids), the sizes of the VLPs are in the expected range of archaeal viruses (Prangishvili et al., 2006). However, the correlative microscopic method described here links metagenomic data to the structure of uncultivated viruses, and thus enabled elucidating morphological traits of viruses whose existence is known only from sequence data. We suggest that this novel approach could be easily adapted to other sample matrices than subsurface biofilms, which *per se* represent a challenge due to the complexity of the biofilm matrix.

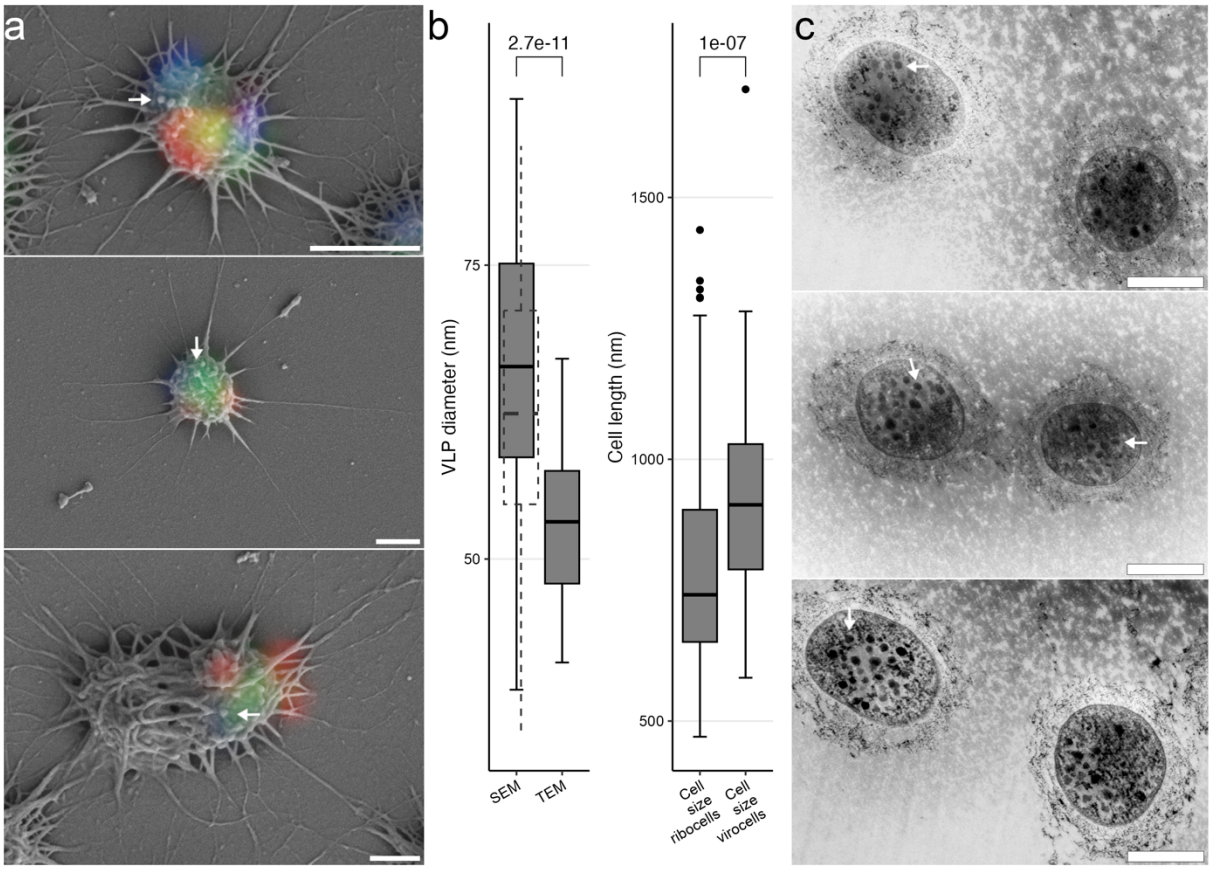

Figure 3.7 | Identification of intracellular and putative extracellular viral particles; **a:** Overlays of fluorescence and scanning electron micrographs (sampled in 2022). Arrows point at putative extracellular VLPs. Blue fluorescence signal corresponds to DAPI, green to the SMARCH714 probe (Moissl et al., 2003) labeling the 16S rRNA of *Ca.* A. hamiconexum (Atto 488) and red the virusFISH probes (Rahlff et al., 2021) labeling the viral genome (Alexa594). **b:** Boxplot indicating the measured size of the VLPs measured in SEM and TEM (average diameter of VLPs in TEM 53 nm (n=56) vs. SEM 65 nm (n=71) t-test *p* value= $2.7 \cdot 10^{-11}$) The dashed boxplot within the SEM column represents the hypothetical data after subtraction of the 4 nm Pt/Pd layer (significance of t-test above boxplots). In comparison to the measured archaeal cell size (30 infected and 145 non-infected cells; Wilcox test, *p* value < 0.001) (significance of Wilcox test above boxplots). **c:** TEM images (sampled in 2018). Arrows point at putative VLPs within *Ca*. A. hamiconexum cells. Scale bars 500 nm.

Microbes of the deep biosphere remain some of the most enigmatic biological entities on Earth due to limitation in sampling opportunities of the deep subsurface. While "omics"

approaches are mostly used to decipher microbial traits in the deep subsurface (Probst et al., 2018), advances at single-cell level to understand ecophysiology of these organisms remain the exception. Our novel protocol enabling the ability to spot rare infection events of individual cells presents a major step forward in understanding the little characterized deep biosphere at individual virocell level and demonstrates specific morphologies from vesicles to size alteration of uncultivated archaea. The spatial-functional distribution within virocells reveals a high degree of sub-cellular organization in deep-branching archaea, which might be required for the viruses to replicate and warrants future investigation necessitating sophisticated method development tied to high-resolution imaging, like TEM (Jahn et al., 2021). While the molecular mechanisms underlying such virus replication in deep-branching archaea remain unknown, we suggest that sub-cellular organizations in ribocells and virocells play an important role in microbial physiology also outside well-characterized model systems and might encompass the entire tree of archaea.

Acknowledgements

The work carried out herein was funded by the German Academic Scholarship Foundation (given to I.B.). A.J.P. acknowledges support from the Ministry of Culture and Science of North Rhine-Westphalia (Nachwuchsgruppe “Dr. Alexander Probst”) and German Research Foundation (DFG grant PR1603/2-1). This project has received funding from the European Research Council (ERC) under the European Union’s Horizon 2020 research and innovation program (grant agreement No. 863664). We thank Sabrina Eisfeld, Ines Pothmann, Maximiliane Ackers, and Agathe Materla for lab management and technical assistance. We thank the team at the Imaging Center Essen and Jennifer Grünert for technical assistance, training on the microscopes, and constructive discussions leading to superior sample preparation protocols.

We declare no conflict of interest.

Supplemental Information

All Supplemental information as revised is supplied on the accompanying CD (see section 7 for more information).

4. General Discussion

4.1. Prokaryotic virocells can be identified at the single-cell level using micro(spectro)scopy

Virocells are biochemically distinct from ribocells

Viruses play a major role in shaping ecosystems and biogeochemical cycles, via the alteration of their host's metabolism, host lyses, shaping microbial communities and causing release of dissolved organic matter (Vincent and Vardi, 2023). To fully understand the ecological impact of viruses, it is necessary to change to point of view from the quantification of virions to access the alteration of infected cells (Correa et al., 2021). Those infected cells resulting in lysis after virion production are called virocells (Forterre, 2011). To study the metabolic changes during viral infections at high resolution, non-destructive methods to identify individual virocells and their maturation progress are needed.

Within the publication "Label-Free Raman Microspectroscopy for Identifying Prokaryotic Virocells", we aimed to identify virocells using Raman microspectroscopy (section 3.1). We were able to show significant biochemical differences in-between infected and uninfected cultures of *P. syringae* by its respective phage *phi6* using multivariate data analysis of single cell focused Raman spectra (Figure 3.3). These differences caused by viral infections were found to be more significant than differences between cells of different growth phases, which are known to be significant (Huang et al., 2004). The complex multivariate data were reduced to three wavenumbers, which contributed significantly to differences between the infected and uninfected population. To facilitate virocell identification, a ratio of these peaks assigned to nucleic acids and proteins was postulated (Equation 3.1). This transformation from multivariate to univariate data has been already commonly used to identify stable isotopically labeled cells (Huang et al., 2007) and is used to implement Raman microspectroscopy as a quick and non-destructive tool subsequent to other techniques for cell or metabolite analysis (Lee et al., 2021a).

In addition, to the separation of virocells and ribocells along the first principal component axis, we observed separation of a subpopulation within the infected culture along the second principal component axis (Figure 3.3), which was mainly influenced by an increase of the lipid fraction. Since *phi6* is known to form a lipid layer in its late maturation stage (Bamford et al., 1976), we postulate, that Raman microspectroscopy is sensitive enough to distinguish viral maturation stages. We tested the applicability of the determined ratio to two more

prokaryotic virus-host systems, where host and virus vary drastically in their biochemical composition from the test system *P. syringae-phi6* (Figure 3.4). In contrast to the increase in *P. syringae-phi6* virocells, the ratio was also able to successfully identify virocells in the *B. subtilis-phi29* system (Figure 3.5) by a significant decrease of the ratio. This shift resembles observed stress responses within bacterial cells *(Teng et al., 2016).* However, while the ratio worked for the bacterial systems (Gram positive/negative with DNA/RNA phages) it revealed only a trend for the archaeal system *M. mazei* MetSV due to higher autofluorescence of the host.

In summary, we were able to show that by comparing spectra of uninfected and infected cultures, multivariate data analyses of single-cell Raman spectra can be used to define univariate markers to separate virocells and ribocells. The sensitivity is high enough to differentiate viral maturation stages, which also means these changes are rather unique for individual virus-host systems.

Virocell characterization can support virion depiction

The virosphere is not represented by viral studies relying on cultivated hosts (Dutilh et al., 2021). Environmental studies provide insights into the actual viral diversity with regard to their morphology, but they lack the direct correlation of these data to viral genomes or linkage to their host identity (Vincent and Vardi, 2023). Archaeal viruses display unique shapes and within their few isolated representatives, and they cause exceptional alterations of their host morphology (Baquero et al., 2021; Krupovic et al., 2018; Liu et al., 2021). To access the ecological role of metagenomically predicted viruses, these data need to be linked not only with their host identity, but also with morphological alteration of the host cell during the infection cycle. A detailed look into environmental virocells, might ultimately lead to the elucidation of virion shapes and a deeper understanding of the virosphere.

After accessing biochemical changes under laboratory conditions in section 3.1, we explored morphological traits of environmental samples in section 3.2. and coupled virusFISH and SEM with conservation of the fine ultrastructure of an uncultivated biofilm. By focusing in detail on individual cells we found a clear spatial separation of chromosomal DNA and ribosomes. In addition, the thoroughly examination of the biofilm lead to the observation of DAPI stained structures smaller than the expected size of microorganisms. We suspected them to be DNA-filled vesicles, whose potential would have been overseen by individual microscopy methods (Figure 3.6). Further exploration of these infrequently observed vesicles, which might

be involved in inter-kingdom gene transfer (Bornemann et al., 2022), represent an interesting perspective on the ecology within these altiarchaeal biofilms.

Measuring the individual sizes of archaeal ribocells and virocells, we observed a significant swelling the later (Figure 3.7). An increase of cell size was only described for cultured virus-host systems so far (Liu et al., 2021) and could promote correlative free virocell identification during EM. The correlative approach further allowed spatial evaluation of the viral signal. In virocells with one DAPI signal, indicating the host chromosome location, the viral signal formed individual spheres indicating an early infection stage. In comparison, virocells with two DAPI signals separated by the cellular ribosomes, indicating an active division process, tend to show an accumulation of viral signal along a potential division septum (Figure 3.6). However, in comparison to ribocells, virocells did not show ultrastructural indication of concluding cell division, resulting in the observed increased cell size. SEM did not allow to draw final conclusions about intracellular structures but revealed changes of surface structures of virocells. Measurements of these structures supports the hypothesis, that they represent virions (Figure3.7). Similar structures have been observed intracellular using TEM. Even though extracellular virions observed via SEM were shown to be significantly larger, the size difference can still be explained by the presence of a capsid in the extracellular state and by technical differences of the used methods. On the one hand, SEM of biological specimens rely on a thin metal layer to increase the conductivity (2 nm of Pt/Pd in our case) and the micrographs have a pixel size in the same range. On the other hand, TEM sample preparation is known to cause a shrinking of the sample (Mollenhauer, 1993). Therefore, both techniques are still hypothesized to show the same virus, despise the measured difference in size. Overall, the results demonstrate, that linking virusFISH and SEM provides the first tool to link metagenomic data with structural changes of uncultivated virocells and the appearance of the respective virions at the cell surface.

In summary the presented spectroscopic and microscopic approaches presented in section 3.1 and 3.2 increase our access to individual virocells. To address their ecological role and metabolic capacities, section 4.2 provides an outlook, how these methods enable a higher temporal resolution and a larger spatial perspective on virocell maturation.

4.2. Towards genome-informed single-virocell multimodal microscopy

RACS fortifies single-virocell transcriptomics

Viral infection alter the gene expression of the host and cause a high transcriptional heterogeneity within a population. Therefore, single-cell methods are required to achieve a sufficient overview of the individual maturation stages (Rosenwasser et al., 2019). Single-cell transcriptomic protocols for prokaryotic cells have been published recently (Imdahl et al., 2020) and will revolutionize our understanding of ribocells and virocell maturation.

The study presented in section 3.1 of this thesis resulted in a ratio to differentiate virocells and ribocells based on three wavenumbers (Equation 3.1). The defined ratio should allow RACS of, *e.g.*, an infected culture for downstream single-cell analyses just as the comparison of peaks to identify ^{13}C-incorporation into phenylalanine. This could provide further evidence, that the observed shift along the second principal component of *P. syringae* Raman spectra was caused by the expression of lipids-encoding genes of *phi6,* by RACS and single cell transcriptomics. Instead of relying on high throughput, single-infected cells can be trapped and measured over time (similar to the study of Wu *et al*. (Wu et al., 2020)) and just be moved into lysis buffer, when a ratio of defined Raman peaks indicates the second maturation stage of *phi6*, to collect cells with similar spectra for (single-cell) transcriptomics.

While a clear drop of the OD for *P. syringae* occurred only 10 h after phage addition, it was already observed 2 h after phage addition for *B. subtilis* (see Materials and methods of section 3.1). The virulence of the virus has a high impact on the duration of virocell proliferation, and varies even between phenotypes of the same viral species (DeLong et al., 2022). For studying the stress response *B. subtilis* in presence of *phi29* in more detail, *in vivo* Raman measurements can help to achieve the needed temporal resolution during fast viral maturation. RACS can provide a crucial additional level of information by making *in vivo* measurements, beyond identifying the presence of cells to sort them. If the transcriptomic analyses agree with the ramanome, cells could be pooled for enriching individual phenotypes for subsequent lipidomic or proteomic studies, linking multi-omic approaches on a single-cell level.

Ramanomics from laboratory conditions into ecosystems

There is still a large method development gap in adapting state-of-the art technologies to environmental single-cell studies es discussed in section 2.1. Various FISH-based approaches already support single-cell genomics (Kaster and Sobol, 2020) and allow to target genomic and

transcriptomic information of interest (Barrero-Canosa et al., 2017; Pernthaler and Amann, 2004), while ramanomics demonstrate insights into biochemical differences at phenotype resolution (García-Timermans et al., 2018; Kuzmin et al., 2017; Teng et al., 2016). Therefore, Raman-FISH can bridge the gap to link metagenomic data with biochemical characteristics of individual cells, while maintaining spatial information of the sample (Schaible et al., 2022). Previous Raman-FISH studies have relied on strong Raman shifts that are easy to identify within spectra regardless of their resolution for the overall microbial fingerprint (*e.g*. stable isotope induced shifts or metabolites with a strong Raman band as cytochromes or carotenoids) (Huang et al., 2007; Schaible et al., 2022).

VirusFISH allows the immediate identification of individual virocells within a population. Therefore, coupling Raman and virusFISH allows testing the feasibility and robustness of the virocell ratio determined in section 3.1 (Equation 3.1), when applied to an environmental sample. Other studies reported successful measurements using long bleaching and acquisition times (Huang et al., 2007), we minimized the required acquisition time by changing from the commonly used 532 nm laser to a 633 nm laser. This wavelength was longer than the excitation needed for the used fluorophores (see Figure caption Figure 4.1 A). Instead of measuring individual cells, we used the high cell density of the biofilm for an area mapping surrounding the infection (Figure 4.1 A). By doing so, a representative number of archaeal spectra is generated in a more automated, time efficient workflow. The introduction of polynucleotides was potentially hypothesized of artificially increase the nucleic acid content of virocells, but the results indicate an increased protein content in the respective area. The average virocell ratio of the sample was found to be below 0.5, which was lower than any previously measured value. Comparing the average Raman spectrum of *Ca.* A. hamiconexum (Figure 4.1 C) with the current body of literature revealed, that this ratio was to be expected as the archaeal biofilm spectra align with commonly described biofilm spectra (Liu et al., 2020). The EPS, composed of the characteristic *hami of Ca.* A. hamiconexum, is representing a substantial higher contribution of proteins compared to planktonic cells measured previously (compare average spectra in Figure 4.1 C with those in Figure 3.3 B and Figure 3.5 B). The hypothesis, that the virocell ratio can still be used to identify virocells within the biofilm was not confirmed within this preliminary experiment. It was hypothesized, that the presence of virocells, identified based on the red virusFISH signal in the fluorescence micrograph, would cause a significant change of the virocell ratio indicated by a strong change in the color in the

overlayed plot, representing the calculated virocell ratio at the respective position. This was not observed, as illustrated in Figure 4.1 A and the respective data in supplemental material III.

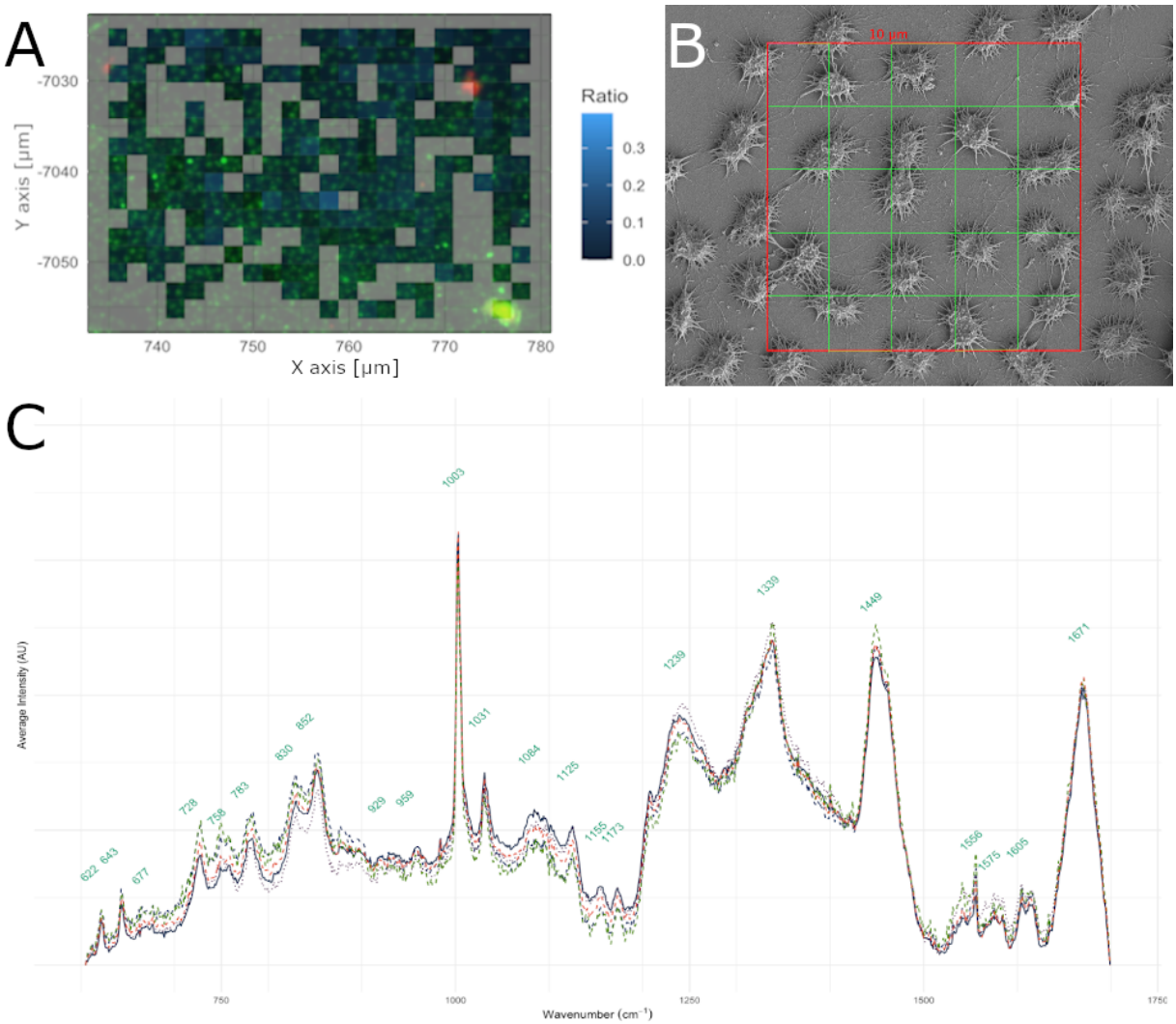

Figure 4.1 | Preliminary virusFISH Raman study. **(A)**: overlay of a fluorescence micrograph (green corresponds to the SMARCH714 probe (Moissl et al., 2003) labeling the 16S rRNA of *Ca.* A. hamiconexum (Atto 488) and red to virusFISH probes (Rahlff et al., 2021)) and a map of the calculated ratio (Equation 3.1). Images were aligned based on the light micrograph taken in the Raman microspectroscope. Empty spaces in the ratio plot represent spectra, which were removed due to insufficient quality or cosmic rays (for details see supplement 4_2); **(B)**: SEM image (from 3.2) with a grid indicating potential measurement positions of a Raman mapping with 2 µm steps; **(C)**: average Raman spectra of *Ca.* A. hamiconexum from the mapping shown in (A). individual lines indicate different clusters based on optimal kmean-clustering. (original data, R script for analyses and plotting of panel (A) and (C) and GIMP file for panel A are deposited in supplement III)

The study performed in section 3.2 allowed further considerations: First, the CLEM approach improved differentiation of virusFISH signals of actual virocells from false positive results. Second, instead of individual spectra, consecutive Raman spectra of a defined area can be recorded due to the high cell density in a biofilm, as presented in Figure 4.1 A. Drawing a hypothetical mapping area in a scanning electron micrograph, reveals the compromise

between generating a significant amount of data for analyses and the laser being actually focused on an individual cell (Figure 4.1 B). As conclusion, mappings can be used to get a general overview of the uninfected majority within the biofilm, but individual measurements or mappings of a narrow area (e.g. 10 x 10 µm) around virocells enables the spectra acquisition of several virocells per sample within an optimized time frame.

The results of this preliminary study indicate that virusFISH and Raman microspectroscopy can be coupled to achieve spectra of sufficient quality for subsequent multivariate data analyses. By using a laser wavelength of 633 nm, the bleaching time necessary of obtain sufficient Raman spectra can be minimized and mappings of uninfected areas can be performed to generate a control group of spectra. *Hami* of *Ca.* A. hamiconexum are suspected to massively increase the intensity of peaks assigned to proteins, which agrees with reference spectra of bacterial biofilms (Liu et al., 2020). This causes a massively lower ratio than previously implemented values for virocell detection of planktonic cells (compare Figure 3.4). In future work, measuring several archaeal virocells with virusFISH-Raman should allow statistical evaluations of their biochemical changes, to identify molecular traits of virocell maturation in an environmental biofilm (Figure 4.2).

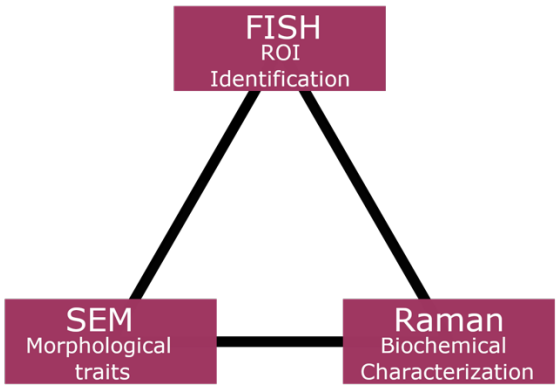

Figure 4.2 | Level of information from different microscopy and spectroscopy approaches. The individual combinations of these techniques each harbor advantages and disadvantages which must be carefully considered during experiment design.

Besides coupling virusFISH with SEM or Raman microspectroscopy, information from these studies can benefit the implementation of coupling Raman and SEM (Figure 4.2). These techniques can be coupled within one instrument, where a Raman unit is added to a regular SEM. The software allows to move the stage between the SEM area and the Raman imaging (Hollricher et al., 2015). Planning to perform correlative microscopy of Raman and SEM of microbial samples comes with limitations on SEM sample preparation. It needs to be evaluated to which extend osmium tetroxide and dehydration alters the Raman spectra.

However, using a highly polished steel slide as already used in section 3.1 for Raman measurements aid in avoiding sputter coating for increased conductivity of the sample in monolayer biofilm sections. Further, the resolution of the electron micrographs does not need to achieve a pixel size of several nanometer; 25 - 50 nm should be sufficient in our example to differentiate virocells of *Ca.* A. hamiconexum from ribocells or bacteria (at a magnification of 2,500- 5,000x). This would allow targeting single cells in a dense biofilm with higher precision than Raman-FISH. Cells of interest can be distinguished by morphological traits, which have to be identified in prior CLEM analyses, as demonstrated in section 3.2. Comparing virusFISH-Raman and Raman SEM studied based on virusFISH-SEM observation would allow label free measurements of this system without random mappings. Label free Raman-SEM measurements would increase the accuracy of the generated data to discriminate biochemical changes of environmental virocells and ribocells.

Turning grayscale into multicolor

CLEM methods like (virus)FISH-SEM and (phage)FISH-TEM are useful for setting different microorganisms in a broader context, *e.g.* their distribution within a biofilm, localizing rare microbes within a community, due to a larger field of view during initial fluorescence imaging (see section 3.2 and (Jahn et al., 2021; Schaible et al., 2022)) or help to link microbial identity and inorganic storage compounds (McGlynn et al., 2018). Some fluorophores can be preserved during embedding for more accurate correlation (McGlynn et al., 2018). Therefore, research hypotheses regarding interactions or morphological properties of the cells can be answered using CLEM.

At the same time, advances in probe design and the considerations to balance sample permeabilization and preservation will also fuel advances in the field of nano-metalprobe *in situ* hybridization (Metal-ISH). The ongoing development of methods based on Gold-FISH, GISH, polygold-FISH and silver-DISH harbors the potential to tackle hypotheses, which purely fluorescence based approaches might not answer as easily (Almstrand et al., 2015; Berg et al., 2020; Schmidt et al., 2012; Ye et al., 2015). These studies detect the identity of cells based on the accumulation of nanoparticles without the need to correlate data of two methods.

The previously discussed combination of morphological traits identified using CLEM and Raman-SEM for optimal spatial resolution of biochemical characteristics could be further refined by these methods, as cells can be identified with EM. The SERS effect described during the silver-DISH protocol opens new possibilities for ramanomics in the field of microbial

ecology (Berg et al., 2020). Within a sample examined in a Raman-SEM setting, cells could be identified based on the metal probe signal, located by the contrast between carbon and metal using a BSE detector (Berg et al., 2020; Schmidt et al., 2012; Ye et al., 2015), which simultaneously enhances the Raman signal during subsequent measurements. Currently, nanoparticles for SERS studies of microorganisms are either attached to the cell surface, or to antibodies which will bind to their respective antigens on the cell surface (Lee et al., 2021a; Wang et al., 2013). These methods are useful under laboratory conditions, especially with regard of biomedical applications (Lee et al., 2021a). For more in-depth application of the SERS effect, it is possible to produce silver nanoparticles inside microbial cells *in situ* by reduction of silver nitrate within the cells, which results in unspecific localization within all cells (Efrima and Bronk, 1998; Weiss et al., 2019). Metal-ISH protocols, by contrast result, in a probe specific labeling, to create a signal amplifying SERS effect only, but within cells of interest (Berg et al., 2020). Applying Metal-ISH to virocell identification would result in a strong Raman signal exclusively from infected cell, without any interference of fluorophores, within a reduced time per spectrum. The measurements could be performed within the Raman microspectroscope without the need of a multimodal setting. However, it would require the establishment of poly- instead of oligonucleotide probes in the Metal-ISH workflow.

All presented studies rely on ion-reduction for the particle synthesis and focus on one metal probe alone (Almstrand et al., 2015; Berg et al., 2020; Schmidt et al., 2012; Ye et al., 2015). Recently the ligand-free generation of monometallic nanocluster were reported for gold and platinum (Ziefuss et al., 2022, 2021). Therefore, it should be possible to perform hybridization using different metal probes within one sample. If the different cells can be distinguished based on the metal composition using EDS (Almstrand et al., 2015; Berg et al., 2020; Ye et al., 2015), it would allow ecological studies in a similar manner as standard FISH protocols, but under consideration of the ultrastructural context. As metal enhancement is frequently discussed (Berg et al., 2020; Schmidt et al., 2012; Ye et al., 2015) it needs to be evaluated, if initially different metal particles can still be distinguished afterwards.

Interestingly, none of the presented studies evaluated the detection of nanogold using TEM, which can be coupled to EDS as well (McGlynn et al., 2018) and should facilitate the particle detection due to a higher resolution. During SEM studies, the problems of unspecific gold signals due to non-specific binding to surface charged minerals or deposition during enhancement steps are reported (Schmidt et al., 2012; Ye et al., 2015). These effects should

have a lower impact on TEM orientated studies, which could elucidate, whether the virusFISH signal originated form assembled virions or unpacked viral genome fragments.

3D-CLEM: from virocell to maturation cycle

In section 3.2 both methods, FM and SEM were only used to displaying two-dimensional (2D) observations, since SEM can just scan the sample surface. However, the biofilm and each individual cell represents a three-dimensional (3D) space in which their components interact. Recent studies of virusFISH indicate a huge impact of viral infection within the multilayered areas of the biofilm (Rahlff et al., 2021; Turzynski et al., 2023). Therefore, after establishing virusFISH, 3D information should be acquired to illuminate the viral impact on virocells and the biofilm as ecosystem. This will enable a more qualitative and quantitative assessment of the intracellular organization of virocells in the same manner as Avci and colleagues elucidated the spatial organization of DNA and ribosomes of archaeal cells (Avci et al., 2021). To exploit the full potential of the generated samples, they can be correlated with EM approaches. Relocating an individual cell in a 3D space, like a biofilm, is challenging, and the scientific question needs to be carefully formulated to choose the right approaches. The results of our study led to further perspectives regarding environmental virocells, their influence on the ecosystem and the challenge, to morphologically describe the ultrastructure of virions.

To address the ecological role of virocells, CLEM will be an important tool that will bridge the scale from individual cells and their surrounding context. The correct concertation of methods enabled localization of the fluorescently labeled viral structures in thin sections of sponge tissue (Jahn et al., 2021) and if the biofilm itself and not the individual cells are considered as system to study, protocols can be adapted. Prior or after the virusFISH protocol the 3D shape of the biofilm can be preserved in noble agar to further avoid delocalization of cells during EM sample preparation as performed by McGlynn *et al*. (McGlynn et al., 2018). In thin sections with a thickness of 100 nm virions of about 200 nm were identified (Jahn et al., 2021). Ultrathin sections between 50 and 100 nm would result in 6 - 12 sections per average uninfected cell and up to 20 for virocells. If all consecutive sections are collected in a 3D reconstruction, this would allow to quantify, how many virions are assembling within the virocell in dependence of virocell size. Provided successful correlation with the fluorescence data, the EM reconstruction will reveal how the virusFISH signal types (multiple smaller spherical signals vs. one large signal) relate to the assembly of virus particles. However, ultrathin sections would result in a challenge to recover a complete biofilm, with a thickness

of multiple cells, without losing any sections (Peddie and Collinson, 2014). McGlynn and colleagues circumvented the 3D fluorescence reconstruction by performing fluorescence imaging of the alreday cut sections and focused on single cross sections (McGlynn et al., 2018).

Volume electron microscopy (volume EM) techniques represent alternatives to ultra-thin sectioning for EM. Methods like electron tomography (ET) of 200 nm to 1000 nm sections, Serial Blockface (SBF)-SEM or focused ion beam (FIB)-SEM or could be used for biofilms in a similar manner as tissue samples (McGlynn et al., 2018; Peddie and Collinson, 2014; Rollenhagen et al., 2020). 200 nm sections can be examined for cells and significant structures. Sections of interest can then be used for ET, where a tilt series of sections is performed for high resolution 3D reconstruction. SBF-SEM and FIB-SEM represent faster and more automated data acquisition of a larger field of view than TEM techniques. For biofilm reconstruction a large field of view is beneficial, but SEM has a lower resolution than TEM (Rollenhagen et al., 2020), which might result in an misestimation in the aim of virion quantification within virocells, but structures of similar size have already been resolved in bacterial biofilms (Remis et al., 2014). These time-consuming techniques will highly benefit from the information of the flock infection stage derived from FM to choose highly infected flocks for this procedure, but compromises between resolution and sample processing need to be carefully considered (Flechsler et al., 2020; Rollenhagen et al., 2020).

For investigating *Ca.* A. hamiconexum biofilms including respective virocells, the dense network of *hami* might limit the dispersal of virions. Therefore, a complete picture of the infection cycle from first particle assembly, via virocell lysis to initial infection of new cells might me achievable in a confined volume. FIB-SEM was already applied to *Ca.* A. hamiconexum cells to illustrate the formation of electron dense rings in dividing cells. In agreement with micrographs, showing fluorescence immuno-staining of FtsZ proteins, these rings indicate the aggregation FtsZ proteins during cell division (Probst et al., 2014). The results in section 3.2 imply an aggregation of viral genomes in the septum area of dividing cells as well (Figure 3.6 e). The increased size of virocells in comparison to ribocells leads to the question if viral infections influence the aggregation of FtsZ proteins. The aggregation of FtsZ in virocells could be elucidated by virusFISH with subsequent immuno-staining of the FtsZ proteins within the same sample or paying attention to the electron dense area in volume EM reconstructions. Linking these so far independently examined events, the aggregation of FtsZ during cell division and the infection with a lytic virus, within virocells of *Ca.* A. hamiconexum,

will shed new light on how viruses influence their host. Inhibiting cell division processes to increase the cell volume of small archaea in a nutrient limited environment, would result in a higher virulence of the virus, since more virions can be produced prior to lysis, and therefore affect the evolution dynamic within the biofilm (DeLong et al., 2022).

The potential of prokaryotic viruses to shape their host environment lies within the ability to hijack the host metabolismus. Virocells have short lifetimes in comparison to ribo(viro)cells and require techniques with high spatial or temporal resolution to depict their metabolic capacity (Correa et al., 2021; Ku et al., 2020). As non-destructive method ramanomics paves the way for *in vivo* single-cell studies of virocell maturation (Wu et al., 2021, p. 21) to link the result of multi-omic studies at a temporal resolution not yet achieved for prokaryotic virocells. Potentially, multimodal approaches including ramanomics overcome limitations of environmental single-cell transcriptomics and allow insights into biochemical alterations of individual indigenous virocells at single cell resolution. Simultaneously, advancements in in Metal-ISH protocols further enhance ramanomics and Metal-ISH and CLEM approaches including TEM, or volumeEM have the potential to decrease the spatial resolution below the cellular level and resolve environmental virocell maturation at sub-cellular level. In the future, genome-informed multimodal microscopy of virocell maturation might allow accurate quantification of environmental viruses and their ecological impact.

4.3. Global impact of the smallest microbial entities

The fate of lysed cells

Virocells of *Ca.* A. hamiconexum are representing only a minor fraction of their biofilm community (Turzynski et al., 2023). However, the impact of cell lysates might impact a wide range of the community. First, surrounding archaeal cells become prone to new viral infections, so they can either turn into virocells, or they need to activate their defense system (Rosenwasser et al., 2019). Secondly, besides virions also cellular organic matter is released, which can be taken up by other microorganisms. During the study in section 3.2 the focus was set on the characterization of archaeal virocells. The signals assigned to individual virocells only represent the first infection stage proposed by Rahlff *et al.*, described as adsorption of the virus to the host cell (Rahlff et al., 2021). Our virusFISH-SEM results indicate that these signals can be correlated to more advances infection stages, since the cells already show an increased cell size (Figure 3.7). Rahlff *et al.* proposed two more infection stages as advanced

infection and lyses (Rahlff et al., 2021). During our CLEM study it was noteworthy that the kind of virusFISH signal assigned to these stages, was not found to correlate with the 16S rRNA signal of *Ca.* A. hamiconexum, but only with DAPI stained cells of different morphologies (Figure 4.3). SEM reveals that these cells tend to be covered in a thin layer of EPS.

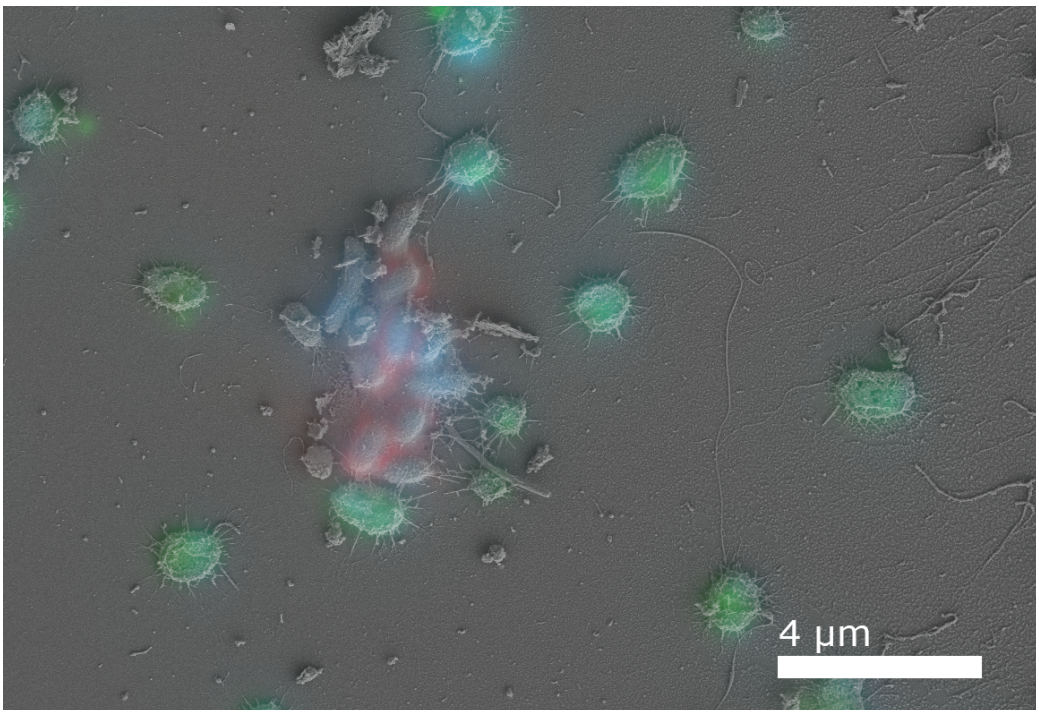

Figure 4.3 |CLEM image indicating virusFISH signal co-localized with non-SMARCH714 labeled cells. Blue fluorescence signal corresponds to DAPI, green to the SMARCH714 probe (Moissl et al., 2003) labeling the 16S rRNA of *Ca*. A. hamiconexum (Atto 488) and red the virusFISH probe (Rahlff et al., 2021) labeling the viral genome (Alexa594). Original data are deposited in the supplemental material IV.

Since the virusFISH signal seems to associate with the EPS, I hypothesize that it is composed of virocell debris after lysis, including unpacked virus DNA. The released nutrients might be taken up by heterotrophic bacteria, which represent about 5 % of the MSI biofilm fraction (Henneberger et al., 2006). The majority of bacteria within the biofilms retrieved from MSI was previously assigned to Deltaproteobacteria with the genus *Desulfobacula* being the most enriched (Probst et al., 2012). It would be interesting to further elucidate the diversity of bacteria associated with this archaeal organic matter. It might further close the gap of knowledge, how virocells fuel the deep terrestrial subsurface microbiome, if direct nutrient uptake is restricted to a subgroup of organisms. For this purpose, the bacterial probes previously described (Henneberger et al., 2006; Probst et al., 2012) can be combined with virusFISH probes for co-localization of the most abundant groups. VirusFISH-TEM could then help to locate whether fluorescent signals similar in Figure 4.3 are surrounding or within the associated bacterial cells. In addition, single thin sections are sufficient to determine whether

virions are present in the debris or not. A high accuracy between the fluorescence signal and the EM micrographs within a 2D space is sufficient for this purpose.

By reconstruction of an altiarchaeal biofilm using volume EM, the effect of advanced lysis events within the biofilm can be accessed in detail. A micrometer-scale 3D reconstruction creates a complete overview, setting virocells of different maturation stages and the invasion of other microorganisms in a spatial context with high ultrastructural resolution. The different virusFISH signals can be precisely assigned to maturation stages and stages below the detection limit of FM can be identified. Using FM, the prediction of the viral lifestyle of environmental viruses became possible (Rahlff et al., 2021). Using results derived from 2D CLEM studies and adapting the protocols to volume EM might enable the description of the maturation cycle of a virus without its host cultivation, overcoming a bottleneck of studying the prokaryotic virosphere.

Targeting virocells for *in situ* virion reconstruction

Once we understand virocell characteristics and can confirm properties to distinguish virion filled virocells from other cells in the biofilm without virusFISH, one challenge remains necessitating a higher resolution than previously discussed TEM techniques. Beyond describing viral maturation stages at a sub-cellular level, a sub nanometer resolution will be required to resolve the structure of virus particles and complete the ultrastructural information about the microbial entity.

Sutton and colleagues were able to resolve the structure of a 85 nm virus within human cells using cryo-electron tomography on 150-200 nm thick lamellae created via cryo-focused ion beam milling (Cryo-FIB) (Sutton et al., 2020). If biofilm flocks are plunge-frozen on a grid, it might be possible to identify virocells based on their increased size and generate lamellae of areas potentially filled with virions in a similar manner. This avoids the time extensive purification that usually is performed to resolve viral structures from cultivated representatives (Spinelli et al., 2014). Recently, cryo-electron tomography of an Asgard archaeon enrichment culture was used for intracellular reconstruction of the characteristic ribosomal structure (Rodrigues-Oliveira et al., 2023). Similar to the challenge of identifying virocells in a biofilm, they were challenged by low cell density and pointed out, that FISH leads to major perturbations of the ultrastructure (Rodrigues-Oliveira et al., 2023). Therefore, CLEM approaches are not recommended for higher resolution molecular reconstruction studies but can help to independently identify cellular morphologies of interest, *e.g.* a certain cell size.

The reconstructions can be compared with the capsid protein structures predicted via Aphafold (see supplemental II Table S1) and it might be possible to determine how many of these capsid proteins form the virion. Ultimately, coupling metagenomics, metatranscriptomics and *in situ* imaging studies might be able to close the gap between free virions, their host identity, viral maturation stages and virion structure of environmental virocells, without cultivation.

Beyond virocells - addressing other viral lifestyles

As briefly described in section 2.2, lysis is not the only mechanism by which viruses influence their host and the ecosystem composition, but there is rather an infection continuum between lytic and lysogenic lifestyles (Correa et al., 2021). Chronic or (pseudo)lysogenic lifestyles are prevalent in ecosystems, yet most of the knowledge about these lifestyles is only derived from isolated representatives, as most of the virosphere can so far only be grasped via metagenomic data (Chevallereau et al., 2022; Mäntynen et al., 2021). Non-lytic viruses produce virions or metabolites derived from AMG, which might be released into the environment, thus playing important ecological roles (Romantschuk and Bamford, 1981; Sun et al., 2022). The methods described to characterize virocells, should be transferrable to other lifestyles to complement the metagenomically advancements detecting them in complex environments (Kieft and Anantharaman, 2022b).

Considering the results to differentiate ribocells and virocells in section 3.1, I hypothesize that ribovirocells can be differentiated from virocells using the similar methods. Since phage *phi6* is described to induce chronic infections within certain hosts (Romantschuk and Bamford, 1981), it represents a convenient candidate to test this hypothesis. Cells should probably not be fixed but measured and tracked in liquid medium over a defined amount of time, while maintaining growth conditions favoring the chronic infection lifestyle. Once the chronic character was verified, the growth conditions could be changed to induce lysis. The transition from chronic to lytic infection and the biochemical differences between these two states, can possibly be described using Raman microspectroscopy. For sufficient resolution on the spectral and temporal scale, single-cell Raman measurements of individual trapped cells over a longer time span (Chen et al., 2009; Wu et al., 2021), should be combined with measuring a sufficient high number of random cells at certain time points to generate a statistical significant dataset (Ali et al., 2018).

In a recent study, DGF was used to target a novel isolated ssDNA phage and could support the presence of a lysogenic carrier state in addition to lysis (Zucker et al., 2022). As DGF was introduced to label genes of interest (Barrero-Canosa et al., 2017), and virusFISH was also adapted from DGF (Rahlff et al., 2021), this study proves the applicability to adapt virusFISH to a broader range of virus host systems. Therefore, DGF-Raman should also be applicable to characterize biochemical changes, whose significance is can only be revealed by multivariate data analyses, in a variety of prokaryotic environmental samples. These changes can be based on different virus-host systems or the presence of genes of interest, as demonstrated by the detection of the *amo*A encoding gene in a lake sample based on DGF (Barrero-Canosa et al., 2017; Rahlff et al., 2021; Wang et al., 2016; Zucker et al., 2022).

In environmental systems it might be interesting to try labeling mRNA derived from the expression of AMGs to test whether the genes are only carried in the viral genome or actually expressed. For this DGF derived protocols cannot be applied as the denaturation steps might enhance mRNA degradation (Barrero-Canosa et al., 2017) and some genes of interest might be too short to label with several polynucleotide probes (e.g., the Ni-Fe hydrogenase subunit identified in section 3.2 [see supplemental table 1 of the study] is only about 360 bases long). Protocols targeting mRNA use oligonucleotides with fluorescent dyes close to the near-infrared range (*e.g.,* Atto594 or Alexa647), to minimize auto fluorescent background signals (Coleman et al., 2007; Taniguchi et al., 2010). This method is especially useful for mRNA quantification (Taniguchi et al., 2010). For qualitative mRNA determination, especially in environmental samples, CARD-FISH based protocols are used (Pernthaler and Amann, 2004; Wagner et al., 1998). Due to the low copy number of mRNA (Taniguchi et al., 2010), most protocols point out the additional requirement to use RNase free solutions and equipment from the time of sampling to hybridization (Coleman et al., 2007; Pernthaler and Amann, 2004; Taniguchi et al., 2010) and deactivation of internal RNase (Pernthaler and Amann, 2004). This would make multimodal studies more challenging, since CARD-FISH heavily affects cellular composition and ultrastructure (Ye et al., 2015) and near infrared dyes like Alexa647 will be excited by the 633 nm laser during Raman microspectroscopy. At the same time, the expressed protein will have a longer lifetime than the respective mRNA (Taniguchi et al., 2010). The expression of AMG is of special interest, when it provides an ecological advantage to the host (Sun et al., 2022). Respective proteins can be targeted by immunolabeling, whereas the antibody generation might benefit from analogs from cultivated microorganisms (Probst

et al., 2014). Whenever the protein function can only be predicted due to close homologues, mRNA-FISH might still be an alternative to time extensive immunolabeling protocols.

Friend or foe

Ca. Altiarchaeum was not only found to be targeted by viruses (Rahlff et al., 2021), but by another, possible symbiotic, DPANN archaeon as well. (Probst et al., 2018; Schwank et al., 2019). The symbiosis was first indicated by significant co-occurrence in metagenomes in water derived from the CO_2 driven, cold-water geyser Crystal Geyser (Probst et al., 2018). Geochemical, Meta- and single-cell genomical surveillance of a complete eruption cycle revealed that *Ca.* Altiarchaeum dominates the deepest groundwater layer, and genomes of *Ca.* Huberarchaeum crystalense were first reconstructed (Probst et al., 2018). Additionally, SEM micrographs dispayed putative Altiarchaeal cells, based on the presence of *hami,* with ultrasmall cell-like structures attached to them (Probst et al., 2018). A later study supported these findings, showing that the co-occurrence of the two organisms within metagenomes can be determined over the time span of serval years and demonstrated a cellular co-localization using FISH (Schwank et al., 2019). A putative symbiotic lifestyle is proposed for a variety of organisms placed within the DPANN superphylum, as they are characterized by a small genome size, have reduced metabolic capacities and the few cultivated representatives only exist within co-cultures (Dombrowski et al., 2019). Similar reduced metabolic capacities and genome sizes are also reported for representatives of the bacterial candidate phyla radiation (CPR) (Brown et al., 2015; Monsees et al., 2019). The symbiotic lifestyle of CPR bacteria is additionally supported by the lack of a ribosomal protein (Brown et al., 2015). Metagenomic studies of Crystal Geyser and other subsurface ecosystems inducate that DPANN archaea and CPR bacteria are ubiquitous and highly abundant within the deep subsurface (Anantharaman et al., 2016; Gios et al., 2023; He et al., 2021; Luef et al., 2015; Probst et al., 2018). Regardless of their reduced metabolic capacities, genomes of the CPR bacteria and DPANN archaea often contain key genes for carbon, nitrogen and sulfur metabolic pathways (He et al., 2021; Probst et al., 2018), indicating that they can contribute to the proposed complex network of metabolic handoffs of subsurface communities (Anantharaman et al., 2016), and potentially impact global biochemical cycles.

Cultivation based studies on few CPR bacteria and DPANN archaea with cultivated host start to shed light on these close microbial interactions (Bor et al., 2020; Hamm et al., 2023; He et al., 2015; Heimerl et al., 2017; Sakai et al., 2022). Heimerl *et al*. depicted contact

between the host and symbionts cytoplasm of a membrane bound system and proofed protein transport from the host into the symbiont using immunogold labeling (Heimerl et al., 2017). Additionally, a recent study used cultivation based cryo-CLEM to demonstrate invasion of a DPANN archaeon into its host and even symbiont associated host lysis, representing the first predatory instead of symbiotic lifestyle within the DPANN superphylum (Hamm et al., 2023). The discovery more examples for a predatory lifestyle of DPANN archaea of in future studies would completely change their ecological role, as they might contribute to nutrient cycling and microbial diversity in the same extend as lytic viruses (Hamm et al., 2023). Simultaneously, there is evidence for viruses infecting these putative host-dependent ultra-small cells (Baker et al., 2010; Munson-McGee et al., 2019, 2015). A putative virus infecting Nanoarchaeota was linked to its host *in silico* and TEM micrographs of VLP were used to assign two possible virion structures to the viral genome (Munson-McGee et al., 2019). Considering an only 300 nm host cell, whose own replication is depending on another cell, being infected to produce a putative 60-400 nm sized virion, opens a new perspective on virus-symbiont-host associations (Munson-McGee et al., 2019).

As presented in section 2.1 cultivation, independent imaging techniques are reliable and robust approaches to support metagenomic derived information about the uncultivated majority. After all, co-cultures of DPANN archaea and CPR bacteria are not even representing the majority of linages within these groups (Dombrowski et al., 2019; Hug et al., 2016). Linking ultrastructural information within genomic identity in environmental samples remains challenging to this day. He *et al.* identified communities with high abundance of CPR bacteria and DPANN archaea in groundwater samples using metagenomics and performed cryo-TEM on symbiont-host systems, without imaging-based cell identification, and postulated host-dependent replication of ultrasmall cells during membrane contact (He et al., 2021, p. 21). As FISH protocols can be adapted to target these ultra-small cells (Munson-McGee et al., 2015; Sakai et al., 2022; Schwank et al., 2019), future genome-informed multimodal studies can expand our knowledge on symbiotic and predatory microbial interactions of the smallest microbial entities: CPR bacteria, DPANN archaea and viruses.

5. Zusammenfassung

Durch die Quantifizierung über die Anzahl von Virus Partikeln, sogenannter Virionen, werden Viren in der Literatur in der Regel als häufigste biologische Entität auf der Erde bezeichnet. Der ökologische Einfluss von Viren entsteht jedoch erst, wenn Virionen auf einen potenziellen Wirt treffen, da Virionen keinen eigenen Metabolismus besitzen. Vor etwa zehn Jahren wurde das sogenannte "Virocell"-Konzept vorgestellt, das die Umprogrammierung von Zellen zur Virionen Produktion und Lyse beschreibt und seitdem die Notwendigkeit adressiert, wie die ökologische Rolle von Viren zu beurteilen ist. Zudem zeigen mikroskopische und metagenomische Methoden eine Vielfalt an Virion- und Genomstruktur in Umweltproben, die nicht durch die Eigenschaften isolierter Viren repräsentiert werden können. Deshalb sind mehr kultivierungsunabhängige Methoden notwendig sind, um diese Virozellen und ihren ökologischen Einfluss zu verstehen.

Das Ziel dieser Dissertation war es, prokaryotische Virozellen mittels bildgestützter Methoden zu identifizieren und charakterisieren. Mittels Raman Mikrospektroskopie wird einen Einblick in die biochemischen Veränderungen von prokaryotischen Kulturen bei Virozellen Induktion im Labor gegeben. Die Analyse der Spektren einzelner Zellen ermöglichte die Formulierung eines univariaten Parameters zur Identifizierung von Virozellen innerhalb flüssiger Kulturen. Dieser wurde durch die Reduktion der multivarianten spektralen Daten auf jene Wellenzahlen mit signifikantem Einfluss ermittelt. Die Biomoleküle, die diesen Wellenzahlen zugeordnet wurden, stimmen mit der Zusammensetzung der Virionen überein und erlauben sogar Rückschlüsse auf beschriebene Entwicklungsstadien der Viren. Um natürliche Virozellen in Umweltproben zu untersuchen, wurde im weiteren Verlauf der Dissertation ein Protokoll für korrelative Licht- und Elektronenmikroskope etabliert. Dieses ermöglicht die Identifizierung von Viren, die zuvor metagenomisch hervorgesagt wurden und anschließende detaillierte Untersuchung der Morphologie der resultierenden Virozellen. Durch statistische Vergleiche wurde der Größenunterschied zwischen Virozellen und nicht infizierten Archaeen und die Größe möglicher Virionen auf der Zelloberfläche im Vergleich zu intrazellulären Partikeln quantifiziert. Durch die detaillierte Untersuchung individueller Zellen wurden neue Vermutungen zur intrazellulären Organisation der Zell- und Virusreplikation aufgestellt. Abschließend wird diskutiert, wie die genutzten und weitere bildgebende Methoden sinnvoll kombiniert werden können, um durch multimodale Anwendungen zu untersuchen, wie Virozellen Ökosysteme beeinflussen.

Zusammenfassend liefert die hier präsentierte Arbeit einen grundlegenden Überblick über Mikroskopische Methoden und der Prozessierung der dabei generierten Daten, um individuelle Virozellen zu identifizierten und zu charakterisieren. Sie stellt einen Wegweiser für die Entwicklung zukünftiger Experimente im Gebiet der prokaryotischen Viren Forschung dar, um den ökologischen Einfluss von Virozellen auf verschiedenen Ebenen zu evaluieren.

6. Bibliography

Abellan-Schneyder, I., Matchado, M.S., Reitmeier, S., Sommer, A., Sewald, Z., Baumbach, J., List, M., Neuhaus, K., 2021. Primer, Pipelines, Parameters: Issues in 16S rRNA Gene Sequencing. mSphere 6, e01202-20. https://doi.org/10.1128/mSphere.01202-20

Ackermann, H.-W., 2003. Bacteriophage observations and evolution. Research in Microbiology 154, 245–251. https://doi.org/10.1016/S0923-2508(03)00067-6

Ali, N., Girnus, S., Rösch, P., Popp, J., Bocklitz, T., 2018. Sample-Size Planning for Multivariate Data: A Raman-Spectroscopy-Based Example. Analytical Chemistry 90, 12485–12492. https://doi.org/10.1021/acs.analchem.8b02167

Almstrand, R., Drennan, D.M., Sharp, J.O., 2015. Polygold-FISH for signal amplification of metallo-labeled microbial cells. Journal of Basic Microbiology 55, 798–802. https://doi.org/10.1002/jobm.201400748

Altinoglu, I., Merrifield, C.J., Yamaichi, Y., 2019. Single molecule super-resolution imaging of bacterial cell pole proteins with high-throughput quantitative analysis pipeline. Sci Rep 9, 6680. https://doi.org/10.1038/s41598-019-43051-7

Amann, R.I., Krumholz, L., Stahl, D.A., 1990. Fluorescent-oligonucleotide probing of whole cells for determinative, phylogenetic, and environmental studies in microbiology. Journal of Bacteriology 172, 762–770. https://doi.org/10.1128/jb.172.2.762-770.1990

Anantharaman, K., Brown, C.T., Hug, L.A., Sharon, I., Castelle, C.J., Probst, A.J., Thomas, B.C., Singh, A., Wilkins, M.J., Karaoz, U., Brodie, E.L., Williams, K.H., Hubbard, S.S., Banfield, J.F., 2016. Thousands of microbial genomes shed light on interconnected biogeochemical processes in an aquifer system. Nature Communications 7, 13219. https://doi.org/10.1038/ncomms13219

Ankrah, N.Y.D., May, A.L., Middleton, J.L., Jones, D.R., Hadden, M.K., Gooding, J.R., LeCleir, G.R., Wilhelm, S.W., Campagna, S.R., Buchan, A., 2014. Phage infection of an environmentally relevant marine bacterium alters host metabolism and lysate composition. ISME J 8, 1089–1100. https://doi.org/10.1038/ismej.2013.216

Auer, H., Mobley, J., Ayers, L., Bowen, J., Chuaqui, R., Johnson, L., Livolsi, V., Lubensky, I., McGarvey, D., Monovich, L., Moskaluk, C., Rumpel, C., Sexton, K., Washington, M., Wiles, K., Grizzle, W., Ramirez, N., 2014. The effects of frozen tissue storage conditions on the integrity of RNA and protein. Biotech Histochem 89, 518–528. https://doi.org/10.3109/10520295.2014.904927

Avci, B., Brandt, J., Nachmias, D., Elia, N., Albertsen, M., Ettema, T., Schramm, A., Kjeldsen, K., 2021. Spatial separation of ribosomes and DNA in Asgard archaeal cells. ISME J. 16. https://doi.org/10.1038/s41396-021-01098-3

Baker, B.J., Comolli, L.R., Dick, G.J., Hauser, L.J., Hyatt, D., Dill, B.D., Land, M.L., VerBerkmoes, N.C., Hettich, R.L., Banfield, J.F., 2010. Enigmatic, ultrasmall, uncultivated Archaea. Proceedings of the National Academy of Sciences 107, 8806. https://doi.org/10.1073/pnas.0914470107

Baltimore, D., 1971. Expression of animal virus genomes. Bacteriol Rev 35, 235–241.

Bamford, D.H., Palva, E.T., Lounatmaa, K., 1976. Ultrastructure and Life Cycle of the Lipid-containing Bacteriophage ϕ6. Journal of General Virology 32, 249–259. https://doi.org/10.1099/0022-1317-32-2-249

Baquero, D.P., Liu, J., Prangishvili, D., 2021. Egress of archaeal viruses. Cellular Microbiology 23, e13394. https://doi.org/10.1111/cmi.13394

Bar-On, Y.M., Phillips, R., Milo, R., 2018. The biomass distribution on Earth. Proceedings of the National Academy of Sciences 115, 6506–6511. https://doi.org/10.1073/pnas.1711842115

Barrero-Canosa, J., Moraru, C., Zeugner, L., Fuchs, B.M., Amann, R., 2017. Direct-geneFISH: a simplified protocol for the simultaneous detection and quantification of genes and rRNA in microorganisms. Environmental Microbiology 19, 70–82. https://doi.org/10.1111/1462-2920.13432

Bechtel, D.B., Bulla, L.A., 1976. Electron Microscope Study of Sporulation and Parasporal Crystal Formation in Bacillus thuringiensis. Journal of Bacteriology 127, 1472–1481. https://doi.org/10.1128/jb.127.3.1472-1481.1976

Benevides, J.M., Overman, S.A., Thomas, G.J., 2003. Raman Spectroscopy of Proteins. Current Protocols in Protein Science 33, 17.8.1-17.8.35. https://doi.org/10.1002/0471140864.ps1708s33

Benevides, J.M., Terwilliger, T.C., Vohník, S., Thomas, G.J., 1996. Raman Spectroscopy of the Ff Gene V Protein and Complexes with Poly(dA): Nonspecific DNA Recognition and Binding. Biochemistry 35, 9603–9609. https://doi.org/10.1021/bi952602e

Benevides, J.M., Tsuboi, M., Bamford, J.K., Thomas, G.J., 1997. Polarized Raman spectroscopy of double-stranded RNA from bacteriophage phi6: local Raman tensors of base and backbone vibrations. Biophysical Journal 72, 2748–2762. https://doi.org/10.1016/S0006-3495(97)78917-3

Berg, J.S., Khachikyan, A., Tienken, D., Littmann, S., Kuypers, M.M.M., Milucka, J., 2020. An intracellular silver deposition method for targeted detection and chemical analysis of uncultured microorganisms. Systematic and Applied Microbiology 43, 126086. https://doi.org/10.1016/j.syapm.2020.126086

Bor, B., Collins, A.J., Murugkar, P.P., Balasubramanian, S., To, T.T., Hendrickson, E.L., Bedree,

J.K., Bidlack, F.B., Johnston, C.D., Shi, W., McLean, J.S., He, X., Dewhirst, F.E., 2020. Insights Obtained by Culturing Saccharibacteria With Their Bacterial Hosts. J Dent Res 99, 685–694. https://doi.org/10.1177/0022034520905792

Bornemann, T.L.V., Adam, P.S., Turzynski, V., Schreiber, U., Figueroa-Gonzalez, P.A., Rahlff, J., Köster, D., Schmidt, T.C., Schunk, R., Krauthausen, B., Probst, A.J., 2022. Genetic diversity in terrestrial subsurface ecosystems impacted by geological degassing. Nat Commun 13, 284. https://doi.org/10.1038/s41467-021-27783-7

Bradley, D.E., 1967. Ultrastructure of bacteriophage and bacteriocins. Bacteriol Rev 31, 230–314.

Brown, C.T., Hug, L.A., Thomas, B.C., Sharon, I., Castelle, C.J., Singh, A., Wilkins, M.J., Wrighton, K.C., Williams, K.H., Banfield, J.F., 2015. Unusual biology across a group comprising more than 15% of domain Bacteria. Nature 523, 208. https://doi.org/10.1038/nature14486

Cai, L., Weinbauer, M.G., Xie, L., Zhang, R., 2023. The smallest in the deepest: the enigmatic role of viruses in the deep biosphere. National Science Review nwad009. https://doi.org/10.1093/nsr/nwad009

Caicedo, J.C., Cooper, S., Heigwer, F., Warchal, S., Qiu, P., Molnar, C., Vasilevich, A.S., Barry, J.D., Bansal, H.S., Kraus, O., Wawer, M., Paavolainen, L., Herrmann, M.D., Rohban, M., Hung, J., Hennig, H., Concannon, J., Smith, I., Clemons, P.A., Singh, S., Rees, P., Horvath, P., Linington, R.G., Carpenter, A.E., 2017. Data-analysis strategies for image-based cell profiling. Nat Methods 14, 849–863. https://doi.org/10.1038/nmeth.4397

Chaikeeratisak, V., Nguyen, K., Khanna, K., Brilot, A.F., Erb, M.L., Coker, J.K.C., Vavilina, A., Newton, G.L., Buschauer, R., Pogliano, K., Villa, E., Agard, D.A., Pogliano, J., 2017. Assembly of a nucleus-like structure during viral replication in bacteria. Science 355, 194–197. https://doi.org/10.1126/science.aal2130

Chen, C., Hou, J., Tanner, J.J., Cheng, J., 2020. Bioinformatics Methods for Mass Spectrometry-Based Proteomics Data Analysis. International Journal of Molecular Sciences 21, 2873. https://doi.org/10.3390/ijms21082873

Chen, D., Shelenkova, L., Li, Y., Kempf, C.R., Sabelnikov, A., 2009. Laser Tweezers Raman Spectroscopy Potential for Studies of Complex Dynamic Cellular Processes: Single Cell Bacterial Lysis. Anal. Chem. 81, 3227–3238. https://doi.org/10.1021/ac8023476

Chen, Z., Chen, L., Zhang, W., 2017. Tools for Genomic and Transcriptomic Analysis of Microbes at Single-Cell Level. Frontiers in Microbiology 8.

Chevallereau, A., Pons, B.J., van Houte, S., Westra, E.R., 2022. Interactions between bacterial and phage communities in natural environments. Nat Rev Microbiol 20, 49–62. https://doi.org/10.1038/s41579-021-00602-y

Coleman, J.R., Culley, D.E., Chrisler, W.B., Brockman, F.J., 2007. mRNA-targeted fluorescent in situ hybridization (FISH) of Gram-negative bacteria without template amplification or tyramide signal amplification. Journal of Microbiological Methods 71, 246–255. https://doi.org/10.1016/j.mimet.2007.09.011

Correa, A.M.S., Howard-Varona, C., Coy, S.R., Buchan, A., Sullivan, M.B., Weitz, J.S., 2021. Revisiting the rules of life for viruses of microorganisms. Nat Rev Microbiol 19, 501–513. https://doi.org/10.1038/s41579-021-00530-x

Daly, R.A., Roux, S., Borton, M.A., Morgan, D.M., Johnston, M.D., Booker, A.E., Hoyt, D.W., Meulia, T., Wolfe, R.A., Hanson, A.J., Mouser, P.J., Moore, J.D., Wunch, K., Sullivan, M.B., Wrighton, K.C., Wilkins, M.J., 2019. Viruses control dominant bacteria colonizing the terrestrial deep biosphere after hydraulic fracturing. Nat Microbiol 4, 352–361. https://doi.org/10.1038/s41564-018-0312-6

Dam, H.T., Vollmers, J., Sobol, M.S., Cabezas, A., Kaster, A.-K., 2020. Targeted Cell Sorting Combined With Single Cell Genomics Captures Low Abundant Microbial Dark Matter With Higher Sensitivity Than Metagenomics. Frontiers in Microbiology 11. https://doi.org/doi.org/10.3389/fmicb.2020.01377

de Bekker, C., Bruning, O., Jonker, M.J., Breit, T.M., Wösten, H.A., 2011. Single cell transcriptomics of neighboring hyphae of Aspergillus niger. Genome Biol 12, R71. https://doi.org/10.1186/gb-2011-12-8-r71

de Boer, P., Hoogenboom, J.P., Giepmans, B.N.G., 2015. Correlated light and electron microscopy: ultrastructure lights up! Nature Methods 12, 503. https://doi.org/10.1038/nmeth.3400

De Gelder, J., De Gussem, K., Vandenabeele, P., Moens, L., 2007. Reference database of Raman spectra of biological molecules. Journal of Raman Spectroscopy 38, 1133–1147. https://doi.org/10.1002/jrs.1734

De Smet, J., Zimmermann, M., Kogadeeva, M., Ceyssens, P.-J., Vermaelen, W., Blasdel, B., Bin Jang, H., Sauer, U., Lavigne, R., 2016. High coverage metabolomics analysis reveals phage-specific alterations to Pseudomonas aeruginosa physiology during infection. ISME J 10, 1823–1835. https://doi.org/10.1038/ismej.2016.3

DeLong, J.P., Al-Sammak, M.A., Al-Ameeli, Z.T., Dunigan, D.D., Edwards, K.F., Fuhrmann, J.J., Gleghorn, J.P., Li, H., Haramoto, K., Harrison, A.O., Marston, M.F., Moore, R.M., Polson, S.W., Ferrell, B.D., Salsbery, M.E., Schvarcz, C.R., Shirazi, J., Steward, G.F., Van Etten, J.L., Wommack, K.E., 2022. Towards an integrative view of virus phenotypes. Nat Rev Microbiol 20, 83–94. https://doi.org/10.1038/s41579-021-00612-w

Deppenmeier, U., Blaut, M., Mahlmann, A., Gottschalk, G., 1990. Reduced coenzyme F420: heterodisulfide oxidoreductase, a proton- translocating redox system in methanogenic

bacteria. PNAS 87, 9449–9453. https://doi.org/10.1073/pnas.87.23.9449

DiMaio, F., Yu, X., Rensen, E., Krupovic, M., Prangishvili, D., Egelman, E.H., 2015. A virus that infects a hyperthermophile encapsidates A-form DNA. Science 348, 914–917. https://doi.org/10.1126/science.aaa4181

Dinno, A., Dinno, M.A., 2017. Package 'dunn. test.' CRAN Repos 10, 1–7.

Dion, M.B., Oechslin, F., Moineau, S., 2020. Phage diversity, genomics and phylogeny. Nat Rev Microbiol 18, 125–138. https://doi.org/10.1038/s41579-019-0311-5

Dombrowski, N., Lee, J.-H., Williams, T.A., Offre, P., Spang, A., 2019. Genomic diversity, lifestyles and evolutionary origins of DPANN archaea. FEMS Microbiology Letters 366, fnz008. https://doi.org/10.1093/femsle/fnz008

Dutilh, B.E., Varsani, A., Tong, Y., Simmonds, P., Sabanadzovic, S., Rubino, L., Roux, S., Muñoz, A.R., Lood, C., Lefkowitz, E.J., Kuhn, J.H., Krupovic, M., Edwards, R.A., Brister, J.R., Adriaenssens, E.M., Sullivan, M.B., 2021. Perspective on taxonomic classification of uncultivated viruses. Current Opinion in Virology 51, 207–215. https://doi.org/10.1016/j.coviro.2021.10.011

Džunková, M., 2022. Single-cell Genomics for Uncovering Relationships between Bacteriophages and their Hosts, Genetic Diversity - Recent Advances and Applications. IntechOpen. https://doi.org/10.5772/intechopen.108118

Efrima, S., Bronk, B.V., 1998. Silver Colloids Impregnating or Coating Bacteria. J. Phys. Chem. B 102, 5947–5950. https://doi.org/10.1021/jp9813903

Ehlers, C., Veit, K., Gottschalk, G., Schmitz, R.A., 2002. Functional organization of a single nif cluster in the mesophilic archaeon Methanosarcina mazei strain Gö1. Archaea 1, 143–150. https://doi.org/10.1155/2002/362813

Flechsler, J., Heimerl, T., Pickl, C., Rachel, R., Stierhof, Y.-D., Klingl, A., 2020. 2D and 3D immunogold localization on (epoxy) ultrathin sections with and without osmium tetroxide. Microscopy Research and Technique 83, 691–705. https://doi.org/10.1002/jemt.23459

Fleeman, R.M., Mikesh, M., Davies, B.W., 2023. Investigating Klebsiella pneumoniae Biofilm Preservation for Scanning Electron Microscopy (preprint). https://doi.org/10.1099/acmi.0.000470.v2

Flemming, H.-C., Wuertz, S., 2019. Bacteria and archaea on Earth and their abundance in biofilms. Nature Reviews Microbiology 17, 247–260. https://doi.org/10.1038/s41579-019-0158-9

Forterre, P., 2013. The virocell concept and environmental microbiology. ISME J. 7, 233–236.

https://doi.org/10.1038/ismej.2012.110

Forterre, P., 2011. Manipulation of cellular syntheses and the nature of viruses: The virocell concept. Comptes Rendus Chimie, De la chimie de synthèse à la biologie de synthèse 14, 392–399. https://doi.org/10.1016/j.crci.2010.06.007

García-Timermans, C., Rubbens, P., Kerckhof, F.-M., Buysschaert, B., Khalenkow, D., Waegeman, W., Skirtach, A.G., Boon, N., 2018. Label-free Raman characterization of bacteria calls for standardized procedures. Journal of Microbiological Methods 151, 69–75. https://doi.org/10.1016/j.mimet.2018.05.027

Gehlert, F.O., Sauerwein, T., Weidenbach, K., Repnik, U., Hallack, D., Förstner, K.U., Schmitz, R.A., 2022. Dual-RNAseq Analysis Unravels Virus-Host Interactions of MetSV and Methanosarcina mazei. Viruses 14, 2585. https://doi.org/10.3390/v14112585

Gibb, S., Strimmer, K., 2012. MALDIquant: a versatile R package for the analysis of mass spectrometry data. Bioinformatics 28, 2270–2271. https://doi.org/10.1093/bioinformatics/bts447

Gios, E., Mosley, O.E., Weaver, L., Close, M., Daughney, C., Handley, K.M., 2023. Ultra-small bacteria and archaea exhibit genetic flexibility towards groundwater oxygen content, and adaptations for attached or planktonic lifestyles. ISME COMMUN. 3, 1–14. https://doi.org/10.1038/s43705-023-00223-x

Giovannoni, S.J., DeLong, E.F., Olsen, G.J., Pace, N.R., 1988. Phylogenetic group-specific oligodeoxynucleotide probes for identification of single microbial cells. Journal of Bacteriology 170, 720–726. https://doi.org/10.1128/jb.170.2.720-726.1988

Golding, C.G., Lamboo, L.L., Beniac, D.R., Booth, T.F., 2016. The scanning electron microscope in microbiology and diagnosis of infectious disease. Sci Rep 6, 26516. https://doi.org/10.1038/srep26516

Hamm, J.N., Liao, Y., Kügelgen, A. von, Dombrowski, N., Landers, E., Brownlee, C., Johansson, E.M.V., Whan, R.M., Baker, M.A.B., Baum, B., Bharat, T.A.M., Duggin, I.G., Spang, A., Cavicchioli, R., 2023. The intracellular lifestyle of an archaeal symbiont. https://doi.org/10.1101/2023.02.24.529834

He, C., Keren, R., Whittaker, M.L., Farag, I.F., Doudna, J.A., Cate, J.H.D., Banfield, J.F., 2021. Genome-resolved metagenomics reveals site-specific diversity of episymbiotic CPR bacteria and DPANN archaea in groundwater ecosystems. Nat Microbiol 6, 354–365. https://doi.org/10.1038/s41564-020-00840-5

He, X., McLean, J.S., Edlund, A., Yooseph, S., Hall, A.P., Liu, S.-Y., Dorrestein, P.C., Esquenazi, E., Hunter, R.C., Cheng, G., Nelson, K.E., Lux, R., Shi, W., 2015. Cultivation of a human-associated TM7 phylotype reveals a reduced genome and epibiotic parasitic lifestyle.

Proceedings of the National Academy of Sciences 112, 244–249. https://doi.org/10.1073/pnas.1419038112

Head, I.M., Saunders, J.R., Pickup, R.W., 1998. Microbial Evolution, Diversity, and Ecology: A Decade of Ribosomal RNA Analysis of Uncultivated Microorganisms. Microb Ecol 35, 1–21. https://doi.org/10.1007/s002489900056

Heimerl, T., Flechsler, J., Pickl, C., Heinz, V., Salecker, B., Zweck, J., Wanner, G., Geimer, S., Samson, R.Y., Bell, S.D., Huber, H., Wirth, R., Wurch, L., Podar, M., Rachel, R., 2017. A Complex Endomembrane System in the Archaeon Ignicoccus hospitalis Tapped by Nanoarchaeum equitans. Frontiers in Microbiology 8. https://doi.org/10.3389/fmicb.2017.01072

Hemphill, H.E., Whiteley, H.R., 1975. Bacteriophages of Bacillus subtilis. Bacteriol Rev 39, 257–315.

Henneberger, R., Moissl, C., Amann, T., Rudolph, C., Huber, R., 2006. New Insights into the Lifestyle of the Cold-Loving SM1 Euryarchaeon: Natural Growth as a Monospecies Biofilm in the Subsurface. Applied and Environmental Microbiology 72, 192–199. https://doi.org/10.1128/aem.72.1.192-199.2006

Hériché, J.-K., Alexander, S., Ellenberg, J., 2019. Integrating Imaging and Omics: Computational Methods and Challenges. Annual Review of Biomedical Data Science 2, 175–197. https://doi.org/10.1146/annurev-biodatasci-080917-013328

Hernsdorf, A.W., Amano, Y., Miyakawa, K., Ise, K., Suzuki, Y., Anantharaman, K., Probst, A., Burstein, D., Thomas, B.C., Banfield, J.F., 2017. Potential for microbial H2 and metal transformations associated with novel bacteria and archaea in deep terrestrial subsurface sediments. ISME J 11, 1915–1929. https://doi.org/10.1038/ismej.2017.39

Hobbs, Z., Abedon, S.T., 2016. Diversity of phage infection types and associated terminology: the problem with 'Lytic or lysogenic.' FEMS Microbiology Letters 363. https://doi.org/10.1093/femsle/fnw047

Hochstein, R.A., Amenabar, M.J., Munson-McGee, J.H., Boyd, E.S., Young, M.J., 2016. Acidianus tailed spindle virus: a new archaeal large tailed spindle virus discovered by culture-independent methods. Journal of virology 90, 3458–3468.

Hollricher, O., Schmidt, U., Breuninger, S., 2015. New Imaging Techniques on the RISE. Optik & Photonik 10, 21–24. https://doi.org/10.1002/opph.201500006

Howard-Varona, C., Hargreaves, K.R., Abedon, S.T., Sullivan, M.B., 2017. Lysogeny in nature: mechanisms, impact and ecology of temperate phages. ISME J 11, 1511–1520. https://doi.org/10.1038/ismej.2017.16

Howard-Varona, C., Lindback, M.M., Bastien, G.E., Solonenko, N., Zayed, A.A., Jang, H.,

Andreopoulos, B., Brewer, H.M., Glavina del Rio, T., Adkins, J.N., Paul, S., Sullivan, M.B., Duhaime, M.B., 2020. Phage-specific metabolic reprogramming of virocells. ISME J. 14, 881–895. https://doi.org/10.1038/s41396-019-0580-z

Huang, W.E., Griffiths, R.I., Thompson, I.P., Bailey, M.J., Whiteley, A.S., 2004. Raman Microscopic Analysis of Single Microbial Cells. Analytical Chemistry 76, 4452–4458. https://doi.org/10.1021/ac049753k

Huang, W.E., Stoecker, K., Griffiths, R., Newbold, L., Daims, H., Whiteley, A.S., Wagner, M., 2007. Raman-FISH: combining stable-isotope Raman spectroscopy and fluorescence in situ hybridization for the single cell analysis of identity and function. Environmental Microbiology 9, 1878–1889. https://doi.org/10.1111/j.1462-2920.2007.01352.x

Hug, L.A., Baker, B.J., Anantharaman, K., Brown, C.T., Probst, A.J., Castelle, C.J., Butterfield, C.N., Hernsdorf, A.W., Amano, Y., Ise, K., Suzuki, Y., Dudek, N., Relman, D.A., Finstad, K.M., Amundson, R., Thomas, B.C., Banfield, J.F., 2016. A new view of the tree of life. Nature Microbiology 1, 16048. https://doi.org/10.1038/nmicrobiol.2016.48

Imdahl, F., Vafadarnejad, E., Homberger, C., Saliba, A.-E., Vogel, J., 2020. Single-cell RNA-sequencing reports growth-condition-specific global transcriptomes of individual bacteria. Nat Microbiol 5, 1202–1206. https://doi.org/10.1038/s41564-020-0774-1

Jahn, M.T., Lachnit, T., Markert, S.M., Stigloher, C., Pita, L., Ribes, M., Dutilh, B.E., Hentschel, U., 2021. Lifestyle of sponge symbiont phages by host prediction and correlative microscopy. ISME J. 1–11. https://doi.org/10.1038/s41396-021-00900-6

Jumper, J., Evans, R., Pritzel, A., Green, T., Figurnov, M., Ronneberger, O., Tunyasuvunakool, K., Bates, R., Žídek, A., Potapenko, A., Bridgland, A., Meyer, C., Kohl, S.A.A., Ballard, A.J., Cowie, A., Romera-Paredes, B., Nikolov, S., Jain, R., Adler, J., Back, T., Petersen, S., Reiman, D., Clancy, E., Zielinski, M., Steinegger, M., Pacholska, M., Berghammer, T., Bodenstein, S., Silver, D., Vinyals, O., Senior, A.W., Kavukcuoglu, K., Kohli, P., Hassabis, D., 2021. Highly accurate protein structure prediction with AlphaFold. Nature 596, 583–589. https://doi.org/10.1038/s41586-021-03819-2

Kasson, P., DiMaio, F., Yu, X., Lucas-Staat, S., Krupovic, M., Schouten, S., Prangishvili, D., Egelman, E.H., 2017. Model for a novel membrane envelope in a filamentous hyperthermophilic virus. eLife 6, e26268. https://doi.org/10.7554/eLife.26268

Kaster, A.-K., Sobol, M.S., 2020. Microbial single-cell omics: the crux of the matter. Appl Microbiol Biotechnol 104, 8209–8220. https://doi.org/10.1007/s00253-020-10844-0

Kattenborn, T., Fassnacht, F.E., Schmidtlein, S., 2019. Differentiating plant functional types using reflectance: which traits make the difference? Remote Sensing in Ecology and Conservation 5, 5–19. https://doi.org/10.1002/rse2.86

Kieft, K., Anantharaman, K., 2022a. Virus genomics: what is being overlooked? Current Opinion in Virology 53, 101200. https://doi.org/10.1016/j.coviro.2022.101200

Kieft, K., Anantharaman, K., 2022b. Deciphering Active Prophages from Metagenomes. mSystems 7, e00084-22. https://doi.org/10.1128/msystems.00084-22

Kimura, M., Jia, Z.-J., Nakayama, N., Asakawa, S., 2008. Ecology of viruses in soils: Past, present and future perspectives. Soil Science and Plant Nutrition 54, 1–32. https://doi.org/10.1111/j.1747-0765.2007.00197.x

Knierim, B., Luef, B., Wilmes, P., Webb, R.I., Auer, M., Comolli, L.R., Banfield, J.F., 2012. Correlative microscopy for phylogenetic and ultrastructural characterization of microbial communities. Environmental Microbiology Reports 4, 36–41. https://doi.org/10.1111/j.1758-2229.2011.00275.x

Koonin, E.V., Senkevich, T.G., Dolja, V.V., 2006. The ancient Virus World and evolution of cells. Biology Direct 1, 29. https://doi.org/10.1186/1745-6150-1-29

Kremer, A., Lippens, S., Bartunkova, S., Asselbergh, B., Blanpain, C., Fendrych, M., Goossens, A., Holt, M., Janssens, S., Krols, M., Larsimont, J.-C., Mc GUIRE, C., Nowack, M. k., Saelens, X., Scher$_{TEL}$, A., Schepens, B., Slezak, M., Timmerman, V., Theunis, C., Van Brempt, R., Visser, Y., Guérin, C. j., 2015. Developing 3D SEM in a broad biological context. Journal of Microscopy 259, 80–96. https://doi.org/10.1111/jmi.12211

Krüger, A., Schäfers, C., Busch, P., Antranikian, G., 2020. Digitalization in microbiology – Paving the path to sustainable circular bioeconomy. New Biotechnology 59, 88–96. https://doi.org/10.1016/j.nbt.2020.06.004

Krupovic, M., Cvirkaite-Krupovic, V., Iranzo, J., Prangishvili, D., Koonin, E.V., 2018. Viruses of archaea: Structural, functional, environmental and evolutionary genomics. Virus Research 244, 181–193. https://doi.org/10.1016/j.virusres.2017.11.025

Ku, C., Sheyn, U., Sebé-Pedrós, A., Ben-Dor, S., Schatz, D., Tanay, A., Rosenwasser, S., Vardi, A., 2020. A single-cell view on alga-virus interactions reveals sequential transcriptional programs and infection states. Science Advances 6, eaba4137. https://doi.org/10.1126/sciadv.aba4137

Kuzmin, A.N., Pliss, A., Prasad, P.N., 2017. Ramanomics: New Omics Disciplines Using Micro Raman Spectrometry with Biomolecular Component Analysis for Molecular Profiling of Biological Structures. Biosensors 7, 52. https://doi.org/10.3390/bios7040052

Ladau, J., Eloe-Fadrosh, E.A., 2019. Spatial, Temporal, and Phylogenetic Scales of Microbial Ecology. Trends in Microbiology 27, 662–669. https://doi.org/10.1016/j.tim.2019.03.003

Laurinavičius, S., Käkelä, R., Bamford, D.H., Somerharju, P., 2004. The origin of phospholipids

of the enveloped bacteriophage phi6. Virology 326, 182–190. https://doi.org/10.1016/j.virol.2004.05.021

Lee, K.S., Landry, Z., Pereira, F.C., Wagner, M., Berry, D., Huang, W.E., Taylor, G.T., Kneipp, J., Popp, J., Zhang, M., Cheng, J.-X., Stocker, R., 2021a. Raman microspectroscopy for microbiology. Nat Rev Methods Primers 1, 80. https://doi.org/10.1038/s43586-021-00075-6

Lee, K.S., Palatinszky, M., Pereira, F.C., Nguyen, J., Fernandez, V.I., Mueller, A.J., Menolascina, F., Daims, H., Berry, D., Wagner, M., Stocker, R., 2019. Publisher Correction: An automated Raman-based platform for the sorting of live cells by functional properties. Nature Microbiology 4, 902–903. https://doi.org/10.1038/s41564-019-0446-1

Lee, K.S., Pereira, F.C., Palatinszky, M., Behrendt, L., Alcolombri, U., Berry, D., Wagner, M., Stocker, R., 2021b. Optofluidic Raman-activated cell sorting for targeted genome retrieval or cultivation of microbial cells with specific functions. Nat Protoc 16, 634–676. https://doi.org/10.1038/s41596-020-00427-8

Leeuwenhoek, A. van, 1800. The Select Works of Anthony Van Leeuwenhoek: Containing His Microscopical Discoveries in Many of the Works of Nature. translator.

Li, J., Zhang, H., Menguy, N., Benzerara, K., Wang, F., Lin, X., Chen, Z., Pan, Y., 2017. Single-Cell Resolution of Uncultured Magnetotactic Bacteria via Fluorescence-Coupled Electron Microscopy. Applied and Environmental Microbiology 83, e00409-17. https://doi.org/10.1128/AEM.00409-17

Liu, J., Cvirkaite-Krupovic, V., Baquero, D.P., Yang, Y., Zhang, Q., Shen, Y., Krupovic, M., 2021. Virus-induced cell gigantism and asymmetric cell division in archaea. Proc Natl Acad Sci USA 118, e2022578118. https://doi.org/10.1073/pnas.2022578118

Liu, X.-Y., Guo, S., Ramoji, A., Bocklitz, T., Rösch, P., Popp, J., Yu, H.-Q., 2020. Spatiotemporal Organization of Biofilm Matrix Revealed by Confocal Raman Mapping Integrated with Non-negative Matrix Factorization Analysis. Analytical Chemistry 92, 707–715. https://doi.org/10.1021/acs.analchem.9b02593

Luef, B., Frischkorn, K.R., Wrighton, K.C., Holman, H.-Y.N., Birarda, G., Thomas, B.C., Singh, A., Williams, K.H., Siegerist, C.E., Tringe, S.G., Downing, K.H., Comolli, L.R., Banfield, J.F., 2015. Diverse uncultivated ultra-small bacterial cells in groundwater. Nature Communications 6, 6372. https://doi.org/10.1038/ncomms7372

Luscombe, N.M., Greenbaum, D., Gerstein, M., 2001. What is Bioinformatics? A Proposed Definition and Overview of the Field. Methods Inf Med 40, 346–358. https://doi.org/10.1055/s-0038-1634431

Lwoff, A., 1953. Lysogeny. Bacteriological Reviews 17, 269–337. https://doi.org/10.1128/br.17.4.269-337.1953

Magnabosco, C., Lin, L.-H., Dong, H., Bomberg, M., Ghiorse, W., Stan-Lotter, H., Pedersen, K., Kieft, T.L., van Heerden, E., Onstott, T.C., 2018. The biomass and biodiversity of the continental subsurface. Nature Geosci 11, 707–717. https://doi.org/10.1038/s41561-018-0221-6

Mäntynen, S., Laanto, E., Oksanen, H.M., Poranen, M.M., Díaz-Muñoz, S.L., 2021. Black box of phage–bacterium interactions: exploring alternative phage infection strategies. Open Biology 11, 210188. https://doi.org/10.1098/rsob.210188

Matturro, B., Rossetti, S., Leitão, P., 2021. CAtalyzed Reporter Deposition Fluorescence In Situ Hybridization (CARD-FISH) for Complex Environmental Samples, in: Azevedo, N.F., Almeida, C. (Eds.), Fluorescence In-Situ Hybridization (FISH) for Microbial Cells: Methods and Concepts, Methods in Molecular Biology. Springer US, New York, NY, pp. 129–140. https://doi.org/10.1007/978-1-0716-1115-9_9

McGlynn, S.E., Chadwick, G.L., O'Neill, A., Mackey, M., Thor, A., Deerinck, T.J., Ellisman, M.H., Orphan, V.J., 2018. Subgroup Characteristics of Marine Methane-Oxidizing ANME-2 Archaea and Their Syntrophic Partners as Revealed by Integrated Multimodal Analytical Microscopy. Applied and Environmental Microbiology 84, e00399-18. https://doi.org/10.1128/AEM.00399-18

McIlroy, S.J., Leu, A.O., Zhang, X., Newell, R., Woodcroft, B.J., Yuan, Z., Hu, S., Tyson, G.W., 2023. Anaerobic methanotroph 'Candidatus Methanoperedens nitroreducens' has a pleomorphic life cycle. Nat Microbiol 1–11. https://doi.org/10.1038/s41564-022-01292-9

Meijer, W.J.J., Horcajadas, J.A., Salas, M., 2001. ϕ29 Family of Phages. Microbiology and Molecular Biology Reviews 65, 261–287. https://doi.org/10.1128/MMBR.65.2.261-287.2001

Metzker, M.L., 2010. Sequencing technologies — the next generation. Nat Rev Genet 11, 31–46. https://doi.org/10.1038/nrg2626

Micheel, C.M., Nass, S.J., Omenn, G.S., Trials, C. on the R. of O.-B.T. for P.P.O. in C., Services, B. on H.C., Policy, B. on H.S., Medicine, I. of, 2012. Omics-Based Clinical Discovery: Science, Technology, and Applications, Evolution of Translational Omics: Lessons Learned and the Path Forward. National Academies Press (US).

Mielke, P.W., 1991. The application of multivariate permutation methods based on distance functions in the earth sciences. Earth-Science Reviews 31, 55–71. https://doi.org/10.1016/0012-8252(91)90042-E

Moissl, C., Rachel, R., Briegel, A., Engelhardt, H., Huber, R., 2005. The unique structure of archaeal 'hami', highly complex cell appendages with nano-grappling hooks. Mol Microbiol 56, 361–370. https://doi.org/10.1111/j.1365-2958.2005.04294.x

Moissl, C., Rudolph, C., Huber, R., 2002. Natural Communities of Novel Archaea and Bacteria with a String-of-Pearls-Like Morphology: Molecular Analysis of the Bacterial Partners. Applied

and Environmental Microbiology 68, 933–937. https://doi.org/10.1128/AEM.68.2.933-937.2002

Moissl, C., Rudolph, C., Rachel, R., Koch, M., Huber, R., 2003. In situ growth of the novel SM1 euryarchaeon from a string-of-pearls-like microbial community in its cold biotope, its physical separation and insights into its structure and physiology. Arch Microbiol 180, 211–217. https://doi.org/10.1007/s00203-003-0580-1

Mollenhauer, H.H., 1993. Artifacts caused by dehydration and epoxy embedding in transmission electron microscopy. Microscopy Research and Technique 26, 496–512. https://doi.org/10.1002/jemt.1070260604

Monsees, I., Klingl, A., Probst, A.J., 2019. Kleine Zellen, große Wirkung — Bakterien der Candidate Phyla Radiation. Biospektrum 25, 719–721. https://doi.org/10.1007/s12268-019-1304-7

Mönttinen, H.A.M., Ravantti, J.J., Poranen, M.M., 2021. Structure Unveils Relationships between RNA Virus Polymerases. Viruses 13, 313. https://doi.org/10.3390/v13020313

Moraru, C., Lam, P., Fuchs, B.M., Kuypers, M.M.M., Amann, R., 2010. GeneFISH – an in situ technique for linking gene presence and cell identity in environmental microorganisms. Environmental Microbiology 12, 3057–3073. https://doi.org/10.1111/j.1462-2920.2010.02281.x

Moter, A., Göbel, U.B., 2000. Fluorescence in situ hybridization (FISH) for direct visualization of microorganisms. Journal of Microbiological Methods 41, 85–112. https://doi.org/10.1016/S0167-7012(00)00152-4

Muhamadali, H., Chisanga, M., Subaihi, A., Goodacre, R., 2015. Combining Raman and FT-IR Spectroscopy with Quantitative Isotopic Labeling for Differentiation of E. coli Cells at Community and Single Cell Levels. Anal. Chem. 87, 4578–4586. https://doi.org/10.1021/acs.analchem.5b00892

Munson-McGee, J.H., Field, E.K., Bateson, M., Rooney, C., Stepanauskas, R., Young, M.J., 2015. Nanoarchaeota, Their Sulfolobales Host, and Nanoarchaeota Virus Distribution across Yellowstone National Park Hot Springs. Applied and Environmental Microbiology 81, 7860–7868. https://doi.org/10.1128/AEM.01539-15

Munson-McGee, J.H., Rooney, C., Young, M.J., 2019. An uncultivated virus infecting a symbiotic Nanoarchaeota in the hot springs of Yellowstone National Park. Journal of Virology JVI.01213-19. https://doi.org/10.1128/jvi.01213-19

Neugebauer, U., Schmid, U., Baumann, K., Ziebuhr, W., Kozitskaya, S., Deckert, V., Schmitt, M., Popp, J., 2007. Towards a Detailed Understanding of Bacterial Metabolism—Spectroscopic Characterization of Staphylococcus Epidermidis. ChemPhysChem 8, 124–137.

https://doi.org/10.1002/cphc.200600507

Nyongesa, S., Weber, P.M., Bernet, È., Pulido, F., Nieves, C., Nieckarz, M., Delaby, M., Viehboeck, T., Krause, N., Rivera-Millot, A., Nakamura, A., Vischer, N.O.E., vanNieuwenhze, M., Brun, Y.V., Cava, F., Bulgheresi, S., Veyrier, F.J., 2022. Evolution of longitudinal division in multicellular bacteria of the Neisseriaceae family. Nat Commun 13, 1–18. https://doi.org/10.1038/s41467-022-32260-w

Oksanen, J., Blanchet, F.G., Kindt, R., Legendre, P., Minchin, P.R., O'hara, R., Simpson, G.L., Solymos, P., Stevens, M.H.H., Wagner, H., 2013. vegan: Community Ecology Package. R package version 2.5-7. Community ecology package, version 2, 1–295.

Paradis, E., Schliep, K., 2019. ape 5.0: an environment for modern phylogenetics and evolutionary analyses in R. Bioinformatics 35, 526–528. https://doi.org/10.1093/bioinformatics/bty633

Peddie, C.J., Collinson, L.M., 2014. Exploring the third dimension: Volume electron microscopy comes of age. Micron 61, 9–19. https://doi.org/10.1016/j.micron.2014.01.009

Pernthaler, A., Amann, R., 2004. Simultaneous Fluorescence In Situ Hybridization of mRNA and rRNA in Environmental Bacteria. Applied and Environmental Microbiology 70, 5426. https://doi.org/10.1128/AEM.70.9.5426-5433.2004

Pernthaler, A., Pernthaler, J., Amann, R., 2002. Fluorescence In Situ Hybridization and Catalyzed Reporter Deposition for the Identification of Marine Bacteria. Applied and Environmental Microbiology 68, 3094. https://doi.org/10.1128/AEM.68.6.3094-3101.2002

Perras, A.K., Wanner, G., Klingl, A., Mora, M., Auerbach, A.K., Heinz, V., Probst, A.J., Huber, H., Rachel, R., Meck, S., Moissl-Eichinger, C., 2014. Grappling archaea: ultrastructural analyses of an uncultivated, cold-loving archaeon, and its biofilm. Frontiers in Microbiology 5. https://doi.org/10.3389/fmicb.2014.00397

Prangishvili, D., Bamford, D.H., Forterre, P., Iranzo, J., Koonin, E.V., Krupovic, M., 2017. The enigmatic archaeal virosphere. Nat Rev Microbiol 15, 724–739. https://doi.org/10.1038/nrmicro.2017.125

Prangishvili, D., Garrett, R.A., Koonin, E.V., 2006. Evolutionary genomics of archaeal viruses: Unique viral genomes in the third domain of life. Virus Research, Comparative Genomics and Evolution of Complex Viruses 117, 52–67. https://doi.org/10.1016/j.virusres.2006.01.007

Prescott, B., Sitaraman, K., Argos, P., Thomas, G.J., 1985. Protein-RNA interactions in belladonna mottle virus investigated by laser Raman spectroscopy. Biochemistry 24, 1226–1231. https://doi.org/10.1021/bi00326a026

Probst, A.J., Holman, H.-Y.N., DeSantis, T.Z., Andersen, G.L., Birarda, G., Bechtel, H.A., Piceno,

Y.M., Sonnleitner, M., Venkateswaran, K., Moissl-Eichinger, C., 2012. Tackling the minority: sulfate-reducing bacteria in an archaea-dominated subsurface biofilm. The Isme Journal 7, 635. https://doi.org/10.1038/ismej.2012.133

Probst, A.J., Ladd, B., Jarett, J.K., Geller-McGrath, D.E., Sieber, C.M.K., Emerson, J.B., Anantharaman, K., Thomas, B.C., Malmstrom, R.R., Stieglmeier, M., Klingl, A., Woyke, T., Ryan, M.C., Banfield, J.F., 2018. Differential depth distribution of microbial function and putative symbionts through sediment-hosted aquifers in the deep terrestrial subsurface. Nat Microbiol 3, 328–336. https://doi.org/10.1038/s41564-017-0098-y

Probst, A.J., Moissl-Eichinger, C., 2015. "Altiarchaeales": Uncultivated Archaea from the Subsurface. Life 5, 1381–1395.

Probst, A.J., Weinmaier, T., Raymann, K., Perras, A., Emerson, J.B., Rattei, T., Wanner, G., Klingl, A., Berg, I.A., Yoshinaga, M., Viehweger, B., Hinrichs, K.-U., Thomas, B.C., Meck, S., Auerbach, A.K., Heise, M., Schintlmeister, A., Schmid, M., Wagner, M., Gribaldo, S., Banfield, J.F., Moissl-Eichinger, C., 2014. Biology of a widespread uncultivated archaeon that contributes to carbon fixation in the subsurface. Nat Commun 5, 5497. https://doi.org/10.1038/ncomms6497

Puppels, G.J., de Mul, F.F.M., Otto, C., Greve, J., Robert-Nicoud, M., Arndt-Jovin, D.J., Jovin, T.M., 1990. Studying single living cells and chromosomes by confocal Raman microspectroscopy. Nature 347, 301–303. https://doi.org/10.1038/347301a0

Rahlff, J., Turzynski, V., Esser, S.P., Monsees, I., Bornemann, T.L.V., Figueroa-Gonzalez, P.A., Schulz, F., Woyke, T., Klingl, A., Moraru, C., Probst, A.J., 2021. Lytic archaeal viruses infect abundant primary producers in Earth's crust. Nat Commun 12, 4642. https://doi.org/10.1038/s41467-021-24803-4

Remis, J.P., Wei, D., Gorur, A., Zemla, M., Haraga, J., Allen, S., Witkowska, H.E., Costerton, J.W., Berleman, J.E., Auer, M., 2014. Bacterial social networks: structure and composition of Myxococcus xanthus outer membrane vesicle chains. Environmental Microbiology 16, 598–610. https://doi.org/10.1111/1462-2920.12187

Rodrigues-Oliveira, T., Wollweber, F., Ponce-Toledo, R.I., Xu, J., Rittmann, S.K.-M.R., Klingl, A., Pilhofer, M., Schleper, C., 2023. Actin cytoskeleton and complex cell architecture in an Asgard archaeon. Nature 613, 332–339. https://doi.org/10.1038/s41586-022-05550-y

Rohwer, F., Edwards, R., 2002. The Phage Proteomic Tree: a Genome-Based Taxonomy for Phage. Journal of Bacteriology 184, 4529–4535. https://doi.org/10.1128/JB.184.16.4529-4535.2002

Rohwer, F., Prangishvili, D., Lindell, D., 2009. Roles of viruses in the environment. Environmental Microbiology 11, 2771–2774. https://doi.org/10.1111/j.1462-2920.2009.02101.x

Rollenhagen, A., Walkenfort, B., Yakoubi, R., Klauke, S.A., Schmuhl-Giesen, S.F., Heinen-Weiler, J., Voortmann, S., Marshallsay, B., Palaz, T., Holz, U., Hasenberg, M., Lübke, J.H.R., 2020. Synaptic Organization of the Human Temporal Lobe Neocortex as Revealed by High-Resolution Transmission, Focused Ion Beam Scanning, and Electron Microscopic Tomography. International Journal of Molecular Sciences 21, 5558. https://doi.org/10.3390/ijms21155558

Romantschuk, M., Bamford, D.H., 1981. ϕ6-Resistant Phage-producing Mutants of Pseudomonas phaseolicola. Journal of General Virology 56, 287–295. https://doi.org/10.1099/0022-1317-56-2-287

Rosenwasser, S., Mausz, M.A., Schatz, D., Sheyn, U., Malitsky, S., Aharoni, A., Weinstock, E., Tzfadia, O., Ben-Dor, S., Feldmesser, E., Pohnert, G., Vardi, A., 2014. Rewiring Host Lipid Metabolism by Large Viruses Determines the Fate of Emiliania huxleyi, a Bloom-Forming Alga in the Ocean. The Plant Cell 26, 2689–2707. https://doi.org/10.1105/tpc.114.125641

Rosenwasser, S., Sheyn, U., Frada, M.J., Pilzer, D., Rotkopf, R., Vardi, A., 2019. Unmasking cellular response of a bloom-forming alga to viral infection by resolving expression profiles at a single-cell level. PLOS Pathogens 15, e1007708. https://doi.org/10.1371/journal.ppat.1007708

Rudolph, C., Moissl, C., Henneberger, R., Huber, R., 2004. Ecology and microbial structures of archaeal/bacterial strings-of-pearls communities and archaeal relatives thriving in cold sulfidic springs. FEMS Microbiology Ecology 50, 1–11. https://doi.org/10.1016/j.femsec.2004.05.006

Rudolph, C., Wanner, G., Huber, R., 2001. Natural Communities of Novel Archaea and Bacteria Growing in Cold Sulfurous Springs with a String-of-Pearls-Like Morphology. Applied and Environmental Microbiology 67, 2336–2344. https://doi.org/10.1128/AEM.67.5.2336-2344.2001

Ryan, C.G., Clayton, E., Griffin, W.L., Sie, S.H., Cousens, D.R., 1988. SNIP, a statistics-sensitive background treatment for the quantitative analysis of PIXE spectra in geoscience applications. Nuclear Instruments and Methods in Physics Research Section B: Beam Interactions with Materials and Atoms 34, 396–402. https://doi.org/10.1016/0168-583X(88)90063-8

Sakai, H.D., Nur, N., Kato, S., Yuki, M., Shimizu, M., Itoh, T., Ohkuma, M., Suwanto, A., Kurosawa, N., 2022. Insight into the symbiotic lifestyle of DPANN archaea revealed by cultivation and genome analyses. PNAS 119. https://doi.org/10.1073/pnas.2115449119

Sakoula, D., Smith, G.J., Frank, J., Mesman, R.J., Kop, L.F.M., Blom, P., Jetten, M.S.M., van Kessel, M.A.H.J., Lücker, S., 2022. Universal activity-based labeling method for ammonia- and alkane-oxidizing bacteria. ISME J 16, 958–971. https://doi.org/10.1038/s41396-021-01144-0

Schaible, G.A., Kohtz, A.J., Cliff, J., Hatzenpichler, R., 2022. Correlative SIP-FISH-Raman-SEM-NanoSIMS links identity, morphology, biochemistry, and physiology of environmental microbes. ISME Commun. 2, 1–10. https://doi.org/10.1038/s43705-022-00134-3

Schie, I.W., Stiebing, C., Popp, J., 2021. Looking for a perfect match: multimodal combinations of Raman spectroscopy for biomedical applications. JBO 26, 080601. https://doi.org/10.1117/1.JBO.26.8.080601

Schmidt, H., Eickhorst, T., Mußmann, M., 2012. Gold-FISH: a new approach for the in situ detection of single microbial cells combining fluorescence and scanning electron microscopy. Systematic and applied microbiology 35, 518–525.

Schreiber, L., Holler, T., Knittel, K., Meyerdierks, A., Amann, R., 2010. Identification of the dominant sulfate-reducing bacterial partner of anaerobic methanotrophs of the ANME-2 clade. Environmental Microbiology 12, 2327–2340. https://doi.org/10.1111/j.1462-2920.2010.02275.x

Schuster, K.C., Urlaub, E., Gapes, J.R., 2000. Single-cell analysis of bacteria by Raman microscopy: spectral information on the chemical composition of cells and on the heterogeneity in a culture. Journal of Microbiological Methods 42, 29–38. https://doi.org/10.1016/S0167-7012(00)00169-X

Schwank, K., Bornemann, T.L.V., Dombrowski, N., Spang, A., Banfield, J.F., Probst, A.J., 2019. An archaeal symbiont-host association from the deep terrestrial subsurface. ISME J 13, 2135–2139. https://doi.org/10.1038/s41396-019-0421-0

Serra, D.O., Richter, A.M., Klauck, G., Mika, F., Hengge, R., 2013. Microanatomy at Cellular Resolution and Spatial Order of Physiological Differentiation in a Bacterial Biofilm. mBio 4, e00103-13. https://doi.org/10.1128/mBio.00103-13

Sharma, A., Schmidt, M., Kiesel, B., Mahato, N.K., Cralle, L., Singh, Y., Richnow, H.H., Gilbert, J.A., Arnold, W., Lal, R., 2018. Bacterial and Archaeal Viruses of Himalayan Hot Springs at Manikaran Modulate Host Genomes. Frontiers in Microbiology 9. https://doi.org/10.3389/fmicb.2018.03095

Singh, M.K., Kenney, L.J., 2021. Super-resolution imaging of bacterial pathogens and visualization of their secreted effectors. FEMS Microbiology Reviews 45, fuaa050. https://doi.org/10.1093/femsre/fuaa050

Spinelli, S., Bebeacua, C., Orlov, I., Tremblay, D., Klaholz, B.P., Moineau, S., Cambillau, C., 2014. Cryo-Electron Microscopy Structure of Lactococcal Siphophage 1358 Virion. Journal of Virology 88, 8900–8910. https://doi.org/10.1128/jvi.01040-14

Sun, M., Yuan, S., Xia, R., Ye, M., Balcázar, J.L., 2022. Underexplored viral auxiliary metabolic genes in soil: Diversity and eco-evolutionary significance. Environmental Microbiology n/a. https://doi.org/10.1111/1462-2920.16329

Suttle, C.A., 2005. Viruses in the sea. Nature 437, 356–361. https://doi.org/10.1038/nature04160

Sutton, G., Sun, D., Fu, X., Kotecha, A., Hecksel, C.W., Clare, D.K., Zhang, P., Stuart, D.I., Boyce, M., 2020. Assembly intermediates of orthoreovirus captured in the cell. Nat Commun 11, 4445. https://doi.org/10.1038/s41467-020-18243-9

Taniguchi, Y., Choi, P.J., Li, G.-W., Chen, H., Babu, M., Hearn, J., Emili, A., Xie, X.S., 2010. Quantifying E. coli Proteome and Transcriptome with Single-Molecule Sensitivity in Single Cells. Science 329, 533–538. https://doi.org/10.1126/science.1188308

Team, R.C., 2018. R: A language and environment for statistical computing; 2015.

Teng, L., Wang, Xian, Wang, Xiaojun, Gou, H., Ren, L., Wang, T., Wang, Y., Ji, Y., Huang, W.E., Xu, J., 2016. Label-free, rapid and quantitative phenotyping of stress response in E. coli via ramanome. Scientific Reports 6, 34359. https://doi.org/10.1038/srep34359

Thévenot, E.A., Roux, A., Xu, Y., Ezan, E., Junot, C., 2015. Analysis of the Human Adult Urinary Metabolome Variations with Age, Body Mass Index, and Gender by Implementing a Comprehensive Workflow for Univariate and OPLS Statistical Analyses. J. Proteome Res. 14, 3322–3335. https://doi.org/10.1021/acs.jproteome.5b00354

Thingstad, T.F., Våge, S., Storesund, J.E., Sandaa, R.-A., Giske, J., 2014. A theoretical analysis of how strain-specific viruses can control microbial species diversity. Proceedings of the National Academy of Sciences 111, 7813–7818. https://doi.org/10.1073/pnas.1400909111

Thomas, G.J., 1999. Raman Spectroscopy of Protein and Nucleic Acid Assemblies. Annual Review of Biophysics and Biomolecular Structure 28, 1–27. https://doi.org/10.1146/annurev.biophys.28.1.1

Turzynski, V., Griesdorn, L., Moraru, C., Soares, A., Simon, S.A., Stach, T.L., Rahlff, J., Esser, S.P., Probst, A.J., 2023. Virus-host dynamics in archaeal groundwater biofilms and the associated bacterial community composition. https://doi.org/10.1101/2023.02.03.526798

Turzynski, V., Monsees, I., Moraru, C., Probst, A.J., 2021. Imaging Techniques for Detecting Prokaryotic Viruses in Environmental Samples. Viruses 13, 2126. https://doi.org/10.3390/v13112126

Verstraete, W., Yanuka-Golub, K., Driesen, N., De Vrieze, J., 2022. Engineering microbial technologies for environmental sustainability: choices to make. Microbial Biotechnology 15, 215–227. https://doi.org/10.1111/1751-7915.13986

Vicar, T., Balvan, J., Jaros, J., Jug, F., Kolar, R., Masarik, M., Gumulec, J., 2019. Cell segmentation methods for label-free contrast microscopy: review and comprehensive comparison. BMC Bioinformatics 20, 360. https://doi.org/10.1186/s12859-019-2880-8

Vidaver, A.K., Koski, R.K., Van Etten, J.L., 1973. Bacteriophage ϕ6: a Lipid-Containing Virus of Pseudomonas phaseolicola. Journal of Virology 11, 799.

Vincent, F., Vardi, A., 2023. Viral infection in the ocean—A journey across scales. PLOS Biology 21, e3001966. https://doi.org/10.1371/journal.pbio.3001966

Wagner, C., Reddy, V., Asturias, F., Khoshouei, M., Johnson, J.E., Manrique, P., Munson-McGee, J., Baumeister, W., Lawrence, C.M., Young, M.J., 2017. Isolation and Characterization of Metallosphaera Turreted Icosahedral Virus, a Founding Member of a New Family of Archaeal Viruses. Journal of Virology 91, e00925-17. https://doi.org/10.1128/JVI.00925-17

Wagner, M., Schmid, M., Juretschko, S., Trebesius, K.-H., Bubert, A., Goebel, W., Schleifer, K.-H., 1998. In situ detection of a virulence factor mRNA and 16S rRNA in Listeria monocytogenes. FEMS Microbiology Letters 160, 159–168. https://doi.org/10.1111/j.1574-6968.1998.tb12906.x

Walter, A., Paul-Gilloteaux, P., Plochberger, B., Sefc, L., Verkade, P., Mannheim, J.G., Slezak, P., Unterhuber, A., Marchetti-Deschmann, M., Ogris, M., Bühler, K., Fixler, D., Geyer, S.H., Weninger, W.J., Glösmann, M., Handschuh, S., Wanek, T., 2020. Correlated Multimodal Imaging in Life Sciences: Expanding the Biomedical Horizon. Frontiers in Physics 8.

Wang, F., Cvirkaite-Krupovic, V., Vos, M., Beltran, L.C., Kreutzberger, M.A.B., Winter, J.-M., Su, Z., Liu, J., Schouten, S., Krupovic, M., Egelman, E.H., 2022. Spindle-shaped archaeal viruses evolved from rod-shaped ancestors to package a larger genome. Cell 185, 1297-1307.e11. https://doi.org/10.1016/j.cell.2022.02.019

Wang, F., Liu, Y., Su, Z., Osinski, T., de Oliveira, G.A.P., Conway, J.F., Schouten, S., Krupovic, M., Prangishvili, D., Egelman, E.H., 2019. A packing for A-form DNA in an icosahedral virus. Proceedings of the National Academy of Sciences 116, 22591–22597. https://doi.org/10.1073/pnas.1908242116

Wang, Y., Huang, W.E., Cui, L., Wagner, M., 2016. Single cell stable isotope probing in microbiology using Raman microspectroscopy. Current Opinion in Biotechnology, Analytical biotechnology 41, 34–42. https://doi.org/10.1016/j.copbio.2016.04.018

Wang, Y., Yan, B., Chen, L., 2013. SERS Tags: Novel Optical Nanoprobes for Bioanalysis. Chem. Rev. 113, 1391–1428. https://doi.org/10.1021/cr300120g

Wang, Z., Gerstein, M., Snyder, M., 2009. RNA-Seq: a revolutionary tool for transcriptomics. Nat Rev Genet 10, 57–63. https://doi.org/10.1038/nrg2484

Weidenbach, K., Nickel, L., Neve, H., Alkhnbashi, O.S., Künzel, S., Kupczok, A., Bauersachs, T., Cassidy, L., Tholey, A., Backofen, R., Schmitz, R.A., 2017. Methanosarcina Spherical Virus, a Novel Archaeal Lytic Virus Targeting Methanosarcina Strains. Journal of Virology 91, e00955-17. https://doi.org/10.1128/jvi.00955-17

Weiss, R., Palatinszky, M., Wagner, M., Niessner, R., Elsner, M., Seidel, M., P. Ivleva, N., 2019. Surface-enhanced Raman spectroscopy of microorganisms: limitations and applicability on the

single-cell level. Analyst 144, 943–953. https://doi.org/10.1039/C8AN02177E

Wilhelm, S.W., Suttle, C.A., 1999. Viruses and Nutrient Cycles in the Sea: Viruses play critical roles in the structure and function of aquatic food webs. BioScience 49, 781–788. https://doi.org/10.2307/1313569

Woese, C., 1998. The universal ancestor. Proc. Natl. Acad. Sci. U.S.A. 95, 6854–6859. https://doi.org/10.1073/pnas.95.12.6854

Woyke, T., Tighe, D., Mavromatis, K., Clum, A., Copeland, A., Schackwitz, W., Lapidus, A., Wu, D., McCutcheon, J.P., McDonald, B.R., Moran, N.A., Bristow, J., Cheng, J.-F., 2010. One Bacterial Cell, One Complete Genome. PLOS ONE 5, e10314. https://doi.org/10.1371/journal.pone.0010314

Wu, M., Li, W., Christie, G., Setlow, P., Li, Y., 2021. Characterization of Heterogeneity and Dynamics of Lysis of Single Bacillus subtilis Cells upon Prophage Induction During Spore Germination, Outgrowth, and Vegetative Growth Using Raman Tweezers and Live-Cell Phase-Contrast Microscopy. Anal. Chem. 93, 1443–1450. https://doi.org/10.1021/acs.analchem.0c03341

Wu, M., Li, W., Christie, G., Setlow, P., Li, Y., 2020. Characterization of Heterogeneity and Dynamics of Lysis of Single Bacillus subtilis Cells upon Prophage Induction During Spore Germination, Outgrowth, and Vegetative Growth Using Raman Tweezers and Live-Cell Phase-Contrast Microscopy. Analytical Chemistry. https://doi.org/10.1021/acs.analchem.0c03341

Xin, X.-F., Kvitko, B., He, S.Y., 2018. Pseudomonas syringae: what it takes to be a pathogen. Nat Rev Microbiol 16, 316–328. https://doi.org/10.1038/nrmicro.2018.17

Ye, J., Nielsen, S., Joseph, S., Thomas, T., 2015. High-Resolution and Specific Detection of Bacteria on Complex Surfaces Using Nanoparticle Probes and Electron Microscopy. PLOS ONE 10, e0126404. https://doi.org/10.1371/journal.pone.0126404

Zhang, M., Zhang, T., Yu, M., Chen, Y.-L., Jin, M., 2022. The Life Cycle Transitions of Temperate Phages: Regulating Factors and Potential Ecological Implications. Viruses 14, 1904. https://doi.org/10.3390/v14091904

Ziefuss, A.R., Steenbock, T., Benner, D., Plech, A., Göttlicher, J., Teubner, M., Grimm-Lebsanft, B., Rehbock, C., Comby-Zerbino, C., Antoine, R., Amans, D., Chakraborty, I., Bester, G., Nachev, M., Sures, B., Rübhausen, M., Parak, W.J., Barcikowski, S., 2021. Photoluminescence of Fully Inorganic Colloidal Gold Nanocluster and Their Manipulation Using Surface Charge Effects. Advanced Materials 33, 2101549. https://doi.org/10.1002/adma.202101549

Ziefuss, A.R., Willeke, M., Miertz, M., Heinemann, A., Rehbock, C., Barcikowski, S., 2022. Influence of Pt Alloying on the Fluorescence of Fully Inorganic, Colloidal Gold Nanoclusters. ChemPhysChem 23, e202200033. https://doi.org/10.1002/cphc.202200033

Zucker, F., Bischoff, V., Olo Ndela, E., Heyerhoff, B., Poehlein, A., Freese, H.M., Roux, S., Simon, M., Enault, F., Moraru, C., 2022. New Microviridae isolated from Sulfitobacter reveals two cosmopolitan subfamilies of single-stranded DNA phages infecting marine and terrestrial Alphaproteobacteria. Virus Evolution 8, veac070. https://doi.org/10.1093/ve/veac070

7. Supporting Data

All supporting data used to generate the results published within this thesis are included on the accompanying CD.

The respective folders with the supplemental material are sorted as followed:

I. 3_1 Supplemental material of section 3.1, as published
II. 3_2 Supplemental material of section 3.2, as submitted after revision
III. 4_2 Supplemental material of section 4.2, raw data and script to generate Figure 4.1
IV. 4_3 Supplemental material of section 4.3, raw images of Figure 4.3

8. List of Abbreviations

^{12}C	most abundant carbon isotope (over 98% abundance)
^{13}C	natural stable isotope of carbon (about 1% abundance)
^{15}N	rare stable isotope of nitrogen
16S rRNA	ribosomal RNA of the 16S subunit of prokaryotic ribosomes
2D	two-dimensional
3D	three-dimensional
A	chance-corrected within-group agreement
AMG	auxiliary metabolic gene
B. subtilis	*Bacillus subtilis*
BSE	backscattered electron detector
Ca. A. hamiconexum	*Candidatus* Altiarchaeum *hamiconexum*
CARD-FISH	catalyzed reporter deposition FISH
CLEM	correlative light and electron microscopy
CPR	candidate phyla radiation
CRISPR	clustered, regularly-interspaced short palindromic repeat
Cryo-FIB	cryo-focused ion beam milling
D	Deuterium
DAPI	4',6-Diamidino-2-phenylindol
DGF	direct-geneFISH
DNA	deoxyribonucleic acid
DPANN	Diapherotrites, Parvarchaeota, Aenigmarchaeota, Nanoarchaeota, Nanohaloarchaeota
ds	double-stranded
e.g.	*exempli gratia* (Lat. For example)
EDS	energy dispersive spectroscopy
EhV	*Emiliania huxleyi* virus
EM	electron microscopy
EPS	extracellular polymeric substances
ET	electron tomography
FACS	Fluorescence-activated cell sorting
FIB	focused ion beam
FISH	fluorescence *in situ* hybridization

GISH	Gold *in situ* hybridization
HRP	horseradish peroxidase
I	intensity
M. mazei	*Methanosarcina mazei*
Metal-ISH	nano-metalprobe *in situ* hybridization
MetSV	*methanosarcina* spherical virus
MGE	mobile genetic element
mRNA	messenger RNA
MRPP	multiresponse permutation procedure
MSI	Mühlbacher Schwefelquelle
Nano-SIMS	nano-scale secondary ion mass spectrometry
OPLS	orthogonal partial least square model
P. syringae	*Pseudomonas syringae*
PALM	photoactivation localization microscopy
PC	principal component
PCA	principal component analyses
phage	bacteriophage
RACS	Raman-activated cell sorting
RNA	ribonucleic acid
SBF	Serial Blockface
SEM	Scanning electron microscopy
SERS	surface-enhanced Raman spectra
silver-DISH	silver deposition *in situ* hybridization
SIM	structured illumination microscopy
ss	single-stranded
STORM	stochastic optical reconstruction microscopy
TEM	transmission electron microscopy
TSA	tyramide signal amplification
vhg	viral hallmark genes
VIP	variable importance on projection
viral FISH	dual viral and cellular FISH
virion	viral particles
virusFISH	virus-targeted direct-geneFISH
VLP	virus-like particle
volume EM	Volume electron microscopy

9. Eidesstattliche Erklärung

Ich bestätige hiermit an Eides statt, dass die vorliegende Arbeit ohne unzulässige Hilfe Dritter und ohne Benutzung anderer als der angegebenen Hilfsmittel angefertigt habe. Die aus anderen Quellen direkt oder indirekt übernommenen Daten und Konzepte sind unter Angabe des Literaturzitats gekennzeichnet.

Essen 31.03.2023

_____

Indra Banas